Program & Abstracts

10th OCARINA International Symposium

The OCU Advanced Research Institute for Natural Science and Technology (OCARINA),
and the OCU Professional Development Program

5th - 6th March, 2019 Conference Room (10th Floor), Media Center and Library,
Osaka City University, 3-3-138 Sugimoto, 558-8585 Osaka, Japan
Organized by Osaka City University

Preface

Welcome

OCARINA, the OCU Advanced Research Institute for Natural Science and Technology is a cross-disciplinary research organization in Osaka City University. Currently, seven research projects that cross the three departments of the Graduate School of Science, Graduate School of Engineering, and Graduate School of Human Life Sciences are participating in OCARINA. OCARINA will host the 10th International Symposium on March 5-6, 2019, where the advanced research results of these projects will be presented.

This year we are planning two mini-symposiums entitled "Progress and future of photosynthetic research" and "Catalysts (tentative)", and invited active researchers in the world. We also will produce the poster session from many younger scientists including students (age under 35) to increase opportunities for lively and informative exchange of views. Approximately 20% of posters will be awarded the poster prize and it will be announced at the banquet.

On behalf of the organizing committee, we encourage the submission of abstracts for the poster session and we hope many people will participate in this symposium and contribute to active discussions.

We look forward to welcoming you to Osaka.

Chair organizer

Michio MIYANO

Adviser to the President of OCU

Director of OCARINA

ご挨拶

大阪市立大学・複合先端研究機構（OCARINA）は、地球規模でのエネルギー、資源、生態系など、環境を含めた全人類に係る複合的および先端的な研究課題に対して、プロジェクト制により研究科横断型で最先端科学・技術を融合して取り組むことにより、学術的・社会的提言並びに人材育成を行い、得られた成果を社会や地域へ効果的に還元することを目的とします。

現在、機構では理学研究科・工学研究科・生活科学研究科の 3 研究科を横断する研究組織を構築し、７つのプロジェクト研究を推進しています。これらのプロジェクト研究の相互理解を深める場として、本シンポジウムを開催いたします。

今年度、本学人工光合成研究センターは開所から 5 周年を迎えました。この節目に、本学で「光合成・人工光合成」分野の研究を牽引されてこられた神谷信夫教授と、同分野の第一線でご活躍されている国内外の先生方による講演を企画しました。

また今年度も、学内理系分野間の相互理解を深めることを目的として、本学「人材育成プロジェクト」と連携したポスターセッションを設けています。学生のポスターは英語によるショートプレゼンテーションとポスター発表により審査され、優秀ポスター賞が贈られます。

ご参加いただきました皆様がたには、活発な討論により異分野交流をお楽しみいただき、今後の異分野融合研究を生み出すきっかけになれば幸いです。どうぞよろしくお願いいたします。

2019 年 3 月

複合先端研究機構・機構長
宮野　道雄

Date

5th March (Tue.), 2019 (Registration:09:00-) 09:30-18:10

6th March (Wed), 2019 (Registration:09:00-) 09:30-16:50

*Symposium Photo: 18:10 on 5th March (Tue.), 2019 at conference room (10th Floor)

Venue

Conference Room (10th Floor) , Media Center, OCU

Banquet

5th March (Tue.) , 2019 18:20-

at Meeting Room for Researching Staff (10th Floor) , Media Center, OCU

Organizer

The OCU Advanced Research Institute for Natural Science and Technology (OCARINA)

Organizing committee

- Dr. Michio MIYANO (Adviser to the President of OCU / Director of OCARINA / Specially Appointed Professor, Graduate School of Human Life Science, OCU)
- Dr. Nobuo KAMIYA (Vice Director, OCARINA/Professor, OCARINA)
- Dr. Naoteru SHIGEKAWA (Vice Director, OCARINA/Professor, Department of Physical Electronics and Informatics, Graduate School of Engineering, OCU)
- Dr. Yutaka AMAO (Director, ReCAP/Professor, OCARINA)
- Dr. Tomoko YOSHIDA (Deputy Director, ReCAP/Professor, OCARINA)
- Dr. Ritsuko FUJII (Associate Professor, OCARINA)
- Dr. Keisuke KAWAKAMI (Specially Appointed Associate Professor, OCARINA)
- Dr. Shusaku IKEYAMA (Specially Appointed Research Associate, OCARINA)
- Dr. Muneaki YAMAMOTO (Specially Appointed Research, OCARINA)
- Dr. Yoshihiro YAMAGUCHI (Tenure-track Specially Appointed Associate Professor, OCARINA)

Invited speakers

- Dr. Alain BOUSSAC (Senior Researcher, Centre national de la recherche scientifique, France)
- Dr. Jian-Ren SHEN (Professor, Research Institute for Interdisciplinary Science, Okayama Univ., Japan)
- Dr. Jian-Ping ZHANG (Professor, Renmin University of China, China)
- Dr. Miwa SUGIURA (Associate Professor, Proteo-Science Center, Ehime Univ., Japan)
- Dr. Takumi NOGUCHI (Professor, Grad. Sch. of Science, Dept. of Material Science, Nagoya Univ., Japan)
- Dr. Yutaka BANNO (Professor, Faculty of Agriculture, Kyushu Univ., Japan)
- Dr. Leny YULIATI (Principal Investigator, Ma Chung Research Center for Photosynthetic Pigments (MRCPP), Indonesia)
- Dr. Hsyueh-Liang WU (Professor, Dept. of Chemistry, National Taiwan Normal Univ., Taiwan)
- Mr. Syunichi NAKAMURA (Deputy Manager for Energy Policy, Environmental Policy Division, Environment Bureau, Osaka City Government, Japan)

Speakers in OCARINA project team

- Dr. Makoto MIYATA (Professor, Department of Biology and Geosciences (Functional Biosciences), Grad. Sch. of Science, OCU)
- Dr. Akihisa TERAKITA (Professor, Department of Biology and Geosciences (Science of Biomolecules), Grad. Sch. of Science, OCU)
- Dr. Nobuo KAMIYA (Vice Director, OCARINA/Professor, OCARINA)
- Dr. Taro NAKAMURA（Professor, Dept. of Biology and Geosciences (Functional Biosciences), Grad. Sch. of Science,OCU）
- Dr. Yasuyuki TSUBOI (Dept. of Molecular Materials Science, Grad. Sch. of Science, OCU)
- Dr. Seiya KOBATAKE (Dept. of Applied Chemistry and Bioengineering, Grad. Sch. of Engineering, OCU)
- Dr. Soichi SAEKI (Associate Professor, Dept. of Mechanical and Physical Engineering (Mechanical Engineering), Grad. Sch. of Engineering, OCU)
- Dr. Yasuhisa NAKASO (Special Researcher, OCARINA, OCU)

日　時

2019年3月5日（火）(受付9:00)　9:30－18:10

2019年3月6日（水）(受付9:00)　9:30－16:50

＊3月5日(火) 会議終了後18:10より、会場にて集合写真を撮りますのでご参集ください。

会　場

大阪市立大学（杉本キャンパス）学術情報総合センター 10階 大会議室 研究者交流室

大阪市住吉区杉本3丁目3番138号 Tel:06-6344-9560

懇親会

2019年3月5日（火）18:20～

学術情報総合センター 10階　研究者交流室

主　催

大阪市立大学複合先端研究機構

組織委員

●宮野道雄（大阪市立大学・学長補佐／複合先端研究機構・機構長／生活科学研究科・特任教授）

●神谷 信夫（大阪市立大学・複合先端研究機構・副機構長／複合先端研究機構・教授）

●重川 直輝（大阪市立大学・複合先端研究機構・副機構長／工学研究科電子情報系専攻・教授）

●天尾　豊（大阪市立大学・人工光合成研究センター・所長／複合先端研究機構・教授）

●吉田 朋子（大阪市立大学・人工光合成研究センター・副所長／複合先端研究機構・教授）

●藤井 律子（大阪市立大学・人工光合成研究センター・分析装置運営部会長／複合先端研究機構・准教授）

●川上 恵典（大阪市立大学・複合先端研究機構・特任准教授）

●池山 秀作（大阪市立大学・複合先端研究機構・特任助教）

●山本 宗昭（大阪市立大学・複合先端研究機構・特任助教）

●山口 良弘（大阪市立大学・複合先端研究機構・テニュアトラック特任准教授）

招待講演者

●Dr. アラン ブサック（原子力開発研究所、フランス）

●Dr. 沈 建仁（岡山大学 異分野基礎科学研究所・教授、日本）

●Dr. 張 健平（中国人民大学・教授、中国）

●Dr. 杉浦 美羽（愛媛大学 プロテオサイエンスセンター・准教授）

●Dr. 野口 巧（名古屋大学 大学院理学系研究科・教授）

●Dr. 伴野 豊（九州大学 農学研究院・教授）

●Dr. Leny YULIATI (Principal Investigator, Ma Chung Research Center for Photosynthetic Pigments (MRCPP))

●Dr. Hsyueh-Liang WU (Professor, Department of Chemistry National Taiwan Normal Univ.)

●Mr. 中村 俊一 (大阪市環境局環境施策部環境施策課・エネルギー政策担当課長代理)

プロジェクトチーム講演者

●宮田 真人（大阪市立大学・理学研究科生物地球系専攻・教授）

●寺北 明久（大阪市立大学・理学研究科生物地球系専攻・教授）

●神谷 信夫（大阪市立大学・複合先端研究機構・教授）

●中村 太郎（大阪市立大学・理学研究科生物地球系専攻・教授）

●坪井 泰之（大阪市立大学・理学研究科物質分子系専攻・教授）

●小畠 誠也（大阪市立大学・工学研究科化学生物系専攻・教授）

●佐伯 壮一（大阪市立大学・工学研究科機械物理系専攻・准教授）

●中曽 康壽（大阪市立大学・複合先端研究機構・特別研究員）

Programme of 10th OCARINA International Symposium

Venue: Media Center, Osaka City University, 3-3-138 Sugimoto, Sumiyoshi-ku, Osaka 558-8585, Japan
All the Presentations & Symposium Photo: at Conference Room L (10F)
Banquet & Poster Awarding Ceremony: at Meeting Room for Researching Staff (10F)

5th March (Tue.), 2019 9:20-18:10

09:00-09:20	Registration
09:20-09:30	Opening 櫻木 弘之 （大阪市立大学・理事兼副学長） Hiroyuki SAKURAGI (Vice President of OCU)
09:30-10:00 O1	Session 1: 先端バイオ (Frontier Biology) 宮田 真人（理学研究科生物地球系専攻・教授）[英語講演] Makoto MIYATA (Department of Biology and Geosciences, Graduate School of Science, OCU) [English lecture] Amazing molecular motors in *Mollicutes* !!!
10:00-10:30 O2	寺北 明久（理学研究科生物地球系専攻・教授）[英語講演] Akihisa TERAKITA and Mitsumasa KOYANAGI (Department of Biology and Geosciences, Graduate School of Science, OCU) [English lecture] Animal Opsins: Non-Visual Functions and Optogenetic Applications
10:30-10:40	休憩 (Break)
10:40-12:10	Poster Session [Presentations in English] ポスター発表者によるショートプレゼンテーション[英語講演] Short Presentations [Presentation in English]
12:10-13:10	昼休憩 (Lunch Break)
13:10-13:50	奇数番号のポスター発表 Poster Viewing 1 (odd number)
15:50-14:30	偶数番号のポスター発表 Poster Viewing 2 (even number)
14:30-14:40	休憩 (Break)
14:40-15:30 S1	光合成・人工光合成ミニシンポジウム Mini-Symposium "Progress and Future of Photosynthetic Research" 特別講演 1（座長：川上 恵典 特任准教授） Special Lecture 1 (Chair: Keisuke KAWAKAMI) アラン ブサック（原子力開発研究所、フランス）[英語講演] Alain BOUSSAC (Centre National de la Recherche Scientifique, France) [English lecture] New Insights on the Oxygen Evolution Mechanism and Chl_{D1}Function in Photosystem II

15:30-15:40	休憩 (Break)
15:40-16:00 I1	招待講演 1（座長：川上 恵典 特任准教授） Invited Lecture 1 (Chair: Keisuke KAWAKAMI) 杉浦 美羽（愛媛大学 プロテオサイエンスセンター・准教授）[英語講演] Miwa SUGIURA (Proteo-Science Center, Ehime Univ.) [English lecture] New Insights on Chl_{D1} Function in Photosystem II from Site-Directed Mutants 光化学系 II における Ch_{D1} の機能
16:00-16:20 I2	招待講演 2（座長：川上 恵典 特任准教授） Invited Lecture 2 (Chair: Keisuke KAWAKAMI) 野口 巧（名古屋大学 大学院理学系研究科・教授）[英語講演] Takumi NOGUCHI (Graduate School of Science Division of Material Science, Nagoya Univ.) [English lecture] Infrared Analyses of Photoreactions in Photosystem II 光化学系Ⅱにおける光反応の赤外分光解析
16:20-16:30	休憩 (Break)
16:30-16:50 I3	招待講演 3（座長：藤井 律子 准教授） Invited Lecture 3 (Chair: Ritsuko FUJII) 張 健平（中国人民大学、中国）[英語講演] Jian-Ping ZHANG (Renmin University of China, China) [English lecture] Light Conversion in Bacterial Photosynthesis
16:50-17:10 I4	招待講演 4（座長：川上 恵典 特任准教授） Invited Lecture 4 (Chair: Keisuke KAWAKAMI) 沈 建仁（岡山大学 異分野基礎科学研究所 、日本）[英語講演] Jian-Ren SHEN (Research Institute for Interdisciplinary Science, Okayama Univ., Japan) [English lecture] Mechanism of Water-Splitting Catalyzed by the Mn_4CaO_5-Cluster of Photosystem II 光化学系 II Mn_4CaO_5 クラスターによる水分解の反応機構
17:10-17:20	休憩 (Break)
17:20-18:10 S2	特別講演 2（座長：川上 恵典 特任准教授） Special Lecture 2 (Chair: Keisuke KAWAKAMI) 神谷 信夫（複合先端研究機構・副機構長・教授）[英語講演] Nobuo KAMIYA (Vice Director, OCARINA) [English lecture] Structure of the Oxygen-Evolving Complex and Valences of the Manganese Atoms in Photosystem II Functioning in Photosynthesis 光合成で機能する光化学系 II・酸素発生クラスターの構造と Mn 原子の価数
18:10-18:20	記念撮影 **Symposium Photo** at Conference Room L (**10th Floor**), Media Center, OCU
18:20-20:30	ポスター賞授賞式・懇親会 **Banquet & Poster Awarding Ceremony**

6th March (Wed.), 2019,　9:30-16:50

09:00-09:30	Registration
09:30-09:50 O3	Session 2: バイオリソース (Bio-Resource) 中村　太郎（理学研究科生物地球系専攻・教授）[日本語講演] Taro NAKAMURA (Department of B o ogy and Geosc ences, Graduate Schoo of Sc ence, OCU) [Japanese ecture] ナショナルバイオリソースプロジェクト酵母 Nat ona B o Resource Project-Yeast
09:50-10:30 I5	招待講演 5（座長：中村 太郎 教授） Inv ted Lecture 5 (Cha r: Taro NAKAMURA) 伴野　豊（九州大学 農学研究院・教授）[日本語講演] Yutaka BANNO (Facu ty of Agr cu ture, Kyushu Un v.) [Japanese ecture] カイコバイオリソースとサイエンスの繋がり Contr but on to Sc ence us ng a S kworm B o-Resources
10:30-10:40	休憩 (Break)
10:40-11:10 O4	Session 3: ナノマテリアル光制御 (Optical Control of Nano-Material) 坪井 泰之（大阪市立大学・理学研究科物質分子系専攻・教授）[日本語講演] Yasuyuk TSUBOI (Department of Mo ecu ar Mater a s Sc ence, Graduate Schoo of Sc ence, OCU) [Japanese ecture] ナノ物質マニピュレーションを目指す新型光ピンセットの開発
11:10-11:40 O5	Session 4: 先端マテリアル (Frontier Materials) 小畠 誠也（工学研究科化学生物系専攻・教授）[日本語講演] Se ya KOBATAKE (Department of App ed Chem stry and B oeng neer ng, Graduate Schoo of Eng neer ng, OCU) [Japanese ecture] フォトクロミック分子結晶のフォトメカニカル挙動 Photomechan ca Behav or of Photochrom c Mo ecu ar Crysta s
11:40-11:50	休憩 (Break)
11:50-12:50 O6	Session 5: バイオメディカル先端医療工学 (Frontier Bio-Medical Engineering) 佐伯 壮一（工学研究科機械物理系専攻・准教授）[日本語講演] Sou ch SAEKI (Department of Mechan ca and Phys ca Eng neer ng, Graduate Schoo of Eng neer ng, OCU) [Japanese ecture] 多機能 OCT を応用した再生医療等製品の品質向上と支援機器の開発 Deve opment of Support Instrumentat on n Regenerat ve Med c ne app y ng Mu t -funct ona OCT
12:50-13:50	昼休憩 (Lunch Break)

13:50-14:20 O7	Session 4: 都市エネルギー・防災 (Urban energy) 中曽 康壽（大阪市立大学・複合先端研究機構・特別研究員）[日本語講演] Yasuh sa NAKASO (OCARINA, OCU) [Japanese ecture] 日本の沿岸都市域に適用する帯水層蓄熱システムの研究開発成果 R&D Resu ts of Aqu fer Therma Storage System App ed to Urban Coasta Areas n Japan
14:20-14:50 O8	中村 俊一 (大阪市環境局 環境施策部環境施策課・エネルギー政策担当課長代理）[日本語講演] Syun ch NAKAMURA (Env ronment Bureau, Osaka C ty Government) [Japanese ecture] 大阪市域における帯水層蓄熱利用の普及促進について Promot on of Aqu fer Therma Energy Storage n Osaka Metropo tan Area
14:50-15:00	休憩 (Break)
15:00-15:40 S3	触媒ミニシンポジウム Mini Symposium on Catalysis 後援：平成 30 年度教育推進本部経費事業「研究科横断型大学院教育改革の推進と化学人材育成」 Supported by the 2018 OCU Professional Development Program 特別講演 3（座長：吉田 朋子） Special Lecture 3 (Chair: Tomoko Yoshida) Leny YULIATI (Ma Chung Research Center for Photosynthetic Pigments, INDONESIA) [English lecture] Metal Oxide Photodeposition towards High Activity of Titanium Dioxide Photocatalyst
15:40-15:50	休憩 (Break)
15:50-16:30 S4	特別講演 4（座長：板崎 真澄） Special Lecture 4 (Chair: Masumi Itazaki) Hsyueh-Liang WU (Department of Chemistry National Taiwan Normal University, Taiwan) [English lecture] Enantioselective Rh-Catalyzed Syntheses of Chiral Nitrogen Containing Compounds
16:30-16:40	休憩 (Break)
16:40-16:50	Closing 神谷 信夫（大阪市立大学・複合先端研究機構・副機構長） Nobuo KAMIYA (Vice Director, OCARINA/Professor, OCARINA)

喫煙エリア


Smoking is prohibited in the campus except for designated area !
Faculty of Science
SmokingArea
OCARINA
OCU Madia Center
Venue:
OCU Madia Center (10F)
SmokingArea

Guidelines for Poster Presentations

(1) Preparation for the poster

- The poster board provided is approximately 160 cm height x 110 cm width.
- Please limit the size of your entire poster or poster sections in it. (Recommended poster size is A0.)
- Please place your poster on the poster board numbered for you.
- Push pin will be available at the site.
- Poster viewing will be start from odd number, and then even number (40 min each). During your time, please stay around the poster.
- Display your poster during OCARINA symposium (5 March, 9:00 - the end of the poster session).

(2) Preparation for the short oral presentation

- All the poster presenters can present own short oral presentation.
- One separate file (pdf or power point format) is available to show during your presentation.
- No animation. Submit the file to the conference secretary.
- Gather and make a queue in front of the stage before starting of the short oral presentation. Allocated time is 1 minute including set up time. Please stand up nearby the microphone and be ready before finishing of the previous talk.

ポスター発表について

（１）貼付ポスターについて（英語）

- ポスターサイズ　A0（ボードサイズは W110 x H160 cm 程度)
- 添　　付：自分のポスター番号（要旨集／ HP）の場所に貼付してください。
- 会　　場：学術情報センター 10F　大会議室
- 貼付期間：3 月 5 日（火）9 時 ～ ポスターセッション終了まで
- ポスター賞の審査を希望する方は、必ず最後まで貼付してください。
- ポスターの撤去は、ご自身でお願いします。放置されたポスターについてはこちらで処分いたします。
- ポスター発表：前半／奇数番号　後半／偶数番号
  ➢ 自分の発表の時間帯は、自身のポスターのそばにいてください。

（２）ポスターショートプレゼンテーションについて（英語、持ち時間 1 分（厳守））

ショートプレゼンテーションの開始時刻には、檀上付近に集まり発表順に並んでください。

- ポスター賞審査方法　　招待講演者及び学内複合先端研究機構プロジェクトメンバー有志の審査員による審査。異分野の研究者に自身の研究を的確に伝えているかどうか。
  （研究の背景・目的・意義・狙いを理解してもらい、討論をする。）
- ポスター賞授与式3 月 5 日（火）18 時 20 分開始の懇親会場にて行います。皆様どうぞご参加ください。

Oral Presentations

March 5th (Tue), 2019

Amazing molecular motors in *Mollicutes* !!!

Makoto Miyata
1) The OCU Advanced Research Institute for Natural Science and Technology
2) Graduate School of Science, Osaka City University

There are numerous species of lifes on the earth. However, if we focus on the structure of force generating molecules, the motility discovered so far can be classified into just 18 types. Interestingly, three of them are found in a small group of bacteria called the class *Mollicutes*. The class *Mollicutes* is thought to have been established after unique evolution through parasitic on higher animals and plants in a short time from Gram positive bacteria, represented by *Bacillus subtilis var. natto*. Recently, we succeeded in clarifiying the core part of the motilities, through a process including (i) analyzing the movement of cells and molecules in detail, (ii) identifying protein molecules involved, (iii) clarifying the structure of motility machinery. Then, we saw unimaginable secrets!

Spiroplasma eriocheiris (right figure) has a regular helicity in the cell and pushes water backward by reversing the handedness from front to back, and swims forward. We isolated the ribbon structure responsible for helix formation and its component "Fibril protein", and clarified their structures at nanometer level. We found that the reversal of cell helicity is caused by the structural switch in Fibril protein, and its structure depends on MreB, which is an actin homolog dictating the shape of cells in other bacteria, and the intracellular energy state.

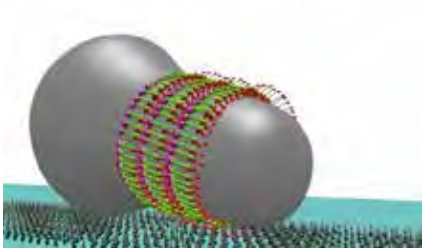

Mycoplasma mobile (right figure) forms an organelle on a cell pole, binds to the host surface and shows gliding motility. Previously, we revealed that a complex including legs composed of four huge proteins works on the surface of cell membrane, and motors hydrolyze ATP on the inside of cell membrane. We isolated the motor and clarified its structure to the atomic resolution by using electron cryomicroscopy. A “Monster" appeared as the combination of phosphoglycerate kinase and ATP synthase which are responsible for ATP synthesis in many organisms, associated with several novel proteins.

References

[1] Miyata, M.; Hamaguchi, T. *Frontiers in Microbiology* **2016,** 7, 960.
[2] Miyata, M.; Hamaguchi, T. *Current Opinion in Microbiology* **2016**, 29,15-219.

Animal opsins: non-visual functions and optogenetic applications

Akihisa Terakita and Mitsumasa Koyanagi

Department of Biology and Geoscience, Graduate School of Science, Osaka City University, Osaka, Japan; OCARINA, Osaka City University, Osaka, Japan

Most animal opsins bind to a retinal as a chromophore to form photosensitive pigments and serve as light-sensitive G protein-coupled receptors (GPCRs), which constitute a large protein family of receptors that sense molecules outside the cell and activate inside signal transduction pathways and, ultimately, generate cellular responses.

Many animals capture light through opsin-based pigments and utilize the light information for visual and non-visual functions including regulation of circadian rhythms. Thousands of opsins have been identified from a wide variety of animas thus far. We have characterized diverse opsins, including novel ones, spectroscopically, biochemically, molecular physiologically and evolutionally [1-4], and also investigated their contribution to biological function [5, 6]. Interestingly, we found that some non-visual opsins have unique molecular properties and such unique peroperties might be suitable for optogenetics applications, which are the combination of genetics and optics to control well-defined events within specific cells of living tissues.

O-2

In lower vertebrates, pineal and its related organs in the brain discriminate UV and visible light. A pineal UV-sensitive opsin, parapinopsin has been considered to be involved in this color discrimination [1, 3]. We recently found that a signle photoreceptor cell containing parapinopsin alone generates color opponency, which is essential cellular photoresponse to detect different wavelenght of lights [6]. Because it has been discussed that maltiple opsins are requiered for color opponency, this finding could propse a new concept for the mechanism of color detection and its evolution. We also found that UV and green light illuminations activate and deactivate parapinopsin, respectively to regulate G protein-mediated signal transduction cascade in the mammalian cultured cells [7]. Therefore we suggest that parapinopsin has optogenetic potentials to control cellular responses and animal behaviours in a light wavelength-dependent manner.

References:

[1] Koyanagi, Kawano et al., *Proc. Natl. Acad. Sci. U.S.A* **2004**, 101, 6687 [2] Koyanagi et al., *Proc. Natl. Acad. Sci. U.S.A* **2013**, 110, 4998 [3] Koyanagi, Wada et al., *BMC Biology* **2015**, 17, 73 [4] Gerrard et al., *Proc. Natl. Acad. Sci. U.S.A* **2018**, 115, 6201-6206
[5] Nagata et al., *Science* **2012**, 355, 469 [6] Wada et al., *Proc. Natl. Acad. Sci. U.S.A* **2018**, 110, 4998 [7] Kawano-Yamashita et al., *PLoS One* **2015**, 10, e0141280

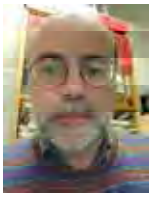

New insights on the Photosystem II O_2 evolution mechanism: The S_2 to S_3 transition.

Alain Boussac[1], A. William Rutherford[2], Miwa Sugiura[3]

[1]I²BC, UMR CNRS 9198, CEA Saclay, 91191 Gif-sur -Yvette, France. [2]Department of Life Sciences, Imperial College, London SW7 2AZ, United Kingdom. [3]Proteo-Science Research Center, Ehime University, Bunkyo-cho, Matsuyama, Ehime 790-8577, Japan.

Abstract:

Oxygenic photosynthesis provides the main input of energy into biology. This process produces food, fibers and fossil fuels, and energizes the atmosphere with O_2. Photosystem II (PSII) is the unique water-oxidizing enzyme of the cyanobacteria, algae and higher plants that is at the heart of oxygenic photosynthesis. The active site of PSII, a Mn_4CaO_5-cluster, advances through five sequential oxidation states (S_0 to S_4) before water is oxidized and O_2 is generated. Both the S_2-state and S_3-state exhibit different EPR properties showing there are several structural conformations for both of them. The S_2-state can be present in either a low spin (S=1/2) or a high spin (S=5/2) configuration. The S_3-state has at least two configurations. one exhibiting an EPR signal from a spin S=3 state and one that is EPR silent but detectable upon near-infrared illumination at 4.2 K by inducing a so-called “split signal”. The S_2 to S_3 transition is a complex state because several events occurs as the preloading of water, the binding of water to the cluster, deprotonation steps and possible structural changes in the cluster. In the present work, the transition between the S_2 and S_3 state has been studied by using EPR spectroscopy, quantum chemical calculations using Density Functional Theory (DFT), and time-resolved UV-visible absorption spectroscopy.

The EPR experiments show that the equilibrium between S_2^{LS} and S_2^{HS} is pH dependent [1], with a pK_a ≈ 8.3 (n ≈ 4) for the native Mn_4CaO_5 and pK_a ≈ 7.5 (n ≈ 1) for Mn_4SrO_5. The DFT results suggest that exchanging Ca with Sr modifies the electronic structure of several titratable groups within the active site, including groups that are *not* direct ligands to Ca/Sr, *e.g.*, W1/W2, Asp61, His332 and His337. This is consistent with the complex modification of the pK_a upon the Ca/Sr exchange. By studying a Val185Thr mutant [2] it is shown that Val185 contributes to the stabilization of the S_2 into the low spin configuration. Indeed, in the V185T mutant a high proportion of S_2 exhibits a high spin, S = 5/2, configuration. By using bromocresol purple as a dye, a proton release was detected in the $S_1Tyr_Z^{\bullet} \rightarrow S_2^{HS}Tyr_Z$ transition in the V185T mutant in contrast to the WT*3-PSII in which there is no proton release in this transition. Instead, in WT*3-PSII, a proton release kinetically much faster than the $S_2^{LS}Tyr_Z^{\bullet} \rightarrow S_3Tyr_Z$ transition was observed, and we propose that it occurs in the $S_2^{LS}Tyr_Z^{\bullet} \rightarrow S_2^{HS}Tyr_Z^{\bullet}$ intermediate step before the $S_2^{HS}Tyr_Z^{\bullet} \rightarrow S_3Tyr_Z$ transition occurs.

S-1

By studying the temperature dependence of the S_2^{HS} to S_3 transition [3] it is found that *i*) upon illumination at 77 K, the S_2^{HS} state is able to progress to the S_3 state ($S_3^{S=3}$) state in a proportion of centers and *ii*) in another proportion of centers, illumination at low temperature advances the S_2^{HS} state to form the S_3 state that lacks the $S_3^{S=3}$ EPR signal (S_3^{inv}), and this still occurs down to 4.2 K.

On the basis of the model proposed (in blue) and drawn by Pantazis [4] and from the present data, the following suggestions are made (in red) for the S_2 to S_3 transition.

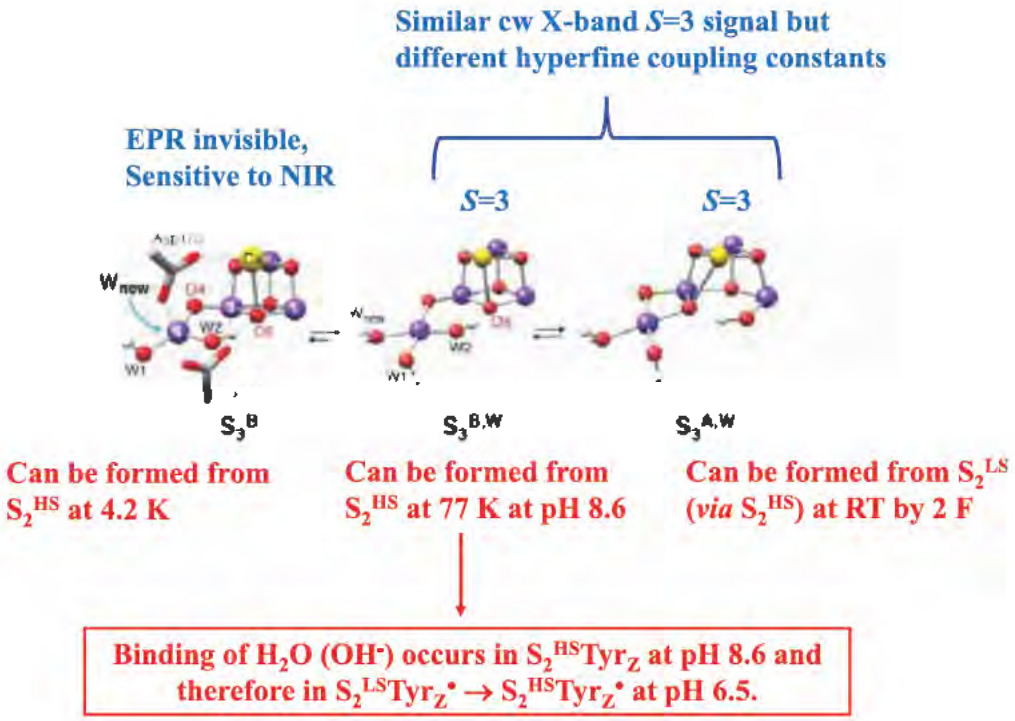

In conclusion we suggest from the present study that both the proton release and the water binding occur in the $S_2^{LS}Tyr_Z^{\bullet} \rightarrow S_2^{HS}Tyr_Z^{\bullet}$ step. It would remain to establish by Pulsed ENDOR measurements if the S_3 state induced at low temperature exhibits or not the same hyperfine coupling constants than the S_3 state induced at room temperature (see [4] for a discussion on this point).

References:

[1] Boussac, A., Ugur, I., Marion, A., Sugiura, M., Kaila, V.R.I., Rutherford, A.W. *Biochim. Biophys. Acta-Bioenerg.* **2018**, 1859, 342.

[2] Sugiura, M., Tibiletti, T., Takachi, I., Hara, Y., Kanawaku, S., Sellés, J., Boussac, A. *Biochim. Biophys. Acta-Bioenerg.* **2018**, 1859, 1259.

[3] Boussac, A. Manuscript in preparation

[4] Pantazis, D. A. *ACS Catal.* **2018**, 8, 9477.

New insights on Chl_{D1} function in Photosystem II from site-directed mutants

Miwa Sugiura

Proteo-Science Research Center, Ehime University, Bunkyo-cho, Matsuyama, Ehime 790-8577, Japan.

The monomeric chlorophyll, Chl_{D1}, which is located between the $P_{D1}P_{D2}$ chlorophyll pair and the pheophytin, $Pheo_{D1}$, is the longest wavelength chlorophyll in the heart of Photosystem II and is thought to be the primary electron donor. Its central Mg^{2+} is liganded to a water molecule that is H-bonded to D1/T179 [1]. Here, site-directed mutants on D1/T179H and D1/T179V, were made in the thermophilic cyanobacterium, *Thermosynechococcus elongatus*, and characterized by a range of biophysical techniques [2]. The Mn_4CaO_5 cluster in the water-splitting site is fully active in both mutants. Changes in thermoluminescence indicate that *i*) radiative recombination occurs *via* the repopulation of $*Chl_{D1}$ itself; *ii*) non-radiative charge recombination reactions appeared to be faster in the T179H-PSII; and *iii*) the properties of $P_{D1}P_{D2}$ were unaffected by this mutation, and consequently iv) the immediate precursor state of the radiative excited state is the $Chl_{D1}^{+}Pheo_{D1}^{-}$ radical pair. Chlorophyll bleaching due to high intensity illumination correlated with the amount of $^1O_2$ generated. Comparison of the bleaching spectra with the electrochromic shifts attributed to Chl_{D1} upon Q_A^- formation, indicates that in the T179H-PSII and in the WT*3-PSII, the Chl_{D1} itself is the chlorophyll that is first damaged by $^1O_2$, whereas in the T179V-PSII a more red chlorophyll is damaged, the identity of which is discussed. Thus, Chl_{D1} appears to be one of the primary damage site in recombination-mediated photoinhibition. Finally, changes in the absorption of Chl_{D1} very likely contribute to the well-known electrochromic shifts observed at ~430 nm during the S-state cycle.

References:

[1] Umena, Y.; Kawakami, K.; Shen, J.–R.; Kamiya, N. *Nature* **2011**, 473 55.

[2] Takegawa, Y.; Nakamura, M.; Nakamura, S.; Noguchi, T.; Sellés, J.; Rutherford, A.W.; Boussac, A.; Sugiura, M. *Biochem. Biophys. Acta* **2019**, 1860 297.

Infrared analyses of photoreactions in photosystem II

Takumi Noguchi
Graduate School of Science, Nagoya University,
Furo-cho, Chikusa-ku, Nagoya, 464-8602, Japan

Abstract:
Photosystem II (PSII) is an enzyme that has a function of water oxidation and quinone reduction utilizing light energy. It provides electrons necessary for CO_2 fixation, and molecular oxygen that is the source of oxygen in the atmosphere. The structure and the reactions of PSII have long been studied using various spectroscopic methods such as fluorescence, electron spin resonance, X-ray absorption, and Fourier transform infrared (FTIR) absorption measurements. In 2011, Kamiya, Shen, and coworkers resolved the X-ray crystallographic structure of the PSII core complexes from a thermophilic cyanobacterium at a high resolution of 1.9 Å [1]. In this structure, oxygen atoms in the water-oxidizing Mn cluster and water molecules were first resolved and the overall structure of the catalytic center of water oxidation was revealed. After the report of this structure, PSII researches, especially on the water oxidation mechanism, entered a new era. Quantum chemical calculations using the density fictional theory (DFT) and quantum mechanics/molecular mechanics (QM/MM) methods based on the atomic coordinates of the X-ray structure became available, and detailed analyses of spectroscopic data have been performed to provide accurate information on the structure and reactions in PSII. Here, I will introduce our results of FTIR studies on PSII in combination of QM/MM calculations based on high-resolution X-ray crystallographic structure. FTIR analysis of vibrations of water molecules around the Mn cluster provided crucial information of the proton transfer mechanism during water oxidation [2]. In addition, vibrations of carboxylate groups and histidine residues interacting with the Mn cluster revealed the role of amino acid residues in the water oxidation mechanism [3, 4]. Furthermore, our FTIR study in combination with genetic introduction of a hydrogen bond to P_{D1} and P_{D2} and QM/MM analysis clarified the distribution of a positive charge on a chlorophyll dimer P680 (P_{D1}/P_{D2}) [5].

I-2

References:

[1] Umena, Y.; Kawakami, K.; Shen, J.-R.; Kamiya, N. *Nature* **2011**, *473*, 55-60.
[2] Nakamura, S.; Ota, K.; Shibuya, Y.; Noguchi, T. *Biochemistry* **2016**, *55*, 597-607.
[3] Nakamura, S.; Noguchi, T. *Proc. Natl. Acad. Sci. U. S. A.* **2016**, *113*, 12727-12732.
[4] Nakamura, S.; Noguchi, T. *J. Am. Chem. Soc.* **2017**, *139*, 9364-9375.
[5] Nagao, R.; Yamaguchi, M.; Nakamura, S.; Ueoka-Nakanishi, H.; Noguchi, T. *J. Biol. Chem.* **2017**, *292*, 7474-7486.

Light Conversion in Bacterial Photosynthesis

Jian-Ping Zhang

Department of Chemistry, Renmin University of China, Beijing 100872, P. R. China

Abstract: In bacterial photosynthesis, light harvesting antennae and reaction centers are responsible for harnessing sunlight. The photosynthetic bacterium *Thermochromatium* (*Tch*.) *tepidum* is a thermophile growing at optimal temperature of 48–50 ºC. Its light harvesting antennae exhibit remarkable thermal stability and nearinfrared absorption. It is important to study the primary excitation dynamics of both isolated and membrane-embedded light harvesting complexes of *Tch. tepidum*, so as to understand the mechanisms of light absorption, thermal stability, photoprotection and resistance to environmental stresses.

We have investigated, by the use of triplet excitation profiles (TEPs),[1] the roles of multi-compositional carotenoids (Cars) in the core light harvesting complexes (*m*-LH1-RCs) from a mutant strain of *Rhodobacter* (*Rba*.) *sphaeroides*.[2] Transient absorption kinetics revealed the triplet excitation transfer from spheroidene (Spe, major composition~85%) to spirilloxanthin (Spx, minor composition ~8%), implying that the two different kinds of Cars coexist in individual *m*-LH1-RC complexes. TEP results showed that Spx is involved in photoprotection by quenching ^{3}BChl*, whereas Spe does so merely for BChls of relatively low site energy. The Spe-to-Spx triplet excitation transfer and their inequivalence in quenching ^{3}BChl* constitute a mechanism of cooperative photoprotection.

We have also investigated, by the using femtosecond time-resolved absorption spectroscopy, the uphill excitation energy transfer (EET) from the core antennae (LH1s) to the reaction centers (RCs) by comparing the *m*-LH1-RC to the native LH1-RC of *Tch. tepidum*. The former exhibits a substantially large RC-LH1 energy difference (ΔE = 630 cm^{-1}, ~3k_BT). The semilogarithmic plot of the EET rate is found to be invresely proportional to ΔE, which consolidates a thermal activation mechanism for the uphill EET. The results are discussed on the basis of the newly reported LH1-RC structure of *Tch*. *tepidum*,[3] which allows us to propose the presence of specific doorway BChls in LH1 in promoting the uphill EET.

References:

[1] Yu J., Fu L.-M., Yu L.-J., Shi Y., Wang P., Wang-Otomo Z.-Y., Zhang J.-P. *J. Am. Chem. Soc.* **2017**, 139, 15984.

[2] Nagashima, K. V., Sasaki, M., Hashimoto, K., Takaichi, S., Nagashima, S., Yu, L.-J., Abe, Y., Gotou, K., Kawakami, T., Takenouchi, M. *Proc. Natl. Acad. Sci. U. S. A*. **2017**, 114, 10906.

[3] Niwa, S.; Yu, L.-J.; Takeda, K.; Hirano, Y.; Kawakami, T.; Wang-Otomo, Z.-Y.; Miki, K. *Nature*, **2014**, 508, 228.

Mechanism of water-splitting catalyzed by the Mn_4CaO_5-cluster of photosystem II

Jian-Ren Shen

Research Institute for Interdisciplinary Science, Okayama University, Japan

Light-driven water-splitting catalyzed by photosystem II (PSII) produces molecular oxygen indispensible for aerobic life on the earth. The structure of dimeric PSII from a thermophilic cyanobacterium *Thermosynechococcus vulcanus* has been solved at a resolution of 1.9 Å [1] using synchrotron radiation (SR) X-rays, which revealed a clear picture of a Mn_4CaO_5-cluster, the catalytic center for water-splitting assocaited with the protein matrix of PSII. The Mn_4CaO_5-cluster is organized in a distorted chair form in which, a Mn_3CaO_4 cluster constitutes the main body of the chair with a cubic shape, and the forth Mn ion is attached to the outside of the cubane by two μ-oxo-bridges O4 and O5. Due to high sensitivity of the Mn ions to radiation damage, some of the inter-atomic distances within this cluster were suggested to be slightly longer than those deduced from EXAS spectroscopic measurements as well as QM/MM calculations. In order to avoid possible radiation damages and eliminate the uncertainties in the inter-atomic distances, we used femtosecond X-ray pulses from an X-ray free electron laser (XFEL) facility SACLA, Japan, to solve the structure of PSII. To obtain a high resolution structure, we used large PSII crystals, and adopted a "fixed-target rotational method" to collect the X-ray diffraction data. This approach required a huge number of large, isomorphous PSII crystals, but allowed us to solve the PSII structure at 1.95 Å resolution [2]. This structure confirmed the unique position of O5, and therefore suggested its possible involvement in the O=O bond formation. We further used a pump-probe approach with a combination of small PSII crystals and serial femtosecond crystallography (SFX) by XFEL to solve the structure of the S_3 intermediate-state induced by 2-flash illumination [3]. The results showed an insertion of a new oxygen in the S_3-state, giving rise to a Mn_4CaO_6 cluster. The newly inserted O6 is located close to O5, suggesting a mechanism of O=O bond formation between O5 and O6.

References

1. Umena, Y.; Kawakami, K.; Shen, J.-R.; Kamiya, N. *Nature* **2011,** 473, 55.
2. Suga, M.; Akita, F.; Hirata, K.; Ueno, G.; Murakami, H.; Nakajima, Y.; Shimizu, T.; Yamashita, K.; Yamamoto, M.; Ago, H.; Shen, J.-R. *Nature* **2015,** 517, 99.
3. Suga, M.; Akita, F.; Sugahara, M.; Kubo, M.; Nakajima, Y.; Nakane, T.; Yamashita, K.; Nakabayashi, M.; Umena, Y.; Yamane, T.; Nakano, T.; Suzuki, M.; Masuda, T.; Inoue, S.; Kimura, T.; Nomura, T.; Yonekura, S.; Yu, L.-J.; Sakamoto, T.; Motomura, T.; Chen, J.-H.; Kato, Y.; Noguchi, T.; Tono, K.; Joti, Y.; Kameshima, T.; Hatsui, T.; Nango, E.; Tanaka, R.; Naitow, H.; Matsuura, Y.; Yamashita, A.; Yamamoto, M.; Nureki, O.; Yabashi, M.; Ishikawa, T.; Iwata, S.; Shen, J.-R. *Nature* **2017,** 543, 131.

Structure of the oxygen-evolving complex and valences of the manganese atoms in Photosystem II functioning in photosynthesis

Nobuo Kamiya, *The OCU Advanced Research Institute for Natural Science and Technology (OCARINA), Osaka City University, Osaka 558-8585, Japan.* E-mail: nkamiya@sci.osaka-cu.ac.jp

Oxygen-evolving complex (OEC) of photosystem II (PSII) extracts electrons from water molecules using solar light energy in photosynthesis. Crystal structureS of PSII and the OEC have been resolved at a high resolution of 1.9 Å [1]. Based on the structural information (PDB-ID: 3WU2), researchers make efforts to elucidate the mechanism of oxygen-evolving reactions in the OEC according to the Kok cycle model. Because the OEC is highly sensitive to X-ray irradiation, X-ray reduction and structure changes induced on the OEC have been discussed on the results mainly from DFT computational calculations. In order to overcome the X-ray reduction problem, we improved the quality of PSII crystals and the procedure of post-crystallization treatments, and succeeded in collecting datasets from highly isomorphous crystals at extremely low X-ray doses. By using 10 and 3 of the isomorphous crystals at pH 6.6, we collected two datasets of diffraction intensities at 0.03 and 0.12 MGy (0.43 MGy for the 3WU2 dataset) and at resolutions of 1.87 and 1.85 Å, respectively [2]. Obtained structures were compared with each other, and a threshold of X-ray dose was found below 0.12 MGy, under which large structural changes were not observed. Furthermore, two alternative OEC structures were found in the two PSII monomers (A, B) in an asymmetric unit of crystal.

According to the same strategies, we collected six datasets from several isomorphous PSII crystals, pH values of which were adjusted at 5.0, 5.7, 6.0, 6.3, 7.0 and 8.0. X-ray doses were at 0.21-0.11 MGy and resolutions, 2.19-1.85 Å. In comparisons of the six structures against the 0.03 MGy structure mentioned above (pH 6.6 and resolution, 1.87 Å), atomic distances in the OEC showed very interesting behaviors depending on the pH values. The five oxo-bridging oxygen atoms (O1-O5) bind four Mn and one Ca atoms in the OEC. The hydrogen-bond distances from O1 to one water molecule (W5) elongated at pH 6.0 from 2.5 Å to 2.8 Å in both of OECs in the A- and B-monomers. The similar behavior was found at the distance from O4 to another water molecule (W6) in the A-monomer, but no change was observed from 2.4 Å in the B-monomer. In the pH range of 5.0-8.0, the distances from O3 to Nε atom of D1-His337 were constant as 2.4 Å and 2.8 Å for the A- and B-monomers, respectively. These are indicating the pH-dependent structural flexibility of the OEC in PSII.

The anomalous dispersion studies have been conducted recently in order to determine valences of the Mn atoms directly in the OEC. These studies showed that the S-states of the Kok cycle were S_1 and S_0 for the A- and B-monomers, respectively. Based on the pH-dependent flexibility and the S-states of the OEC, the oxygen-evolving mechanism of PSII will be discussed in my talk.

[1] Y. Umena, K. Kawakami , J.-R. Shen, N. Kamiya, *Nature* **473** (2011) 55-60.
[2] A.Tanaka, Y. Fukushima, N. Kamiya, *JACS*, **139**, (2017) 1718-1721.

Oral Presentations

March 6th (Wed), 2019

National BioResource Project-Yeast

Taro Nakamura

Graduate School of Science, Advanced Research Institute for Natural Science and Technology, Osaka City University, Sugimoto 3-3-138, Sumiyoshi-ku, Osaka

The National BioResource Project (NBRP) starts in FY 2002 to comprehensively promote life sciences. In the project, the systems of collection, preservation, and deposition have been established for bioresources, such as experimental animals, plants, and microbes (systems, groups, tissues, cells, and genetic materials of animals, plants, and microbes and their information as research and development materials) that are important for the nation to organize strategically.

Yeast is an important eukaryotic model organism. This is especially true of the fission yeast *Schizosaccharomyces pombe* and the budding yeast *Saccharomyces cerevisiae*, which are making significant contributions to research in a variety of areas within the life sciences. NBRP-Yeast has established a framework to collect, stock and distribute strain and DNA resources of mainly the two species. Through phases 1 and 4 (FY 2002 - 2018) of the NBRP, the NBRP-Yeast has become one of the top international yeast resource centers. Here, I will introduce the recent activity of NBRP-Yeast.

Contribution to Science using the Silkworm Bio-Resources

Yutaka Banno

Institute of Genetic Resources, Graduate School of Bioresources and Bioenvironmental Kyushu University

Motooka 744, Nishi-ku, Fukuoka 819-0395, Japan

The economic importance of silk has prompted exhaustive research on the Silkworm, *Bombyx mori*. There are also many kinds of silkworm strains, collected from world. The Japanese breeders and scientists have developed advanced strains for sericulture and academic resources. These strains are core resources in National-Bio-Resource Project (NBRP) started in 2002 with support by the Japanese government. Now, 29 species including silkworm are open for worldwide use. Purpose of NBRP is Collection, Preservation and Distribution of bio-resources that are basic materials for life science researches. Following resources are available by contact to NBRP silkworm (http://silkworm.nbrp.jp/). 1. Domesticated silkworm (*Bombyx mori*): mutant strains, consomic strains and transgenic strains. 2. Wild silkworm: 8 species within 6 genus (*Bombyx*, *Antheraea, Samia, Rhodinia, Actias, and Trilocha*). 3. Genome: cDNA clone of *B. mori* and *S. cynthia ricini*, Fosmid clone of *B. mandarina*, Assembled RNA-seq data of *B. mori*, *S. cynthia ricini*, and *Trilocha varians*. Before starting this project, available season of resources supply of silkworm strains was limited in spring. However it is available to access to resources during all seasons with progress of NBRP. Development of genome editing technology in *Bombyx mori* has resulted in the rapid increase in number of strains. It is an urgent issue to establish effective systems for the preservation of increasing strains. Because diapause egg of *Bombyx mori* cannot be preserved more than one year. and all strains should be reared once a year. There are two kinds of long time preservation methods in *B. mori*. One uses frozen sperm and the other uses frozen ovaries. The former are artificially inseminated to female moths and the latter are implanted to castrated female larvae. In 2013, we have started to provide transgenic strains which were restored by using frozen ovaries. Practical applications of cryopreservation help us to reduce the labor of rearing silkworm and the risks of losing particular strains through unexpected accident such as disease or contamination.

Optical Tweezers for Manipulation of Nanomaterials

TSUBOI, Yasuyuki
Centered Graduate School of Science, Osaka City University, 3-3-138 Sugimoto, Sumiyoshi, Osaka, 558-8585, Japan

Light can exert a mechanical force on a small object. It is called optical force or radiation pressure, by which light can trap and manipulate a small object. The optical manipulation science falls in 3 categories in accordance of the size of object. In the regime of smallest size, it is known as the laser cooling for trapping atoms, for which the Novel prize in Physics 1997 was given. In a regime of a larger size where light wavelength is sufficiently larger than the object, nowadays optical tweezers are commercially available and widely used to manipulate living cells in medical science.

On the other hand, an optical manipulation study in an intermediate regime of nanomaterials has hitherto been limited. Optical manipulation of nanomaterials such as DNA, proteins, artificial polymers, molecular clusters, quantum dots and so on would be fruitful and intriguing, because various chemical processes involving phase transition, ordering, crystallization, molecular aggregation, patterning, chemical reactions, etc. should be induced and controlled due to intermolecular interactions in the manipulation processes. Under such situation, we expect the birth and growth of "the optical manipulation chemistry".

However, it is rather difficult to stably trap nanomaterials since trapping potential energy ($U = (1/2)\ \alpha E^2$) should be much smaller than the thermal energy ($|U| << kT$). For stable and efficient optical manipulation of nanomaterials, we have proposed and developed novel techniques for optical manipulation, whose details are described in the following.

O-4

1) **Resonant optical manipulation** Using a traditional optical tweezes with a focused laser beam, we succeeded in optical trapping of a small protein (egg white lysozyme) and amino acid lusters in aqueous solution[1]. However, trapping efficiency was low. Long time and intense laser light was necessary to detect a sign of trapping of these molecules. For enhancing the trapping force $\boldsymbol{F}$, we proposed a method of resonant trapping whose concept is like this. When trapping laser light resonantly excites a targeted particle, F should be much enhanced due to an increase in α (or in other words, light-matter interactions should be enhanced). As a trapping target, we single out a heme protein, myoglobin. The trapping behavior was analyzed using a confocal Raman microscope. Only under a resonant condition where laser light electronically excite the cofactor heme, myoglobin molecules were obviously trapped at a focal point with great efficiency[2]. Such behavior was well consistent with a theoretical model proposed by prof. Hajime Ishihara. These are direct evidence of the resonant optical manipulation.

2) Plasmonic Optical Manipulation Plasmonic enhanced electromagnetic field is applicable not only to SERS but also to chemical reaction promotion[3], and also even to optical trapping[4]. Plasmon-based

optical trapping is quite intriguing and is currently attracting much attention in nano-photonics and related research fields, since optical trapping based on surface plasmon can potentially overcome several disadvantages of conventional optical trapping technique using a focused laser beam. For example, small palm-top lasers with low light intensity are applicable to plasmonic optical tweezers for trapping of nanomaterials.

So far, we have succeeded in efficient plasmonic trapping of quantum dots[5], polymer beads[6], artificial chain polymers[7] and revealed trapping behaviors using microspectroscopies. Moreover, we developed a femtosecond plasmonic optical tweezer. This enables us switchable trapping for DNA in a persistent fixation mode or a trap-and-release mode[8].

3) NASSCA Optical Manipulation According to these previous studies on plasmonic optical manipulation, it has several practical issues that need to be overcome. In many cases, it has suffered from thermal effects (Marangoni convection and thermophoresis) that frequently hindered stable trapping of nanomaterials[9].

Here, we proposed an alternative approach using a nano-structured material that can enhance the optical force and be applied to optical tweezer[10]. The material is metal-free black silicon (MFBS), the plasma etched nano-textured Si. We demonstrate that MFBS-based optical tweezers can efficiently manipulate small particles with characteristic features. The MFBS-based optical tweezers can overcome disadvantages of plasmonic optical tweezers, because of no detrimental thermal forces, and so on. We call this technique NASSCA optical tweezers (Nano-Structured SemiConductor Assisted optical tweezers). The concept of NASSCA optical tweezer is illustrated in the figure shown below.

O-4

Thus we have proposed novel concepts to enhance optical forces for manipulation of various molecular nanomaterials. These 3 optical manipulation techniques will open a new channel to the optical manipulation chemistry.

I would like to express my sincere thanks to all our collaborators, supervisors, and all the members of my lab.

References (published by us)

[1] *J. Phys. Chem. C* **2010**, 114, 5589. [2] *J. Phys. Chem. C* **2013**, 117, 10691.
[3] *J. Am. Chem. Soc.* **2013**, 135, 6643. [4] *J. Phys. Chem. Lett.* **2014**, 5, 2957.
[5] *J. Phys. Chem. Lett.* **2010**, 1, 2327. [6] *J. Phys. Chem. C* **2013**, 117, 2500.
[7] *J. Phys. Chem. C* **2012**, 116, 14610. [8] *J. Am. Chem. Soc.* **2013**, 135, 6643.
[9] *Nature Nanotechnology* **2016**, 11, 5. [10] *Scientific Reports* **2017**, 7, 12298. (selected as T0P 100 papers in 2017).

Photomechanical behavior of photochromic molecular crystals

Seiya Kobatake

Graduate School of Engineering, Osaka City University

Photochromic compounds undergo a photochemically reversible transformation reaction between two isomers. Such molecules in organic crystals, which are regularly oriented and fixed in the crystal lattice, may be potentially useful for optoelectronic devices. To apply photochromic diarylethene crystals to photonics, electronics, mechanics, and medical fields, the materials are required to change large physical property by photoirradiation. We have so far reported on photoresponsive crystal shape change of diarylethene crystals [1]. In this paper, we have focused on recent development of novel photomechanical phenomena of crystals.

A crystal of diarylethene **1a** was found to undergo a reversible thermodynamic single-crystal-to-single-crystal phase transition accompanying a change in crystal length, which was clarified by differential scanning calorimetry measurement, X-ray crystallographic analysis, and direct microscopic observation of the crystal length. Furthermore, upon irradiation with UV light, the diarylethene crystal exhibited an unusual photomechanical behavior [2]. The photoinduced reversible crystal twisting of diarylethene **2a** was observed upon alternating irradiation with UV and visible light [3]. The crystal twisting takes place in both a left-handed helix and a right-handed helix. A ribbon-like crystal of diarylethene **3a** exhibited bending, cylindrical helix, and twisting depending on the illumination direction [4]. The control of photomechanical crystal deformation by illumination direction provides a convenient and useful way to generate a variety of photomechanical motions from a single crystal. Moreover, tiny nano-rod crystals with a thickness of a few hundreds nm were fabricated using an anodic aluminum oxide filter as a template, in which diarylethene molecules was crystallized [5,6]. The nano rod also underwent photoinduced bending.

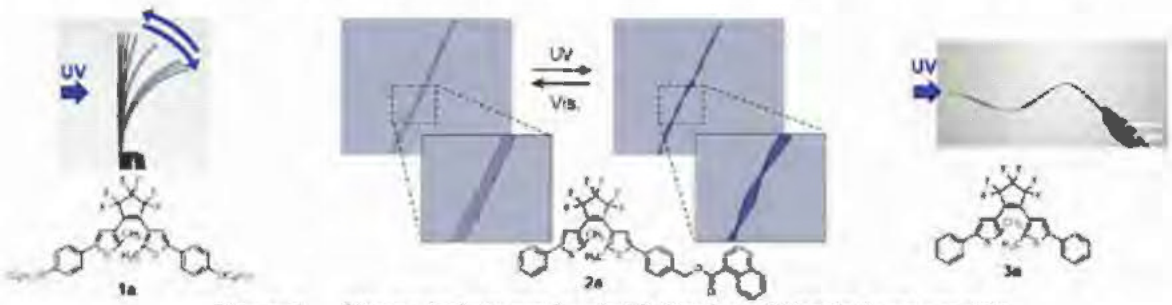

Figure 1. Unusual photomechanical behavior of diarylethene crystals.

References

[1] Kobatake, S.; Takami, S.; Muto, H.; Ishikawa, T.; Irie, M. *Nature* **2007**, *446*, 778.
[2] D. Kitagawa, K. Kawasaki, R. Tanaka, S. Kobatake, *Chem. Mater.* **2017**, *29*, 7524.
[3] D. Kitagawa, H. Nishi, S. Kobatake, *Angew. Chem. Int. Ed.* **2013**, *52*, 9320.
[4] D. Kitagawa, H. Tsujioka, F. Tong, X. Dong, C. J. Bardeen, S. Kobatake, *J. Am. Chem. Soc.* **2018**, *140*, 4208.
[5] F. Tong, D. Kitagawa, X. Dong, S. Kobatake, C. J. Bardeen, *Nanoscale* **2018**, *10*, 3393.
[6] X. Dong, F. Tong, K. M. Hanson, R. O. Al-Kaysi, D. Kitagawa, S. Kobatake, C. J. Bardeen, *Chem. Mater.* **2019**, in press.

Development of Support Instrumentation in Regenerative Medicine applying Multi-functional OCT

Souichi SAEKI[1]

[1] *Graduate School of Engineering, Mechanical & Physical Engineering, Osaka City University. 3-3-138, Sugimoto, Sumiyoshi-ku, Osaka, 558-8585*

Abstract:

In recent years, the regenerative therapy of osteoarthritic cartilage [1] and skin equivalent [2] has attracted attention due to clinical transplantation of 3-dimensional autologous cultured cartilage and skin. However, a non-contact and invasive diagnosing method of bio-mechanical functions, e.g. viscosity and elasticity, has never been established yet. In this study, we have constructed and validated the ultrasonic-assisted Doppler OCT system (UA-OCDV), which can provide viscoelastic and pharmacokinetic characteristics inside tissue tomographically and non-contactly using a high intensity focused ultrasound transducer as a loading devise. The proposed system was applied to 3-dimensional human dermal equivalent, then the tomographic phase map could display the discrimination of tissue viscoelasticity. This phase difference could be caused by the spatio-temporal interaction between elastic shear wave and acoustic streaming, which are generated by acoustic radiation pressure. In conclusions, UA-OCDV has good potential to visualize tissue function tomographically and non-contactly.

O-6

References:

[1] Tohyama, H., et al,.: Atelocollagen-associated autologous chondrocyte implantation for the repair of chondral defects of the knee: a prospective multicenter clinical trial in Japan, J. Orthopaedic Science, (2009), vol.14, pp.579-588.

[2] Saito, N., et al.,: Interstitial fluid flow-induced growth potential and hyaluronan synthesis of fibroblasts in a fibroblast-populated stretched collagen gel culture, Biochimica et Biophysica Acta - General Subjects, 1861, (2017), pp.2261-2273.

Development of Aquifer Thermal Energy Storage System with High Performance Thermal Well and future spread measures

Yasuhisa Nakaso

Research Fellow, 3-9-11,Sugimoto,Sumiyoshi-ku,Osaka City, Japan

Abstract:

Large urban areas in high energy consuming density are required to applicable practical scale renewable energy technologies without damaging urban environment like global warming and heat island problem. From 10 years before, we are trying to develop ground water utilization as 'ubiquitous' heat source.

Now, we can realize direct groundwater heat source utilization under iron and salt ion rich location in the coastal urban area, that leads hard well clogging easily and so on which was difficult to use, and this technical development project is assisted by Japanese Ministry of the Environment and Osaka city government.

We set up the well in the Umekita redevelopment area in the northern part of JR Osaka Station, and we can pump up groundwater total 550,000m^3, get a heat power and immediately recharge the groundwater from another well to original same aquifer.

This is better way that reduce the influence of land subsidence problem in the urban area with keeping groundwater level in local area, and we confirmed it could be operated stably for a long period by using airtight structure.

In this presentation, we show the background and the outline of this technology development and introducing the next project in Maishima as Osaka bay area.

Promotion of aquifer thermal energy storage in Osaka metropolitan area

Shunichi Nakamura

Deputy manager, Osaka City Government, 1-5-1, Abenosuji, Abeno-ku, Osaka, Japan

Abstract:

Aquifer thermal storage (ATES) is a technology that extracts thermal energy from groundwater and efficiently air-condition the building, and is expected as a measure for energy saving, CO_2 emission reduction, and urban heat island. Osaka City, with its abundant groundwater in shallow aquifers, promotes aquifer thermal storage, taking advantage of the feature of the area that large commercial buildings are concentrated.

As a part of its efforts, Osaka City Government, in the commissioned research for the Ministry of the Environment, conducted a research project of ATES in the development district of Umekita, in collaboration with academia, industry and government. As a result, energy saving effect of 35% compared with the conventional air conditioning system has been confirmed without causing impact on the surrounding environment such as ground subsidence.

However, in Osaka, groundwater collection has been strictly restricted due to ground subsidence caused by pumping groundwater excessively in the past, so large-scale ATES cannot be installed. Accordingly Osaka City Government examined the data of the demonstration experiment in Umekita district with academic experts and submitted to the Ministry of the Environment the deregulation measures that allow groundwater collection subject to restoring same amount of groundwater to the same aquifer only for the purpose of heating and cooling the building.

When this deregulation is approved, large-scale aquifer thermal storage will be able to installed in Osaka metropolitan area where urban development will be planned in the near future such as Umekita or Yumeshima, and it is expected to contribute to significant energy saving and CO_2 reduction in Osaka.

Metal Oxide Photodeposition towards High Activity of Titanium Dioxide

Leny Yuliati[1,2]

[1]*Ma Chung Research Center for Photosynthetic Pigments, Universitas Ma Chung, Villa Puncak Tidar N-01, Malang 65151, East Java, Indonesia*

[2]*Department of Chemistry, Faculty of Science and Technology, Universitas Ma Chung, Villa Puncak Tidar N-01, Malang 65151, East Java, Indonesia*

Heterogeneous photocatalysis is one promising approach to solve environmental problems via safe and green technology. Titanium dioxide (TiO_2) has been recognized as a highly active photocatalyst for degradation of organic pollutants. Various approaches have been made to improve the performance of TiO_2 photocatalysts such as by deposition of metal oxide as co-catalyst. One promising method is photodeposition method, which offers mild conditions as the process can be carried out at room temperature, and thus, would not affect the original properties of TiO_2 photocatalyst in terms of crystallinity, particle size, and anatase-rutile ratio. In this talk, the photodeposition of copper [1], lanthanum [2], and iron oxides [3] on the TiO_2 will be discussed at the point of view of properties and photocatalytic activity for degradation of 2,4-dichlorophenoxyacetic acid.

The TiO_2 was modified with copper species by the photodeposition method at room temperature under UV light irradiation [1]. The X-ray absorption near edge structure (XANES) analysis showed that copper species existed as Cu^{2+}. Exploring the photocatalytic activities of copper oxide photodeposited on TiO_2 under UV, visible, and solar light irradiation resulted in different trends. Under UV light irradiation, the photocatalytic activity increased by a maximum factor of 4.3 compared to the unmodified TiO_2 when TiO_2 was loaded with 0.75 mol% CuO. In contrast, under visible light and solar simulator irradiation, the optimum loading of CuO was much lower (0.1 mol%) and enhancements of 22.5 and 2.4 times higher activities were observed, respectively. These results showed that the different masking effects due to the different light sources led to different optimum amounts of CuO, and the added CuO mostly contributed to the visible light activity of TiO_2. Therefore, in addition to the increased charge separation and improved visible light absorption, the masking effect shall also be considered in designing highly active photocatalysts under visible and solar light irradiation. In the proposed mechanism, the Cu^{2+} species was suggested to be the active sites to accept the excited electrons from TiO_2.

Different from copper species, in the case of using lanthanum species photodeposited on TiO_2, the lanthanum species only improved the UV photocatalytic activity of TiO_2 up to 5.5 times higher photocatalytic activity [2]. X-ray photoelectron spectroscopy (XPS) analysis showed

that photodeposition of lanthanum increased the formation of Ti^{3+}, while the electrochemical impedance and photocurrent results showed that the enhanced TiO_2 photocatalytic activity was caused by the increased charge separation in the TiO_2 photocatalyst, owing to the additional formation of Ti^{3+} states. Therefore, the optimum amount of lanthanum species that gave the optimum photocatalytic performance under UV light irradiation could be also related to the optimum amount of Ti^{3-}, which can additionally act as an acceptor for the excited electrons.

As for the iron oxide photodeposited on TiO_2, it was confirmed that the iron species would exist as Fe_2O_3 [3]. The formation of a heterojunction between Fe_2O_3 and TiO_2 nanoparticles was suggested to promote the good charge transfer and suppressed electron-hole recombination. Under UV light irradiation, the photocatalytic activity of TiO_2 could be enhanced up to 3 times higher when 0.5 mol% Fe_2O_3 was photodeposited on the TiO_2. The photocatalyst was shown to have good stability and reusability for the 2,4-D degradation. A further investigation on the role of the active species on Fe_2O_3/TiO_2 confirmed that the crucial active species were both holes and superoxide radicals. All these studies demonstrated that photocatalytic activity of TiO_2 can be enhanced by photodeposition of copper, lanthanum, or iron oxides. While the photodeposited copper oxides contributed to the visible light harvesting of TiO_2, the addition of lanthanum and iron oxides gave higher enhancement on the activity of TiO_2 under UV light irradiation.

S-3

[1] Siah, W. R.; Lintang, H. O.; Shamsuddin, M.; Yoshida, H.; Yuliati, L. *Catal. Sci. Technol.* **2016**, *6*, 5079.
[2] Siah, W. R.; Lintang, H. O.; Yuliati, L. *Catal. Sci. Technol.*, **2017**, *7*, 159.
[3] Lee, S. C.; Lintang, H. O.; Yuliati, L. *Beilstein J. Nanotechnol.* **2017**, *8*, 915.

Enantioselective Rh-Catalyzed Syntheses of Chiral Nitrogen Containing Compounds

Hsyueh-Liang Wu

Department of Chemistry, National Taiwan Normal University

Abstract: An enantioselective Rh(I)-catalyzed conjugate addition reaction of α-substituted β-nitroacrylates with various arylboronic acids using Rh(I)-chiral diene catalysts is described. The addition reaction proceeds under mild conditions in a range of common organic solvents and additives offers the corresponding quaternary carbon-containing α,α-disubstituted β-nitropropionate products in up to 63% yield with up to 99% ee (eq 1).[1] While 2,5-dinaphthyl substituted chiral diene **L1** is proved optimal for the asymmetric arylation of α-substituted β-nitroacrylates, employing Rh/**L1** catalyst in the arylation of β-nitroacrylates sees only moderate selectivity. Enhanced asymmetric induction, in the arylation of β-nitroacrylates, is observed when applying Rh/**L2a** catalyst (eq 2).[2,3]

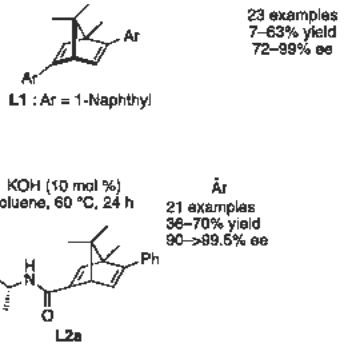

References:

[1] Fang, J.-H.; Jian, J.-H.; Chang, H.-C.; Kuo, T.-S.; Lee, W.-Z.; Wu, P.-Y.; Wu, H.-L. *Chem. Eur. J.* **2017**, *23*, 1830–1838.

[2] Syu, J.-F.; Lin, H.-Y.; Cheng, Y.-Y.; Tsai, Y.-C.; Ting, Y.-C.; Kuo, T.-S.; Janmanchi, D.; Wu, P.-Y.; Henschke, J. P.; Wu, H.-L. *Chem. Eur. J.* **2017**, *23*, 14515–14522.

[3] Jian, J.-H.; Hsu, C.-L.; Syu, J.-F.; Kuo, T.-S.; Wu, P.-Y.; Wu, H.-L. *J. Org. Chem.* **2018**, 83, 12184–12191

Poster Presentations

List of Poster Presentations

P-01 Ikumi Nakamura “Iridium-Catalyzed sp^3 C－H bond Alkylation of Indoline Delivatives with Terminal Alkenes”

P-02 Shunichi Kubota “Acid-Catalyzed Chirality-Transferring Intramolecular Friedel-Crafts Reaction of α-Hydroxy-α-alkenylsilanes”

P-03 Kana Sakamoto “Iridium-Catalyzed Enantioselective Hydroarylation of Chromene Derivatives”

P-04 Risa Yoshimoto “Rhodium(III)-Catalyzed 1,4-Addition of Arylboronic Acids to α,β-Unsaturated Carboxylic Acids”

P-05 Keishi Hirosawa “Iridium-Catalyzed Dehydrogenative Coupling of Aromatic Carboxylic Acids with Internal Alkynes”

P-06 Kohei Yasuda “Catalytic Asymmetric Synthesis of β-OH-DOPA”

P-07 Yuta Omura “Short Step Syntheses and Properties of Nitrogen-Containing Pyrenes”

P-08 Yasunari Kamata “Synthesis and Properties of Unsymmetrical Dinuclear Copper Complex”

P-09 Motoaki Nishimura “Regulation of catilytic acitivity of N-methylpyrolidine by the stumulaus-resposible zinc porphyrin receptor”

P-10 Takayuki Miyamae “Synthesis and Properties of Condensed Phenoxazine Dimer”

P-11 Naoki Yokoyama “Syntheses and Properties of Ortho-bridged Triphenylamines by Two Oxygens and Sulfur or Nitrogen Atoms”

P-12 Gentaro Sakamoto “High Stability of $Ir(OH)_3$ Supported on a Bottom-Up Mesoporous Silica During Photocatalytic Water Oxidation”

P-13 Yuka Kimoto “Synthesis of coordination polymers involving 1,10-phenanthroline-5,6-diolate iron (III) complex as a monomer unit”

P-14 Mayu Maetani “Structure analysis of the solid organic molecule-hydrogen peroxide adducts”

P-15 Mari Yamane “pH-dependent catalytic activity of Prussian blue analogs with CN-deficient sites for hydrolysis of organophosphates”

P-16 Shoma Yorozu “Preparation of Mesoporous Assemblies Composed of Prussian Blue Nanospheres”

P-17 Hiroyuki Oshima “Immobilization of Enzymes in a Bottom-up Mesoporous Silica Nanoparticles Assembly”

P-18 Yusuke Minami “Selective hydrogen production based on the formate decomposition with platinum nano particles dispersed by polyvinylpyrrolidone”

P-19 Kokoro Yoshioka “Photocatalytic CO_2 reduction with water including methanol over Ag loaded Ga_2O_3”

P-20 Masato Akatsuka “The study on photocatalytic CO_2 reduction over Ga_2O_3 photocatalyst with water”

P-21 Akiyo Ozawa “Solvothermal synthesis of black phosphorus nanosheets”

P-22 Ryota Ito “CO_2 reduction with water over various metal oxides supported Ga_2O_3 photocatalysts”

P-23 Kenta Sonoda “Preparation of gallium oxide nanofilm photocatalyst using graphene oxide template”

P-24 Daiki Kitajima “In-situ UV-Vis diffuse reflectance measurements of silver loaded gallium oxide photocatalyst”

P-25 Seiji Wada “Detection of “color changes” with a single kind of opsin in the zebrafish pineal organ”

P-26 Genki Nakata “Behavioral investigation of non-visual photoreception with pineal-specific opsin-knockout zebrafish”

P-27 Tomoka Saito “Evaluation of the pineal wavelength discrimination based on a pineal-specific opsin parapinopsin in the zebrafish behaviours”

P-28 Takashi Nagata “A novel type of opsin with optogenetic potential: Animal opsin-based photopigment as a potential dark-active and light-inactivated G protein-coupled receptor”

P-29 Bokoku Shen “Comparative analyses of light responses between the pineal photoreceptors expressing “bistable” and “bleaching” opsins using transgenic zebrafish”

P-30 Masaki Mizutani “Gliding ghost of Mycoplasma gallisepticum”

P-31 Toshiaki Arata “Structural dynamics of epi-genome related heterochromatin protein HP1 studied by spin labeling ESR spectroscopy”

P-32 Daiki Matsuike “Two different conformations of Gli123 protein, essential for Mycoplasma mobile gliding”

P-33 Takuma Toyonaga “Structure of motor evolved by combination of ATP synthase and phosphoglycerate kinase for Mycoplasma mobile gliding”

P-34 Yuya Sasajima “Internal Ribbon Structure Driving Helicity-Switching Swimming in Spiroplasma”

P-35 Daichi Takahashi “Dynamics and Structure of MreB proteins from Spiroplasma eriocheiris”

P-36 Hana Kiyama “Reproduction of Spiroplasma swimming motility using synthetic bacteria and elucidation of its mechanism”

P-37 Maya Nakatani “Structural and functional analysis of fatty acid kinase of T. thermophilus HB8”

P-38 Yuhei Tahara “Application to microbial surface structure observation of Quick-Freeze and Deep-Etch (QFDE) replica microscopy”

P-39 Nanako Iwamoto “The effect of Ca^{2+} on molecular mass and viscosity of poly-γ-glutamic acid infermentative production”

P-40 Masahiro Oyama “Exploration of novel factors related to gene expression of drug efflux pumps in S. cerevisiae”

P-41 Karina Yoshikawa “Molecular dissection of the transport of the spore surface protein Isp3 in fission yeast”

P-42 Daiki Masuda “Identification and characterization of genes involved in constructing spike structure of fission yeast spore surface”

P-43 Soichiro Seki “Excess accumulation of carotenoids in a siphonous green alga, *Codium fragile* upon different light strengths”

P-44 Shinji Kanda “Fabrication of Diamond/Cu Direct Bonding for Power Device Applications”

P-45 Shotaro Horikawa “Bonding strength evaluation of Al foil/AlN junctions by surface activated bonding”

P-46 Zexin Wan “Analysis of SiC/Si Bonding Interface with Thermal Annealing Treatment by XPS”

P-47 Takuya Higashiguchi “Photoinduced Shape Change of Crystals Composed of a Diarylethene with a Long Alkyl Chain”

P-48 Yuya Seto “Photoluminescence Switching of Quantum Dot Coated with Diarylethenes by Photochromic Reaction”

P-49 Katsuya Shimizu “Bright and Tunable Emission of BODIPY in Solid State”

P-50 Kazuya Tamejima “Simultaneous observation of nanoparticles and hexane droplets in hexane/water emulsion by quick freeze replica electron microscopy”

P-51 Daisuke Furukawa “Study on Micro-Tomographically Functional Imaging of Blood Flow in Vascular Plexuses using Optical Coherence Doppler Velocigraphy”

P-52 Koji Yamane “Development of Micro-tomographic Visualizing System of Mechanical Properties inside Regenerated Tissue using UA-OCDV”

P-53 Miki Yanagisawa “Construction on Medical Diagnosing System by Photo-thermal Doppler OCT (PT-OCDV) using photosensitizer”

Iridium-Catalyzed sp^3 C–H bond Alkylation of Indoline Delivatives with Terminal Alkenes

Ikumi Nakamura,[a] Daisuke Yamauchi,[b] Takahiro Nishimura[a]

[a] *Graduate School of Science, Osaka City University,*

[b] *Graduate School of Science, Kyoto University*

Recent progress of the transition metal-catalyzed direct functionalization of inactive C–H bonds has enabled a highly efficient C–C bond formation in synthetic organic chemistry. Recentry we reported Ir-catalyzed sp^3 C–H alkylation of *N*-methyl-*N,N'*-diphenylurea with terminal alkenes [1]. However, the alkylation of a secondary C–H bond of *N*-ethyl-*N,N'*-diphenylurea did not occur. We report here Ir-catalyzed sp^3 C–H alkylation of indoline derivatives with terminal alkenes [2]. The reaction proceeded in the presence of a hydroxoiridium/1,5-cyclooctadiene catalyst to give the corresponding 2-alkylated indoline derivatives in high yields.

Previous Work

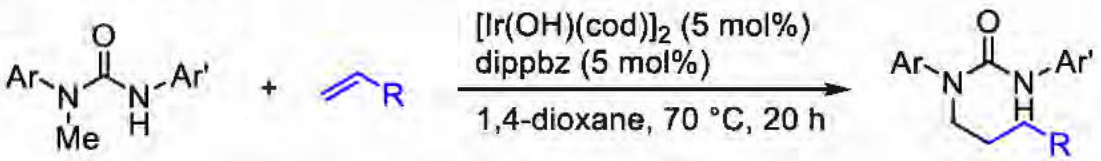

This Work

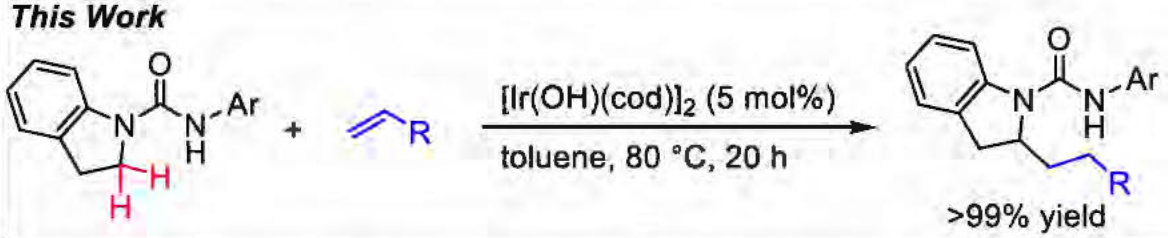

dippbz: 1,2-Bis(diisopropylphosphino)benzene, cod: 1,5-cyclooctadiene

[1] Yamauchi, D.; Nishimura, T.; Yorimitsu, H. *Angew. Chem., Int. Ed.* **2017**, *56*, 7200.

[2] Nakamura, I.; Yamauchi, D.; Nishimura, T. *Asian J. Org. Chem.* **2018**, *7*, 1347.

Acid-Catalyzed Chirality-Transferring Intramolecular Friedel-Crafts Reaction of α-Hydroxy-α-alkenylsilanes

Shunichi Kubota, Wataru Akagi, Naoko Ikeda, Masato Higashino, Tetsuro Shinada, Yasufumi Ohfune, Kazuhiko Sakaguchi and Takahiro Nishimura

Graduate School of Science, Osaka City University, Sugimoto, Sumiyoshi, Osaka 558-8585, Japan

The treatment of optically active α-hydroxy-α-alkenylsilane (*S*)-**1** with catalytic amounts of trimethylsilyl trifluoromethanesulfonate (TMSOTf) as a Lewis acid in the presence of 3Å molecular sieves (MS) gave enantio-enriched intramolecular Friedel–Crafts cyclization product, vinylsilane-tethered tetrahydronaphthalene (*S*)-**2** (82%), together with allylic rearrangement product, γ-hydroxyvinylsilane (*R*)-**3** (15%). In spite of the acidic reaction conditions, the chirality of **1** (>99% ee) was completely transferred to **2** (98% ee) and **3** (>99% ee). Contraly to this, the reaction of the Ph-substituted analog **4** (>99% ee) under the same reaction conditions gave racemic **5** (0% ee) in 92% yield. The silyl group attached to the chiral carbon played a crucial role in the chirality transfer probably due to the destabilization of the adjacent carbocation (α-silyl cation) [1].

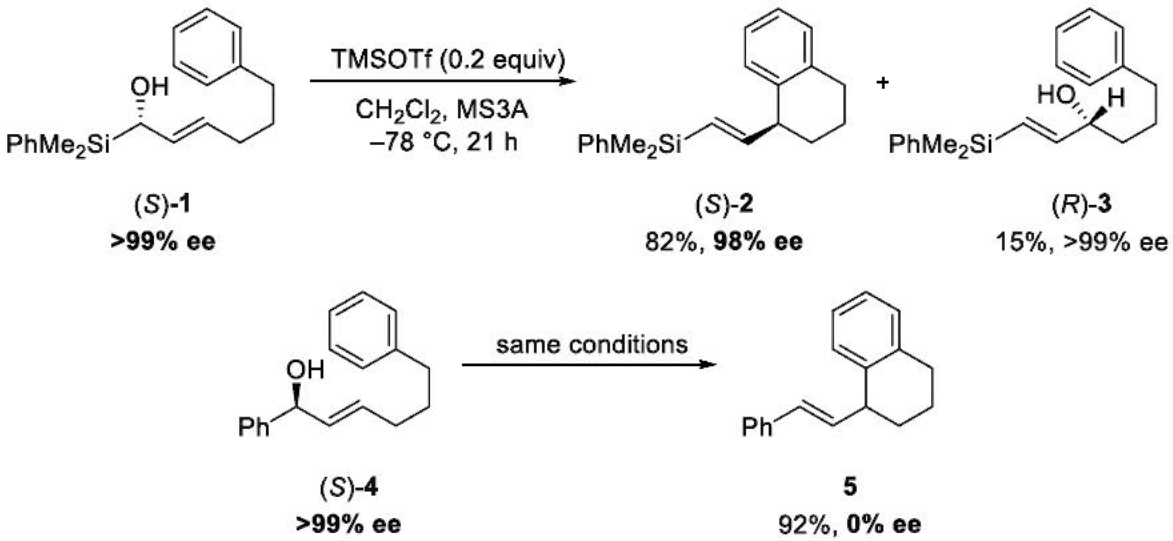

(*S*)-**1** **>99% ee**

(*S*)-**2** 82%, **98% ee**

(*R*)-**3** 15%, >99% ee

(*S*)-**4** **>99% ee**

5 92%, **0% ee**

[1] Apeloig, Y and Stanger, A. *J. Am. Chem. Soc.* **1985**, *107*, 2806–2807.

Iridium-Catalyzed Enantioselective Hydroarylation of Chromene Derivatives

○Kana Sakamoto, Takahiro Nishimura*

Graduate School of Science, Osaka City University, Sumiyosi, Osaka 558-8585

Hydroarylation, which is the direct addition of aromatic compounds to unsaturated bonds, has attracted much attention in view of facile and efficient synthesis of alkylated aromatic compounds. Recently, we reported iridium-catalyzed regio- and enantioselective hydroarylation of alkenyl ethers such as allylic ethers and homoallylic ethers with 2-phenylpyridine derivatives.[1] The reaction involves olefin isomerization of alkenyl ethers to 1-alkenyl ethers resulting in the instrallation of the aryl group at the α-carbon atom of the alkoxy group. Here we report the enantioselective hydroarylation of chromene derivatives with aromatic ketones catalyzed by an iridium/chiral bisphosphine complex.[2] The reaction gave a variety of 2-arylchromane derivatives in high yields with high enantioselectivity.

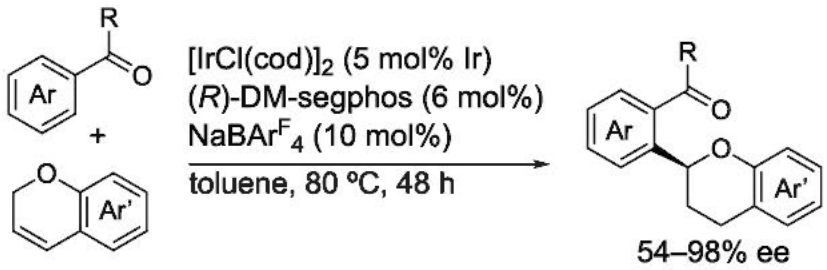

[1] Y. Ebe, M. Onoda, T. Nishimura, H. Yorimitsu, *Angew. Chem., Int. Ed.* **2017**, *56*, 5607.

[2] K. Sakamoto, T. Nishimura, *Adv. Synth. Catal.* **2019**, in press.

Rhodium(III)-Catalyzed 1,4-Addition of Arylboronic Acids to α,β-Unsaturated Carboxylic Acids

Risa Yoshimoto, Yoshinosuke Usuki, Tetsuya Satoh
Department of Chemistry, Graduate School of Science, Osaka City University, 3-3-138 Sugimoto, Sumiyoshi-ku, Osaka 558-8585, Japan

Transition-metal-catalyzed 1,4-conjugate additions of organometallic reagents to α,β-unsaturated compounds have been regarded as useful synthetic tools for preparing β-substituted carbonyl molecules. Among various organometallic reagents, organoboron reagents were widely used due to their ready availability, stability, and low toxicity. In this type transformation, palladium(II)-, rhodium(I)-, or ruthenium(II)-catalysis is usuallu utilized. [1] In contrast, the rhodium(III)-catalyzed version has been less explored.

In this work, we have found that treatment of arylboronic acids with α-trifluoromethylacrylic acid in the presence of a rhodium(III) catalyst gives 1,4-conjugate addition products, β-aryl-α-trifluoromethylpropanoic acids, selectively. Furthermore, we have developed the rhodium(III)-catalyzed β-alkenylation of α-trifluoromethylacrylic acid to produce 5,5,5-trifluoro-1,3-butadiene derivatives selectively through C–H bond cleavage and decarboxylation.

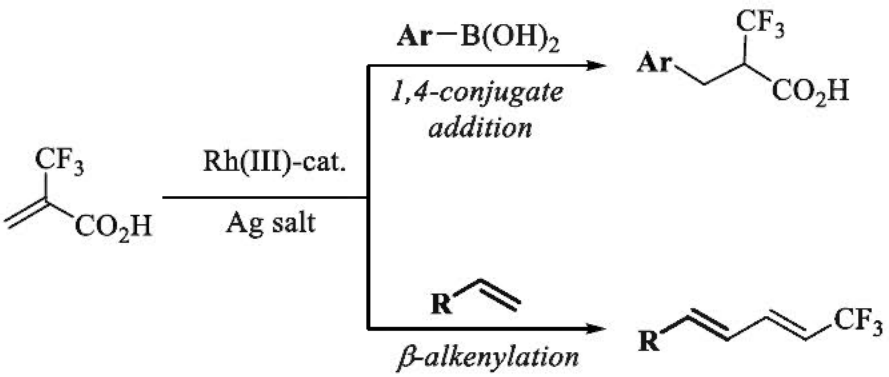

References

[1] For reviews, see:
(a) Fagnou, K.; Lautens, M. *Chem. Rev.* **2003**, *103*, 169.
(b) Hayashi, T.; Yamasaki, K. *Chem. Rev.* **2003**, *103*, 2829.
(c) Miura, T.; Murakami, M. *Chem. Commun.* **2007**, 217.

Iridium-Catalyzed Dehydrogenative Coupling of Aromatic Carboxylic Acids with Internal Alkynes

Keishi Hirosawa, Yoshinosuke Usuki, and Tetsuya Satoh
Department of Chemistry, Graduate School of Science, Osaka City University, 3-3-138 Sugimoto, Sumiyoshi-ku, Osaka 558-8585, Japan

Transition-metal catalyzed dehydrogenative coupling of aromatic substrates with unsaturated compounds is a useful method for synthesizing π-conjugated molecules from readily available, stable starting materials. In this work, we have found that 5,6,7,8-tetraphenyl-1-naphthol derivatives can be prepared through the iridium-catalyzed dehydrogenative 1:2 coupling of salicylic acids with diphenylacetylene (eq. 1). 1-Naphthol derivatives possessing a phenyl group at their 8-position have attracted attention due to their luminescent properties.[1]

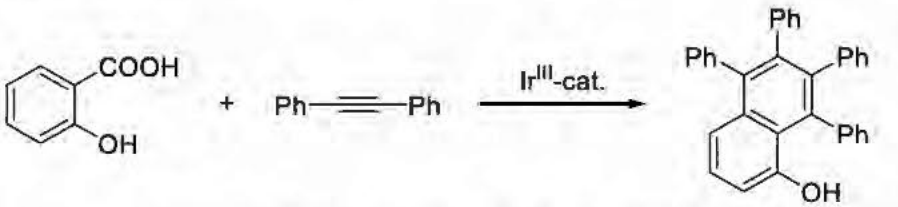

(1)

Interestingly, the same product as in eq. 1 can be obtained as a major product in the reaction of *p*-hydroxybenzoic acid (eq. 2). Plausible mechanism for explaining these regioselectivities observed will be presented.

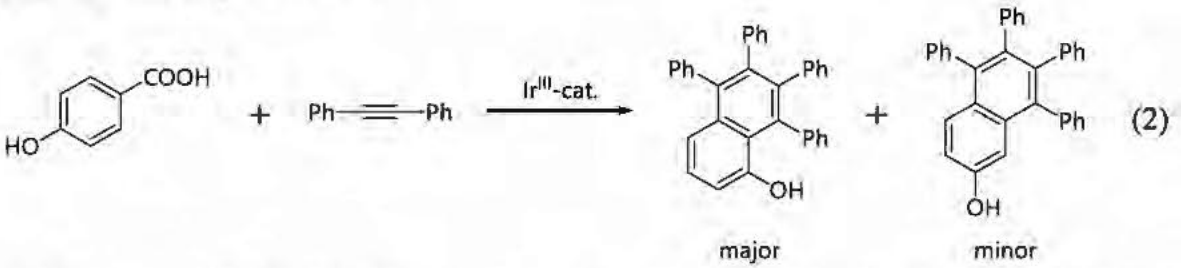

(2)

[1] H. Nakajima, M. Yasuda, K. Shimizu, N. Toyoshima, Y. Tsukahara, T. Kobayashi, S. Nakamura, K. Chiba, A. Baba, *Bull. Chem. Soc. Jpn.* **2011**, *84*, 1118.

Catalytic Asymmetric Synthesis of β-Hydroxy DOPA

Kohei Yasuda, Yoko Yasuno, Tetsuro Shinada

Graduate School of Science, Osaka City University

3-3-138 Sugimoto, Sumiyoshi, Osaka 558-8585, Japan

Phomopsin A (**1**)[1] and ustiloxin D (**2**)[2] are the natural products which exhibit potent tubulin polymerization inhibitory activity. In this presentation, we would like to report the stereoselective syntheses of (2*S*,3*S*)-**5** and (2*S*,3*R*)-**6** as their β-hydroxy DOPA units from ketone **3** and **4** by Ru catalyzed asymmetric transfer hydrogenation via dynamic kinetic resolution.[3]

Asymmetric transfer hydrogenation of **3** provided (2*S*,3*S*)-**5** under the condition using Ru catalyst with a (*S*,*S*)-chiral ligand, HCO_2H and Et_3N. On the other hand, switching the stereoselectivity of C3 was achieved when *N*-methylated ketone **4** was subjected to the asymmetric transfer hydrogenation using a (*R*,*R*)-ligand.

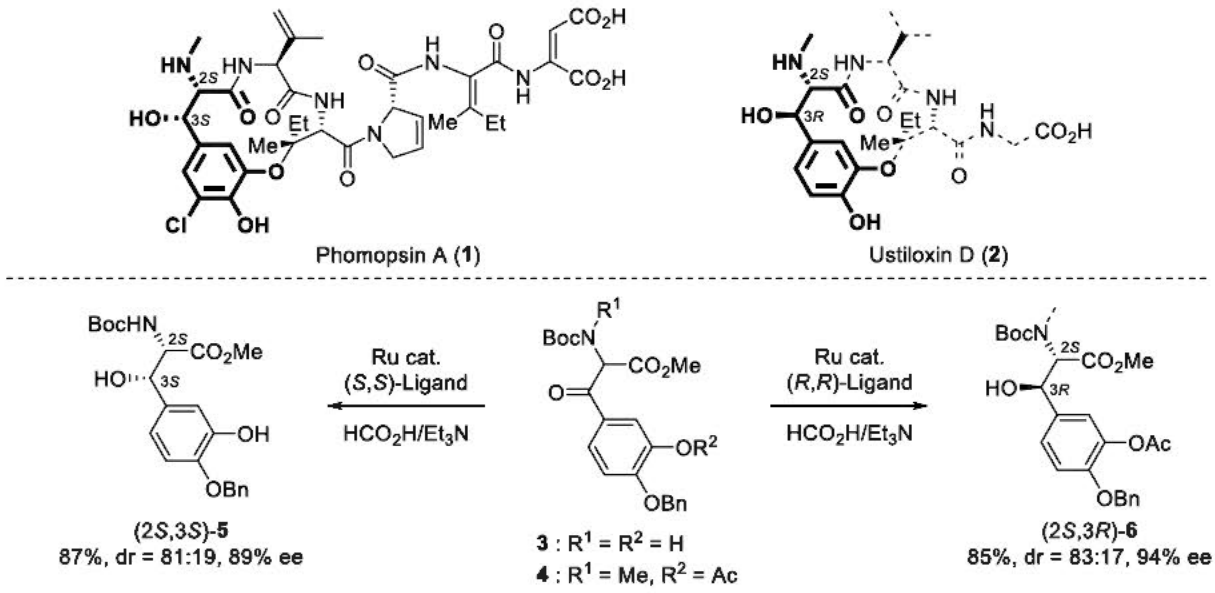

[1] Culvenor, C. C. J.; Beck, A. B.; Clarke, M.; Cockrum, P. A.; Edgar, J. A.; Frahn, J. L.; Jago, M. V.; Lanigan, G. W.; Payne, A. L.; Peterson, J. E.; Peterson, D. S.; Smith, L. W.; White, R. R. *Aust. J. Biol. Sci.* **1977**, *30*, 269.

[2] Koiso, Y.; Narita, M.; Iwasaki, S.; Sato, S.; Sonoda, R.; Fujita, Y.; Yaegashi, H.; Sato, Z. *Tetrahedron Lett.* **1992**, *33*, 4157.

[3] Brinton, S. L.; Piret, V.; Christine, H.; Peter, S. *Org. Lett.* **2010**, *12*, 5274.

Short Step Syntheses and Properties of Nitrogen-Containing Pyrenes

Yuta Omura,[1] Yoshimitsu Tachi,[1] Keiji Okada,[1,2] Masatoshi, Kozaki[1,2]

[1]Graduate School of Science, Osaka City University, [2]Osaka City University, Advanced Research Institute for Natural Science and Technology (OCARINA)

Abstract: Incorporating nitrogen atoms into pyrene frameworks can create valuable materials that are drawing extensive attention as organic semiconductors, potential DNA intercalators, and main building units in molecular machines. We developed a short-step synthesis of 2,4,10-triazapyrene **3a** involving two sequential C–H substitutions: Pd-catalyzed cross-coupling reactions via C–H arylation followed by intramolecular Cu-catalyzed C–H functionalization (Scheme 1).

Scheme 1. Synthesis of 2,4,10-triazapyrene **3a**

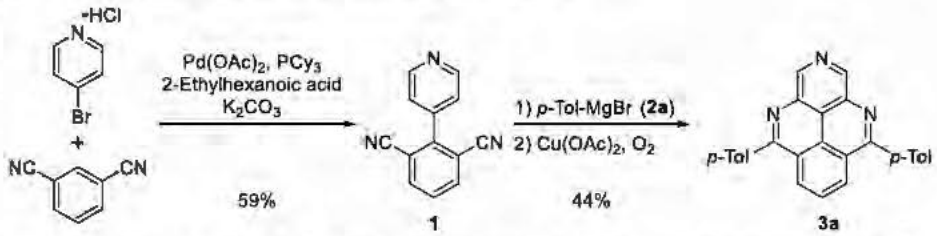

This method was successfully applied to the preparation of 1,4,10-triaza- **4**, 4,10-diaza- **5**, and 1,3,4,10-tetraazapyrenes **6** (Figure 1).

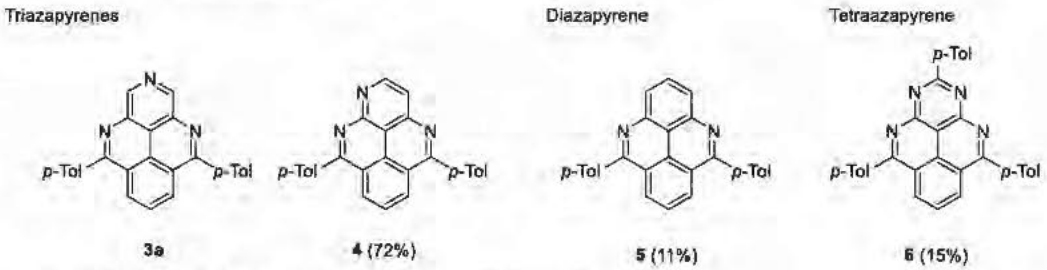

Figure 1. Synthesis of nitrogen-containing pyrenes.

Crystal structure analysis of 5,9-di(4-methylphenyl)-2,4,10-triazapyrene showed that the planar triazapyrene core have π-stack packing. Incorporating nitrogen atoms into the pyrene framework bathochromically shifted the lowest energy onsets of the absorption bands and increased the first reduction potentials. The nitrogen-containing pyrenes showed fluorescenece with a weaker intensity (Φ_f = 0.041–0.12). The number and position of nitrogen atoms influenced the extents of these effects.

Reference

Y. Omura, Y. Tachi, K. Okada, M. Kozaki *J. Org. Chem.* **2018**, in press. DOI: 10.1021/acs.joc.8b02962

Synthesis and Properties of Unsymmetrical Dinuclear Copper Complex

Yasunari Kamada, Masatoshi Kozaki, Yoshimitsu Tachi

Graduate School of Science, Osaka City University

Abstract: Unsymmetrical dinuclear metal complexes are expected to have unique properties through cooperative effects between metals in different coordination environments. Symmetric dinuclear copper complexes reacted with oxygen molecules (O_2) to produce active oxygen complexes with Cu_2O_2 cores bridged in a μ-η^2:η^2-peroxo and *trans*-μ-1,2-peroxo shapes (Figure 1)[1]. On the other hand, a novel active-oxygen complex (μ-η^1:η^2-peroxo)Cu_2 was obtained using unsymmetrical dinuclear copper complexes[2]. In order to investigate the ligand effect and the reactivity of dicopper-dioxygen complexes in unsymmetrical coordination environments, we designed and synthesized unsymmetrical pentapyridine ligand (**L**) that provides a tetradentate and a tridentate coordination site (Figure 2). Unsymmetrical dinuclear copper complexes were prepared with unsymmetrical ligand **L** and their properties were investigated.

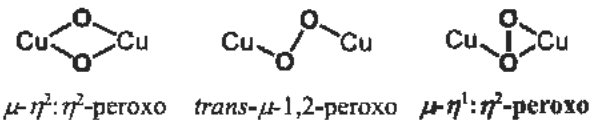

μ-η^2:η^2-peroxo *trans*-μ-1,2-peroxo **μ-η^1:η^2-peroxo**

Figure 1. Cu_2O_2 core structure

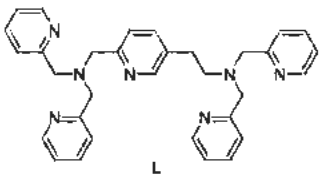

Figure 2. Structure of **L**

$[Cu^I(MeCN)_4]PF_6$ and **L** were reacted in a glovebox to form dinuclear copper(I) complex $[Cu^I_2(\mathbf{L})](PF_6)_2$ (**1a**). **1a** was identified by means of various spectroscopic methods and redox potentials of each Cu site were determined by cyclic voltammetry (CV). The formation of the Cu_2O_2 complex by the reaction of **1a** with dioxygen molecule was monitored by UV-vis spectroscopy, and it showed the absorption band around 349 nm, corresponding to the Ligand-to-Metal Charge Transfer (LMCT) transition. The details of these findings will be reported.

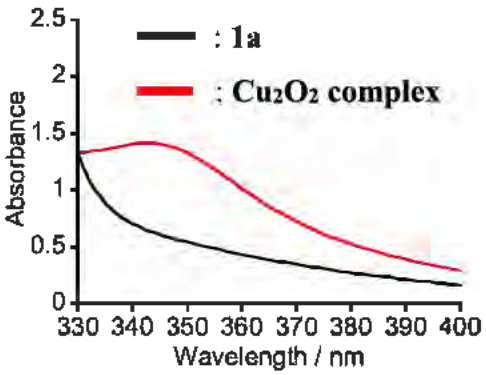

References:

[1] Jacobson, R.; Tyeklar, Z.; Farooq, A.; Karlin, K. D.; Liu, S.; Zubieta, J. *J. Am. Chem. Soc.* **1988**, *110*, 3690–3692.

[2] Tachi, Y.; Aita, K.; Teramae, S.; Tani, F.; Naruta, Y.; Fukuzumi, S.; Itoh, S. *Inorg. Chem.* **2004**, *43*, 4558–4560.

Regulation of catilytic acitivity of *N*-methylpyrolidine by the stumulaus-resposible zinc porphyrin receptor

Tomoaki, Nishimura; Yoshito, Sasaki; Yoshimitsu, Tachi;
Keiji Okada,; Masatoshi, Kozaki
Graduate School of Science, Osaka City University

Abstract: A stimulus-responsive molecule **1** was designed and prepared to control ligand-binding ability of multiple receptor sites, two zinc tetraphenylporphyrin (ZnTPP) and one zinc diethynyldiphenylporphyrin (ZnDEDPP), by effector molecule **2**. Spectroscopic titrations indicated that stable supramolecular complex **1•2** ($K = 6.7 \times 10^6$ M^{-1}) was produced via the cooperative formation of multiple hydrogen bonds and coordination bonds. As the result, the binding of a ligand to ZnTPP was competitively inhibited by **2**. In addition, the formation of **1•2** brought about conformational change of the side arms to cover both faces of ZnDEDPP with shielding panels (HAB). As a result, the binding constant of ZnDEDPP in **1•2** with 4-phenylpyridine was decreased to 8.9% of that in **1**. Namely, the ligand-binding ability of ZnDEDPP was suppressed by allosteric mechanism. The effector molecule can reduce ligand-binding ability of both ZnTPP and ZnDEDPP in **1** by competitive and allosteric mechanism, respectively. The catalytic activity of *N*-methylpyrrolidine in Michael addition was successfully regulated by **1**. We will present molecular design and the allosteric effect in detail.

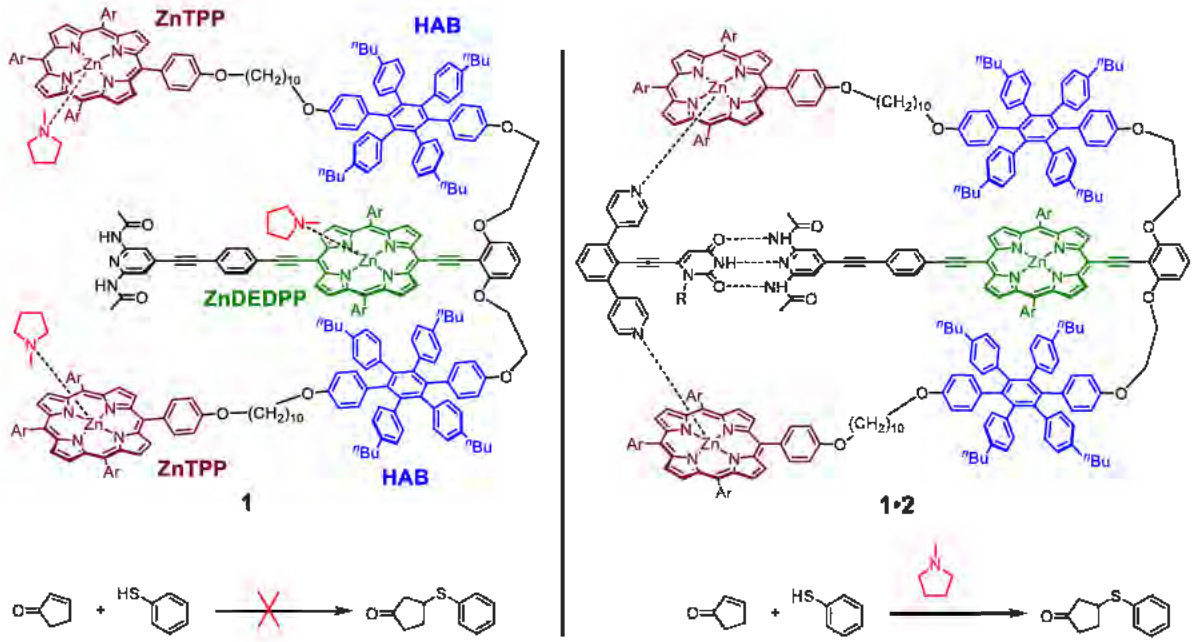

References

[1] Sasaki, Y.; Suzuki, S.; Okada, K.; Kozaki, M. *Tetrahedron Lett.* **2016**, *57*, 4082–4085.

Synthesis and Properties of Condensed Phenoxazine Dimer

Takayuki Miyamae,[1] Makoto Haraguchi,[1] Yoshimitsu Tachi,[1]
Masatoshi Kozaki,[1,2] Keiji Okada[1,2]

[1]Graduate School of Science, Osaka City University, [2]Osaka City University Advanced Research Institute for Natural Science and Technology (OCARINA), Sugimoto, Osaka 558-8585.

Abstract: Phenoxazine (**PXZ**) is a good electron donor, and can be used as a building block of the electron rich condensed materials. We have previously prepared phenoxazine-condensed trioxytriphenylamine (**TOT**),[1] which is a stronger electron donor than **PXZ**, and takes a planar form in radical cation state. The planarity in radical cation state is very important to apply to magnetic materials.

Recently, Higashibayashi and coworkers reported 1,1',9,9',10,10'-biphenothiazine (**BPTZ**) as phenothiazine (**PTZ**) derivative, which was shown to be a butterfly-shaped molecule and has a low oxidation potential.[2] We expected that 1,1',9,9',10,10'-biphenoxazine (**BPXZ**) could have a planar form in the radical cation state.

In this work, we designed **BPXZ**, which was obtained as a stable compound in 5 steps from known compounds. Cyclic voltammogram showed that **BPXZ** had a low oxidation potential (E_{ox} = –0.20 V vs Fc/Fc^+ in THF). Furthermore, we successfully prepared radical cation **BPXZ**$^{\bullet+}$•SbF_6^-. X-ray crystallography revealed that neutral **BPXZ** was in a shallow butterfly-shape and **BPXZ**$^{\bullet+}$ had a highly planar form (Figure 2). The detailed synthesis and properties of **BPXZ** and **BPXZ**$^{\bullet+}$•SbF_6^- are reported.

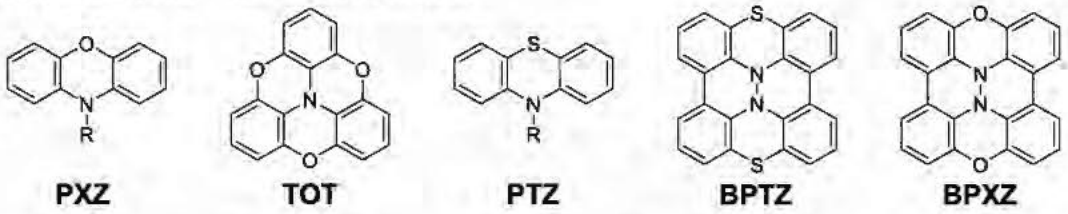

Figure 1. Phenoxazine and phenothiazine derivatives

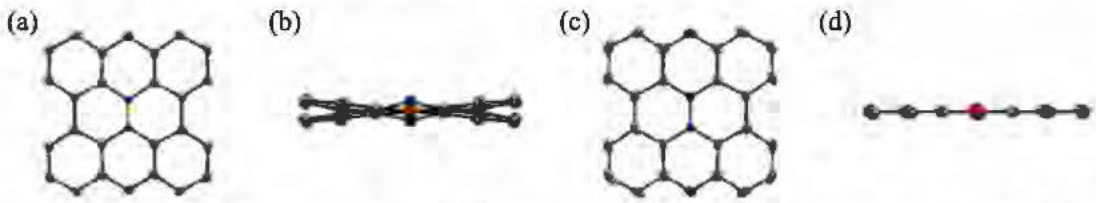

Figure 2. ORTEP views for (a), (b) **BPXZ** and (c), (d) **BPXZ**$^{\bullet+}$•SbF_6^- (set at 50% probability level): (a), (c) top and (b), (d) side views, respectively. Counter ions and hydrogen atoms were omitted for clarity.

[1] Okada, K. et al. *Angew Chem., Int. Ed.* **2005**, *44*, 4056–4058.
[2] Higashibayashi, S. et al. *Asian J. Org. Chem.* **2018**, *7*, 1797–1801.

Syntheses and Properties of Ortho-bridged Triphenylamines by Two Oxygens and Sulfur or Nitrogen Atoms

Naoki Yokoyama, Nobuaki Tanaka, Masatoshi Kozaki, Daisuke Shiomi, Kazunobu Sato, Takeji Takui, Keiji Okada

Graduate School of Science, Osaka City University

Abstract:

Triphenylamines, typical electron donors, have been widely investigated as functional materials. We have hitherto prepared trioxytriphenylamine (**TOT**) and isolated its radical cation species as a stable compound under an aerated condition.[1] Furthermore, the (nitronyl nitroxide)-substituted **TOT** radical cation (**NNTOT**$^+$) has been found to undergo magnetic phase transition into an organic weak ferromagnet at low temperature.[2]

In this work, we designed and synthesized monothio- and monoimino-**TOT** analogues (**DOTT**, **DOIT**, respectively). We here report on the synthesis of neutral and radical cation species for **DOTT** and **NNDOTT** and the synthesis of **DOIT**. **DOTT** and **DOIT** were synthesized in 4 steps from known **(Anis)$_2$X** (X = S or MeN) and characterized by ^{1}H NMR spectra and MS. **DOTT** showed two reversible oxidative waves in cyclic voltammetry at +0.15 V and +0.99 V (vs Fc/Fc$^+$); **DOIT** showed two reversible oxidative waves at –0.28 V and +0.46 V (vs Fc/Fc$^+$), respectively. **NNDOTT** was prepared by cross coupling reaction[3] of **NN-AuPPh$_3$** with iodo-**DOTT** and characterized by MS, ESR spectrometry, and elemental analysis. The detailed synthese of these compounds are reported. The X-ray structure analyses and magnetic properties of **NNDOTT** radical cation species will be also presented.

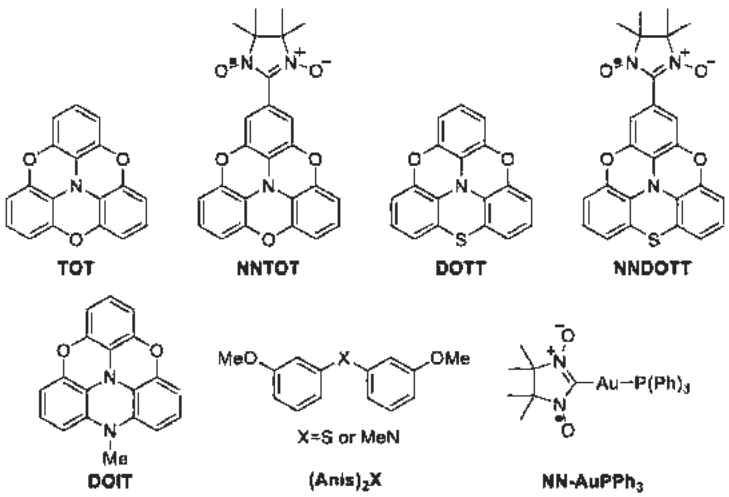

Reference:

[1] Okada, K. et al. *Angew. Chem., Int. Ed.* **2005**, *117*, 4124–4126.
[2] Okada, K. et al. *Chem. –Asian J.* **2012**, *7*, 1607–1609.
[3] Okada, K. et al. *Chem. Lett.* **2014**, *43*. 678–680.

High Stability of $Ir(OH)_3$ Supported on a Bottom-Up Mesoporous Silica During Photocatalytic Water Oxidation

Gentaro Sakamoto[1], Hiroyasu Tabe[1,2], Yusuke Yamada[1]

[1]*Graduate School of Engineering, Osaka City University,* [2]*Advanced Research Institute for Natural Science and Technology, Osaka City University*

3-3-138 Sugimoto Sumiyosi-ku, Osaka-shi, 558-8585, JAPAN

Abstract: Artificial photosynthesis using visible light is a promising method to convert solar energy into chemical energy. Artificial photosynthesis consists of four processes: light harvest, charge separation, water oxidation and substrate reduction. Among them, the water oxidation reaction is the most difficult process, because this reaction accompanied with transfer of four electrons and four protons. Therefore, the development of highly efficient and high durable water oxidation catalyst is strongly demanded to realize practical artificial photosynthesis.

Iridium hydroxide ($Ir(OH)_3$) nanoparticles known as a highly active catalyst for water oxidation were incorporated into a mesoporous support composed of the bottom-up mesoporous silica to suppress catalytic deactivation.[1] The supported $Ir(OH)_3$ catalyzed photocatalytic water oxidation by visible-light irradiation in a buffer solution containing persulfate ion ($S_2O_8^{2-}$) and tris(2,2'-bipyridine) ruthenium(II) ion ($[Ru(bpy)_3]^{2+}$) as a sacrificial electron acceptor and a photosensitizer, respectively. The O_2 yields at the fourth run were 80 % and 30 % for $Ir(OH)_3$ with and without the support, respectively (Figure 1). $Ir(OH)_3$ nanoparticles were also incorporated into bottom-up mesoporous silica-alumina ($Al\text{-}SiO_2$), resulting in further enhancement of the stability with the yield (95 %) at the fourth run (Figure 2).

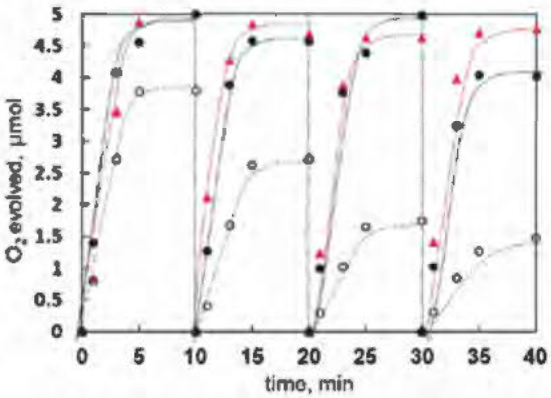

Figure 1. Time courses of O_2 evolution by visible-light irradiation (white light) of a phosphate buffer (2.0 mL, 50 mM, pH 8.0) containing $[Ru(bpy)_3]SO_4$ (1.0 mM), $Na_2S_2O_8$ (5.0 mM), and $Ir(OH)_3$ (0.11 mM, dashed line) or $Ir(OH)_3/SiO_2$-CA(5.0 mg, [Ir] = 0.072 mM, solid line) or $Ir(OH)_3/Al\text{-}SiO_2$-CA (5.0 mg, [Ir] = 0.13 mM, impregnation method, red line) in four repetitive experiments.

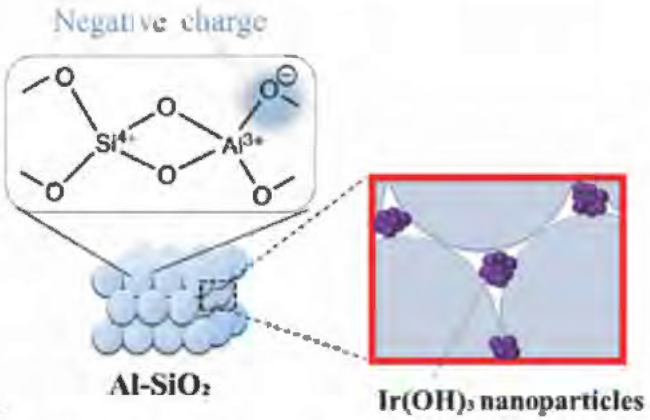

Figure 2. Immobilization of $Ir(OH)_3$ nanoparticles in the pore of $Al\text{-}SiO_2$ nanoparticles assembly

References: [1] Yamada, Y.; Tadokoro, H.; Naqshbandi, M.; Canning, J.; Crossley, M.; Suenobu, T.; Fukuzumi, S. *ChemPlusChem* **2016**, 81, 521.

Synthesis of coordination polymers involving 1,10-phenanthroline-5,6-diolate iron(III) complex as a monomer unit

Yuka Kimoto[1], Hiroyasu Tabe[1,2], Yusuke Yamada[1]

[1]*Graduate School of Engineering, Osaka City University,* [2]*Advanced Research Institute for Natural Science and Technology (OCARINA), Osaka City University*

3-3-138 Sugimoto, Sumiyosi-ku, Osaka-shi, 558-8585, JAPAN

Abstract: Coordination polymers composed of metal ions and bridging ligands have recently emerged as promising candidates for heterogeneous catalysts because of their high activity and tunability with defined active sites. Especially, bridging ligands with an asymmetric structure can bind two different metal ions, resulting in a coordination polymer catalyst with highly tunable degrees of coordinative saturation and electronic structures by choosing an appropriate combination of the metal ions. The catalytic activity of coordination polymers can be tuned by not only combination of metal ions in the framework but also introduction of functional groups to bridging ligands. We report herein synthesis of a metal complex composed by iron(III) ion and 1,10-phenanthroline-5,6-diolate (L) as a building block of a heterometallic coordination polymer (Figure 1). Formation of $[Fe^{III}L_3]^{3-}$ complex by selective coordination of O atoms of L to Fe(III) ions were confirmed by UV-visible spectroscopy (Figure 2a).[1] The absorbance at 480 nm assignable to LMCT band was gradually increased by the addition of Fe(III) ion up to L / Fe(III) = 3. No further increase in the absorbance was observed at L / Fe(III) > 4, strongly supporting the formation of $[Fe^{III}L_3]^{3-}$ (Figure 2b). Then, we added another metal ion (M^N) to a solution containing $[Fe^{III}L_3]^{3-}$ ion to obtain a coordination polymer having selective coordination bonds between M^N and N atoms of L.

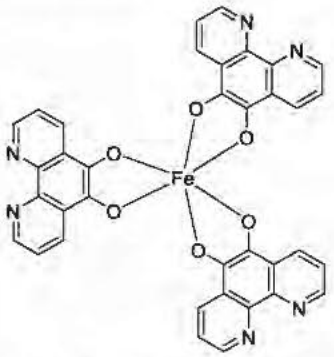

Figure 1. The structure of tris(1,10-phenanthroline-5,6-diolate)iron(III) complex.

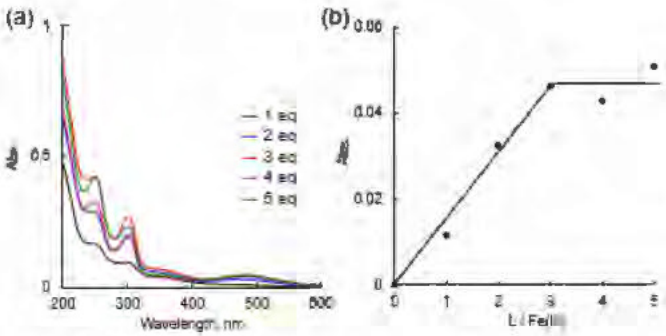

Figure 2. (a) UV-visible spectra of an aqueous solution (3.0 mL) containing $Fe^{III}(NO_3)_3$ (7.36 μM) and 1–5 equivalent of 1,10-phenanthroline-5,6-diol. The peak at around 480 nm indicates the formation of tris(*O*,*O*'-1,10-phenanthroline-5,6-diolate)iron(III) ion. (b) The plot of the absorbance at 480 nm vs. L / Fe(III).

References: [1] M. J. Sever; J. J. Wilker *Dalton Trans.* **2004**, 1061, 1072.

Structure analysis of the solid organic molecule-hydrogen peroxide adducts

Mayu Maetani[1], Hiroyasu Tabe[1,2], Yusuke Yamada[1]

[1]*Graduate School of Engineering, Osaka City University,* [2]*Advanced Research Institute for Natural Science and Technology (OCARINA), Osaka City University*

3-3-138 Sugimoto Sumiyosi-ku, Osaka-shi, 558-8585, JAPAN

Introduction

Hydrogen peroxide (H_2O_2) is a useful oxidizing agent for various selective oxidation reactions, pulp- or paper bleaching, disinfectant. H_2O_2 is produced by the anthraquinone process in industry or the direct synthesis from gaseous hydrogen and oxygen using a Pd catalyst in a laboratory. H_2O_2 is also found in biological systems. For example, H_2O_2 produced in plant roots are used for nutrient absorption, control of root elongation and tissue reinforcement, however, excess H_2O_2 is decomposed by disproportionation catalyzed by catalase. Adsorption of the excess H_2O_2 from biological systems without decomposition can be a novel method to produce H_2O_2.

Urea and sodium bicarbonate are known to form clathrate compounds with H_2O_2 in which amino, carbonyl and carbonate groups strongly interact with H_2O_2 in the crystals by hydrogen bonds (Figure 1).[1] We report herein that several organic molecules having functional groups available as the hydrogen bond donor and acceptor were examined to scrutinize a relationship between the structures of organic molecules and the amount of adsorbed H_2O_2.

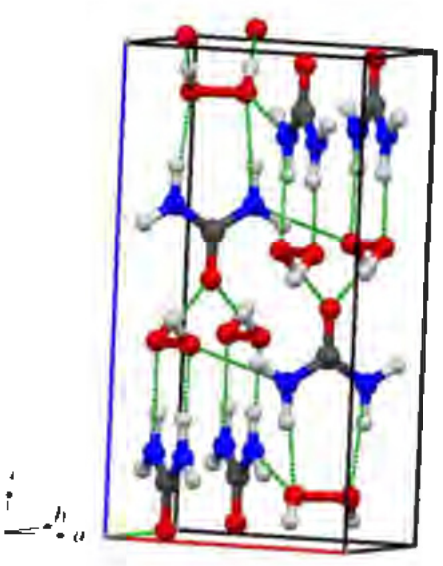

Figure 1. Crystal structure of the urea-hydrogen peroxide adduct. Hydrogen bonds are represented by dashed lines.

Various organic molecules were recrystallized from an aqueous solution of H_2O_2 (30 vol%). The amount of H_2O_2 molecules immobilized in the crystal were determined by the weight gain after the recrystallization, the thermogravimetric analysis (TGA), and the spectrometric change of oxo[5,10,15,20-tetra(4-pyridyl)porphyrinato]titanium(IV) of an aqueous solution of the crystals. X-ray single-crystal structure analysis of the H_2O_2 adduct suggested that H_2O_2 molecules are tightly bound to amino groups and carboxylate groups of the organic molecules by hydrogen bonds.

[1] Fritchie, C. J.; McMullan, R. K. *Acta Cryst.* **1981**, B37, 1089.

pH-dependent catalytic activity of Prussian blue analogs with CN-deficient sites for hydrolysis of organophosphates

Mari Yamane[1], Hiroyasu Tabe[1,2], Yusuke Yamada[1]

[1]*Graduate School of Engineering, Osaka City University,* [2]*Advanced Research Institute for Natural Science and Technology (OCARINA), Osaka City University*

3-3-138 Sugimoto Sumiyosi-ku, Osaka-shi, 558-8585, JAPAN

Organophosphates used as agricultural chemicals sometimes cause poisoning incidents all over the world. The toxicity of organophosphates can be lessened by hydrolytic decomposition. Recently, polymeric cyano-bridged metal complexes known as Prussian blue analogs (PBAs) have been reported to act as heterogeneous catalysts for hydrolysis of organophosphates.[1] The active sites of PBAs are usually metal ions coordinated by N atoms of cyano ligands (M^N). On the other hand, metal ions coordinated by C atoms (M^C) are not active sites because M^C forms coordinatively saturated sites. Lack of some cyano ligands from the framework results in formation of coordinatively unsaturated sites on M^C, where enhancement of catalytic activity per unit area is highly expected (Figure 1, left).

$Na_3[Fe^{II}(CN)_5(H_2O)]$ was prepared through a ligand exchange reaction of $Na_3[Fe^{II}(CN)_5(NH_3)]$ in HEPES buffer solution containing NaCl.[2] $Cu^{II}_{1.5}[Fe^{II}(CN)_5(H_2O)]$, $Cu^{II}_{1.5}[Fe^{II}(CN)_5(NH_3)]$ and $Cu^{II}_2[Fe^{II}(CN)_6]$ were prepared by mixing an aqueous solution containing each precursor complex and $Cu^{II}(NO_3)_2$. Hydrolysis of organophosphates was demonstrated in the presence of catalysts (10 mg) in HEPES buffer solutions (pH 6.0 or pH 8.3, 100 mM) containing disodium 4-nitrophenyl phosphate (NPP, 25 mM) (Figure 1, right). The conversion of NPP was observed by monitoring the increase of absorbance of the 4-nitrophenolate ion at 400 nm using UV−visible absorption spectroscopy. $Cu^{II}_{1.5}[Fe^{II}(CN)_5(L)]$ (L = H_2O, NH_3) showed the higher catalytic activity for NPP hydrolysis than $Cu^{II}_2[Fe^{II}(CN)_6]$. Hydrolysis reactions examined in buffer solutions at various pH suggested that the reaction mechanism depends on the acidity or basicity of the reaction solution.

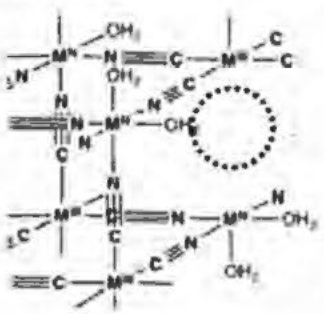

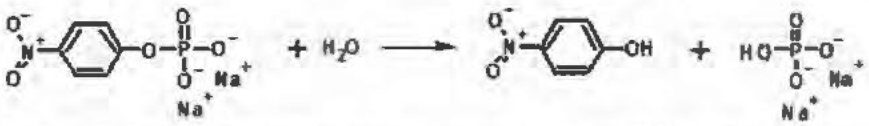

Figure 1. (left) A coordinatively unsaturated site on M^C produced by deleting a part of CN ligands and (right) a scheme of hydrolysis of disodium 4-nitrophenyl phosphate.

[1] Tabe, H.; Terashima, C.; Yamada, Y. *Catal. Sci. Technol.* **2018,** 8, 4747.

[2] Gutierrez, M. M.; Olabe, J. A.; Amorebieta, V. T.; *Inorg. Chem.* **2011,** 50, 8817.

Preparation of Mesoporous Assemblies Composed of Prussian Blue Nanospheres

Shoma Yorozu[1], Mari Yamane[1], Hiroyasu Tabe[1,2], Yusuke Yamada[1]
[1]*Graduate School of Engineering, Osaka City University,* [2]*Advanced Research Institute for Natural Science and Technology (OCARINA), Osaka City University*
3-3-138 Sugimoto Sumiyosi-ku, Osaka-shi, 558-8585, JAPAN

Abstract: Several pesticides used all over the world are a class of organophosphates. Residual organophosphates found in foods and soils can be efficiently removed by adsorbents at low concentrations. However, organophosphates at high concentrations should be catalytically decomposed to assure safety. Prussian blue analogues have been reported to act as efficient catalysts for organophosphates hydrolysis (Figure 1a).[1] However, the catalytic activity is insufficient for organophosphate hydrolysis at low concentrations because of weak interaction between organophosphates and the catalyst surfaces. The binding of organophosphates can be enhanced in confined spaces, such as mesopores. Adsorption ability can be provided for a catalyst by assembling the catalytic nanospheres in a densely packed form, in which interparticles spaces act as mesopore. In this research, size-controlled Prussian blue nanoparticles were hydrothermally synthesized to prepare a mesoporous assembly. The particle sizes were precisely controlled as small as 80 nm under optimized conditions (Figure 1b). The nanospheres assemblies of Prussian blue were examined for their activity for adsorption and hydrolytic decomposition of organophosphates.

(a)

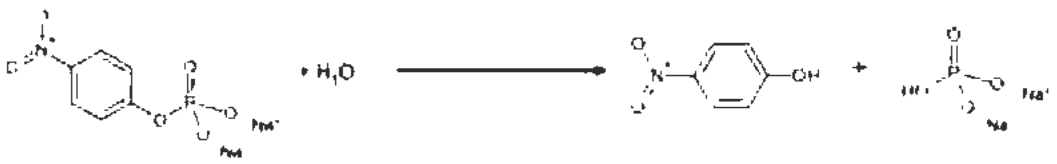

(b)

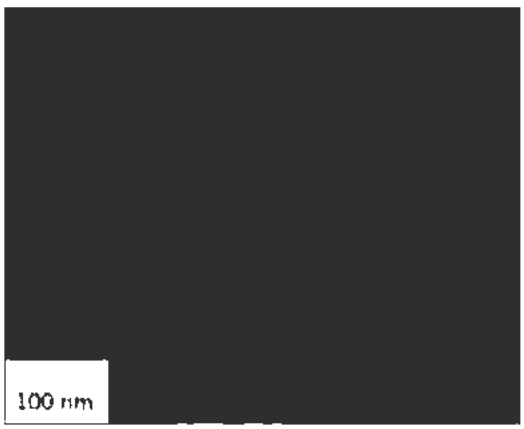

Figure 1. (a) Scheme of hydrolysis of disodium *p*-nitrophenylphosphate.
(b) Scanning electron microscope (SEM) image of a mesoporous assembly composed of Prussian blue nanospheres.

Reference:[1] Tabe, H.; Terashima, C.; Yamada, Y. *Catal. Sci. Technol.* **2018,** *8*, 4747.

Immobilization of Enzymes in a Bottom-up Mesoporous Silica Nanoparticles Assembly

Hiroyuki Oshima[1], Hiroyasu Tabe[1,2], Shusaku Ikeyama[2],
Yutaka Amao[2], Yusuke Yamada[1]
[1]*Graduate School of Engineering, Osaka City University,* [2]*Advanced Research Institute for Natural Science and Technology (OCARINA), Osaka City University*
3-3-138 Sugimoto Sumiyosi-ku, Osaka-shi, 558-8585, JAPAN

Abstract: Enzymes are biological catalysts composed of proteins and prosthetic groups. A huge number of enzymes are used not only in biological processes but also in industrial processes, because they exhibit excellent catalytic activity under atmospheric pressure and room temperature. Enzymes are a kind of homogeneous catalysts, indicating that they are usually in the same phase of substrates. Catalyst separation and recovery without enzyme loss and denature are realized by using the catalyst supports such as mesoporous silica, however, enzyme immobilization is not always successful, because of tremendous multi-step procedures including preparation of a mesoporous support suitable for each enzyme under harsh reaction conditions. Herein, we focus on a bottom-up mesoporous silica nanoparticles assembly as a support suitable for various enzymes. [1] The nanoparticles assembly can be prepared by evaporation of colloidal silica nanoparticles under ambient conditions. Interparticle spaces in the nanoparticles assembly can be regarded as flexible mesopores for various enzymes. Thus, enzymes were immobilized by simple evaporation of a mixed dispersion of colloidal silica nanoparticles and enzymes (Figure 1). We immobilized enzymes such as formate dehydrogenase, alcohol dehydrogenase and acid phosphatase, which have different size and charge properties, in the bottom-up mesoporous silica nanoparticles assembly. The diffuse-reflectance UV-visible spectra and the infrared (IR) spectra of the assemblies suggested the successful immobilization of enzymes.

Figure 1. Immobilization of enzymes in a bottom-up mesoporous silica nanoparticles assembly by air-drying a dispersion of colloidal silica nanoparticles and enzymes.

Reference: [1] Yamada, Y.; Tadokoro, H.; Naqshbandi, M.; Canning, J.; Crossley, M.; Suenobu, T.; Fukuzumi, S. *ChemPlusChem* **2016**, 81, 521.

Selective hydrogen production based on the formate decomposition with platinum nano particles dispersed by polyvinylpyrrolidone

Yusuke Minami[1], Shusaku Ikeyama[2], Yutaka Amao[1,2]

[1]*Faculty of Science, Osaka City University*

[2]*The Advanced Research Institute for Natural Science and Technology, Osaka City University*

The society that depends on fossil fuels has serious environmental and energy problems. In recent years, the concentration of carbon dioxide in the atmosphere has been increasing rapidly. To solve those problems, hydrogen has attracted attention as an alternative energy.

Hydrogen is a gas at a room temperature and an atmospheric pressure, so it has a problem in safety when it is transported and stored. Formic acid is a liquid at a room temperature and contains a 4.3 wt.% hydrogen, so it is suitable for a hydrogen carrier.

Platinum nano particles dispersed by polyvinylpyrrolidone (Pt-PVP) catalyze hydrogen and carbon dioxide production from formic acid decomposition at a room temperature. However, the catalytic mechanism for the hydrogen and carbon dioxide production from formic acid with Pt-PVP has not been clarified yet. To clarify the mechanism with Pt-PVP, we investigated pH and formate ion concentration dependability of hydrogen production rate with Pt-PVP. Hydrogen production rate was increased with increasing proton concentration up to 100 μM, and then reached constant value. Hydrogen production rate was also increased with increasing formate ion concentration up to 1 M. Moreover, the electronic state of Pt-PVP were also observed by EXAFS and Pt L_3-edge XANES. These results indicated that electron-rich platinum nano particles have a high catalytic activity of formic acid decomposition into hydrogen and carbon dioxide.

From these results, we suggested the possible catalytic mechanism for the hydrogen and carbon dioxide production from formic acid with Pt-PVP(Figure 1). An elementary reaction which has an elimination process of carbon dioxide caused by β-hydrogen elimination suggested as a rate limiting step.

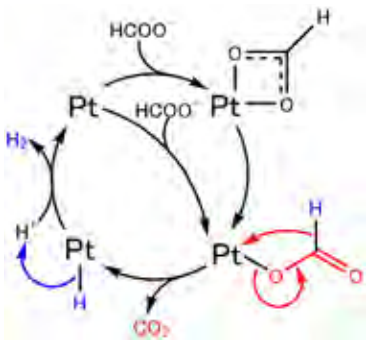

Figure 1. Catalytic mechanism of hydrogen production based on formic acid decomposition with Pt-PVP

Photocatalytic CO_2 reduction with water including methanol over Ag loaded Ga_2O_3

Kokoro Yoshioka[1]; Muneaki Yamamoto[2]; Akiyo Ozawa[1]; Tetsuo Tanabe[2]; Tomoko Yoshida[2]

[1]Applied Chemistry and Bioengineering, Graduate School of Engineering, Osaka City University, [2]Advanced Research Institute for Natural Technology, Osaka City University

Gallium oxide (Ga_2O_3) photocatalyst can promote CO_2 reduction with water to produce CO, H_2 and O_2 under UV light irradiation. It had been reported that Ag loading on Ga_2O_3 as a co-catalyst (Ag/Ga_2O_3) significantly improves the photocatalytic activity for CO_2 reduction to CO[1, 2]. However, the role of Ag co-catalyst is unclear. In order to clarify the role of Ag, it is necessary to control and understand chemical and physical characters of Ag co-catalysts loaded on Ga_2O_3. In preliminary work, we have found that the aggregation and dissolution of Ag were suppressed with using reducing agent of methanol solution. In this study, we have investigated the effect of methanol addition in water on photocatalytic CO_2 reduction with water over Ga_2O_3 with Ag co-catalyst. In the photocatalytic reduction tests, the prepared sample was dispersed into either "1 M $NaHCO_3$" or "1 M $NaHCO_3$+ 20 vol% methanol" aqueous solution under CO_2 gas flow and irradiated with photons given by a 300 W Xe lamp. Reaction products dominated with CO, H_2 and O_2 were analyzed by GC-TCD. The loading state of Ag co-catalyst was investigated by UV-vis DR measurements and SEM.

In photocatalytic CO_2 reduction tests, the addition of methanol showed higher CO selectivity than the case of without methanol. Fig. 1 compares UV-vis DR spectra of Ag/ Ga_2O_3 sample before and after the reaction. After the reaction with methanol, the localized surface plasmon resonance (LSPR) peak became larger. This suggests that the addition of methanol enhaced reduction of Ag species to make metallic nanoparticles and also inhibited elution of Ag. Thus, we have tentatively concluded that methanol assists the reduction of Ag deposited on Ga_2O_3, enhancing Ag nanoparticles formation and suppressing their aggregation or dissolution. We will also discuss about relationship between Ag loading state and photocatalytic activity quantitatively in OCARINA symposium.

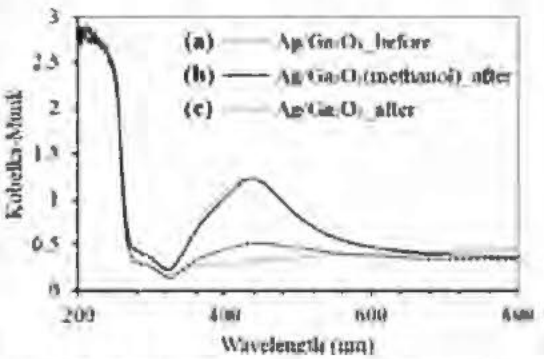

Fig. 1 UV-vis DR spectra of Ag/Ga_2O_3 sample , (a) before the reduction test, and after 5 hous redcution tests (b)with and (c)wituout methanol.

References:

[1] K. Iizuka, T. Wato, Y. Misaki, K. Saito and A. Kudo, *J. Am. Chem. Soc.*, **2011**, 133, 20863-20868

[2] N. Yamamoto, T. Yoshida, S. Yagi, Z. Like, T. Mizutani, S. Ogawa, H. Nameki and H. Yoshida, *e-j. Surf Sci. Nanotech.*, **2014**, 12, 263-268

The study on photocatalytic CO_2 reduction over Ga_2O_3 photocatalyst with water

M. Akatsuka,[a] T. Yoshida,[b] Y. Kawaguchi[a], M. Yamamoto,[b]
A. Ozawa,[a] T. Tanabe[b]
[a] *Graduate School of Engineering, Osaka City University.*
[b] *Advanced Research Institute for Natural Science and Technology, Osaka City University*

Gallium oxide (Ga_2O_3) photocatalysts can reduce CO_2 with H_2O to produce CO, however the reaction rate of CO production is very low. It has been reported that the loading of Ag on Ga_2O_3 promoted CO production [1], on the other hand, improvement of Ga_2O_3 structure should be also essential. Recently, we found that the photocatalytic activity of Ga_2O_3 depended on the calcination temperature for a Ga_2O_3 precursor in the preparation stage. Therefore, in this study, we will discuss the reason why the CO production was enhanced by controlling calcination temperature.

Ga_2O_3 samples were prepared by calcination of $Ga(NO_3)_3 \cdot 8H_2O$ powder in the air at given temperatures (673 - 1173 K) for 4 h. We carried out photocatalytic CO_2 reduction with H_2O over the Ga_2O_3 samples. Fig.1 shows CO production rate for each Ga_2O_3 sample. Ga_2O_3 prepared by calcination at 823 K (Ga_2O_3(823 K)) showed a specifically high activity for CO production, although the H_2 production rate for this sample was comparable with those for Ga_2O_3 (673, 773, 873 K). It was found that the H_2 production rate increases with the surface area of the sample.

In XRD measurement of Ga_2O_3(823 K), very weak and broad diffraction peaks were observed, suggesting the formation of β-Ga_2O_3 phase with low crystallinity. Taking into account that a low crystalline photocatalyst has many defects to promote the recombination of excited electron-hole pairs, high CO production activity for Ga_2O_3(823 K) would be resulted from an improvement of CO_2 adsorption process rather than electrons and holes diffusion process. Here we performed FT-IR measurements for chemisorbed species on Ga_2O_3(823 K) by introduction of CO_2. Fig.2 compares FT-IR spectra of as prepared Ga_2O_3(823 K) and Ga_2O_3(823 K) after one week evacuation for the removal of adsorbed water molecules. Large absorption peaks of CO_2 as monodentate bicarbonate were clearly observed for the latter sample, showing the strong influence of water adsorption. It was also revealed that the photocatalytic active Ga_2O_3(823 K) can adsorb much more CO_2 amount than the inactive Ga_2O_3(973 K).

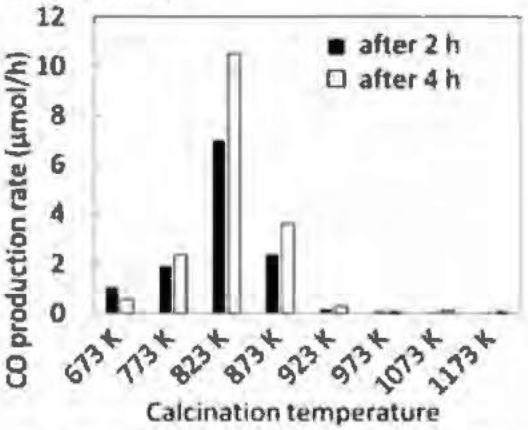

Fig. 1 CO production rates for Ga_2O_3 samples prepared by calcination at different temperarures.

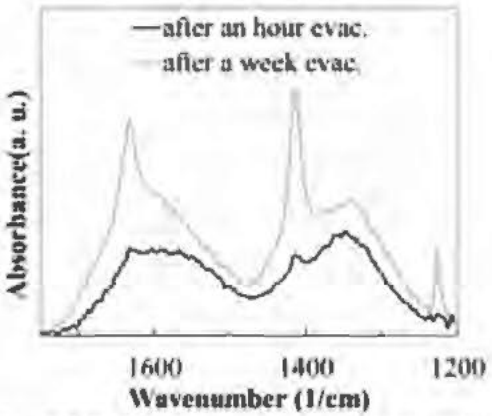

Fig. 2 FT-IR spectra of Ga_2O_3(823 K) and Ga_2O_3(823 K) after one week evacuation taken under CO_2 flowing condition

References: [1] Yoshida H., Zhang L., Sato M., *et al. Catal. Today*, **2015**, 251, 132.

Solvothermal synthesis of black phosphorus nanosheets

Akiyo Ozawa[1,2], Yukihiro Kuniyoshi[2], Tetsuro Tanabe[3], Tomoko Yoshida[3]

1 Applied Chemistry and Bioengineering, Graduate School of Engineering, Osaka City University, 3-3-138, Sugimoto, Sumiyoshi-ku, Osaka, Japan

2 Corporate Research Laboratories, Research & Development Division, Sakai Chemical Industry, Co., Ltd., 5-1, Ebisujima-cho, Sakai-ku, Sakai, Japan

3 Osaka City University Advanced Research Institute for Natural Science and Technology, 3-3-138, Sugimoto, Sumiyoshi-ku, Osaka, Japan

The crystalline structure of black phosphorus (BP) is puckered honeycomb with out-of-plane ridges in which each phosphorus (P) atom is covalently linked to three neighbouring single-layer P atoms, while individual layer sheets are stacked vertically by van der Waals interaction. Zhu et al. have demonstrated that BP nanosheets prepared by a facile solid-state mechanochemical method or ball-milling of bulk BP has photocatalytic activity on hydrogen evolution from water [1]. However, synthesis of BP usually needs high temperature and high pressure, which is costly and difficult to synthesize in large amount. Additionally, BP degrades rapidly when exfoliated to nanoscale dimensions.

Tian et al. prepared BP nanosheets consisted of few layers with one-pot solvothermal synthesis using white P as a starting material [2]. They claimed very high efficiency of the prepared BP nanosheets on photocatalytic water splitting. However white P is difficult to handle. Because it spontaneously ignites in air at above 40 ° C, and is toxic to the human body. In this study, we have tried to synthesise BP nanosheets safely with the one-pot solvothermal method using another phosphorus source. X-ray diffraction analysis of the synthesized sample confirmed the formation of BP. And the sample clearly showed layered structure as depicted in its images of a scanning electron microscope and transmission electron microscopy(Fig. 1(a) and Fig. 1(b), respectively). Absorption edge of the sample in diffuse reflectance spectra was around 850 nm. All these results indicated success in the BP synthesise. Furthermore, we have clarified necessary conditions for the synthesis.

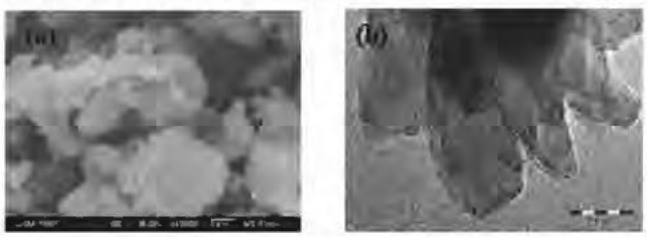

Figure 1. SEM image (a), TEM image (b) of synthesized BP nanosheets.

References

[1] X. J. Zhu, T. Zhang, Z. Sun, H. Chen, J. Guan, X. Chen, H. Ji, P. Du, S. Yang, *Adv. Mater.* **2017**, 29, 1605776

[2] B. Tian, B. Smith, M.C. Scott, R. Hua, Q. Lei, Y. Tian, *Nat. Commun.* **2018**, 9, 1397

CO_2 reduction with water over various metal oxides supported Ga_2O_3 photocatalysts

Ryota Ito[1], Masato Akatsuka[1], Akiyo Ozawa[1], Muneaki Yamamoto[2], Tetsuo Tanabe[2], Tomoko Yoshida[2]

1Applied Chemistry and Bioengineering Graduate School of Engineering, Osaka City University.

2 Advanced Research Institute for National Science and Technology, Osaka City University.

Abstract: Recently Ga_2O_3 has attracted a lot of interests as a photocatalyst for CO_2 reduction with water [1]. However, its photocatalytic activity for CO_2 reduction remains still low. In previous work, we have succeeded to improve the photocatalytic activity of Ga_2O_3 employing Al_2O_3 as catalysis support. In the present study, we have tried to improve the CO_2 reduction activity of Ga_2O_3 changing Al_2O_3 support to other metal oxide suport.

Metal oxides supported GaO_3 samples were prepared by an impregnation method of metal oxides with aqueous solution of gallium nitrate followed by dry and calcination in air at 823 K for 4 h. As for the metal oxide support, MgO, Al_2O_3, ZSM-5, TiO_2, ZnO, Y_2O_3, ZrO_2, La_2O_3, CeO_2, Nd_2O_3, and Yb_2O were employed. The weight ratio of Ga_2O_3 and a metal oxide suport was set to be 40 wt% because 40 wt% Al_2O_3 supported Ga_2O_3 (Ga_2O_3/Al_2O_3) showed the highest CO production rate. The photocatalytic CO_2 reduction with water using the prepared sumples as a catalyst was carried out and compared their photocatlytic activity.

The results are showin in Fig.1 and Fig.2 which compare the CO production rate and CO selectivity for all prepared samples. La_2O_3 supported Ga_2O_3 (Ga_2O_3/La_2O_3) showed the highest CO production rate. Moreover, the CO production rate for Ga_2O_3/La_2O_3 increased with reaction time. Simultaneously, the crystal structure of Ga_2O_3/La_2O_3 appreciably changed generating a new crystalline phase of $NaLa(CO_3)_2$, which is pobably produced by the reaction of La_2O_3 with $NaHCO_3$ aqueous solution. Since no reaction proceeded on simple La_2O_3 used as a photocatalyst, transformation of La_2O_3 into $NaLa(CO_3)_2$ would be the key to promote CO_2 reduction.

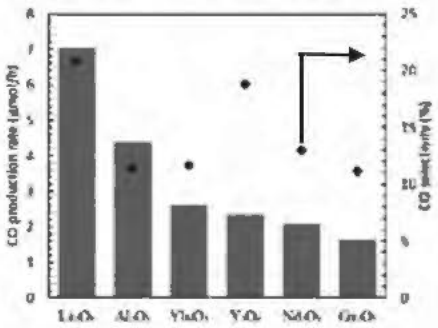

Fig.1 CO production rate after 5h reaction for samples showing higher activity than Ga_2O_3

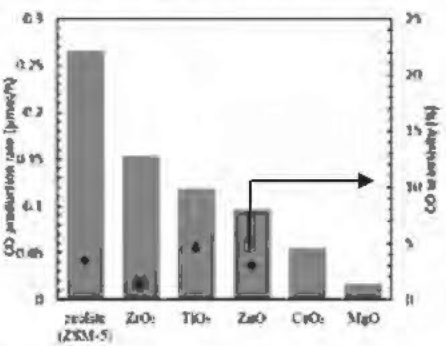

Fig.2 CO production rate after 5h reaction for samples showing lower activity than Ga_2O_3

References: [1] N. Yamamoto, T. Yoshida, S. Yagi et al., e-J Surf. Sci. Nanotech., Vol. 12 (2014) 263-268.

Preparation of gallium oxide nanofilm photocatalyst using graphene oxide template

Kenta Sonoda[1], Muneaki Yamamoto[2], Tetsuo Tanabe[2], Tomoko Yoshida[2]
[1]*Department of Engineering, Osaka City University, Osaka, Japan*
[2]*Advanced Research Institute for Natural Science and Technology, Osaka City University, Osaka, Japan*

Gallium oxide (Ga_2O_3) is well known as a photocatalyst having relatively high catalytic activity with the assistnce of Ag co-catalyst for water splitting and CO_2 reduction with water. We have suggested that the photocatlytic reduction very likely proceeds at the interfaces or boudaries between small grains of Ga_2O_3 and Ag nanoclusters on them [1]. Accordingly, we have tried to improve the catalytic activity with replacement of Ga_2O_3 grains to submicro- to nano- sized Ga_2O_3 sheets (referred as nanofilms), which would allow uniform and dence dispersion of Ag nanoclusters. To realize this, we have developed a method to fabricate Ga_2O_3 nanofilms with using graphene oxide (GO) as a template. Then Ag was loaded on the nanofilms and examined their activity for photocatalytic reduction of CO_2 with water.

Ga_2O_3 nanofilms were fabricated by following procedures. At first, gallium tri-n-butoxide was deposited (adsorbed) on GO, then the GO was autoclaved in cyclohexane at 453 K for 6 hours [2], followed by calcination at a given temperature of 823 – 1123 K.

TEM images of thus fabricated Ga_2O_3 nanofilms are shown in Fig. 1. The images confirm full removal of GO template and formation of nanofilms for samples calcined at 823 – 1123 K. Their crystal structures were analysed by XRD measurements as showin in Fig.2. The nanofilms calcined at 823 K and 1123 K were consisted of single phase, γ-Ga_2O_3 and β-Ga_2O_3, respectively, while those calcined at 923 K and 1023 K, mixed-phases of β- and γ-Ga_2O_3. At the conference, we will show the reaction activities of the Ga_2O_3 nanofilms with loading Ag cocatlyst for photocatalytic reduction of CO_2 with water.

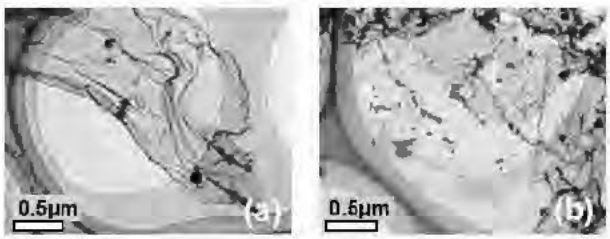

Figure 1. TEM images of Ga_2O_3 nanosheets fabricated by calcination at 823 K (a) and 1123 K (b).

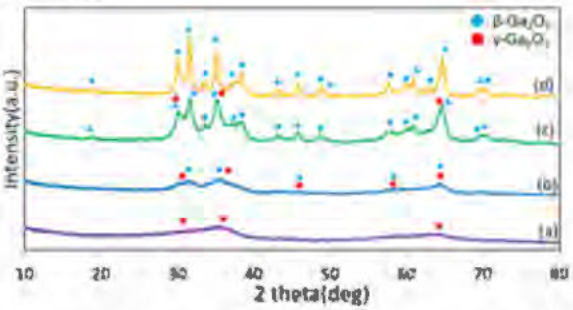

Figure 2. XRD patterns of Ga_2O_3 nanosheets fabricated by calcination at 823 K (a), 923 K (b), 1023 K (c) and 1123 K

References:
[1] Yamamoto, M. *et al.*, *J. Mater. Chem. A* **2015**, 3, 16810.
[2] Takenaka, S. *et al.*, *J. Phys. Chem. C* **2015**, 119, 12445.

In-situ UV-Vis diffuse reflectance measurements of silver loaded gallium oxide photocatalyst

Daiki kitajima[1], Muneaki Yamamoto[2], Tetsuo Tanabe[2], Tomoko Yoshida[2]

[1]*Department of Engineering, Osaka City University, Osaka, Japan*

[2]*Advanced Research Institute for Natural Science and Technology, Osaka City University, Osaka Japan*

It is well known that photocatalytic reduction of CO_2 with water is enhanced by Ag co-catalyst. Nevertheless its role on the photocatalytic reduction process is not understood well. Furthermore the Ag co-catalyst is often subjected to change its chemical and physical state during the reduction, i.e. it is oxidized in water and dissolved as Ag^+, and Ag^+ is photodeposited again resulting in the aggregation to be larger Ag particles, and accordingly lose its photocatalytic activity. Therefore, it is quite important to know physical and chemical state of the Ag co-catalyst and their change during the photoreaction process. In the preset work we have tried to observe in-situ UV-Vis diffuse reflectance (DR) for the surface of Ga_2O_3 with Ag co-catalyst (Ag loaded Ga_2O_3) during the photocatalytic reduction of CO_2 with water, because UV absoption edge gives information on Ga_2O_3 and the absorption caused by localized surface plasmon resonance (LSPR) of Ag nano-particles gives information on themselves. In this study, in-situ DR measurements have been conducted at four different atmospheres either Ar, CO_2, Ar/H_2O or CO_2/H_2O under light irradiation.

Fig. 1 compares time courses of the intensities of LSPR peaked at 450 nm under the light irradiation. As seen in the figure, the LSPR peak appeared immediately after starting the light irradiation and increased with the irradiation time. It found that the peak intensity increased even after 120 min when water vapor was introduced. Fig. 2 shows DR spectra normalized with the highest intensity of each peak after 120 min of the light irradiation. The peaks appeared around 350 nm, 450 nm and 600 nm are attributed to Ag small clusters, Ag nanoparticles and larger Ag nanoparticles, respectively. Main difference among all spectra appears in the intensity of longer wavelength region which is caused by the absorption of larger Ag particles. The peak intensity at 600 nm was low at CO_2 atmosphere. This suggests that the adsorption of CO_2 on the surface of Ga_2O_3 and/or the Ag particles suppressed the appearance of large Ag particles or size growth of Ag nano-particles.

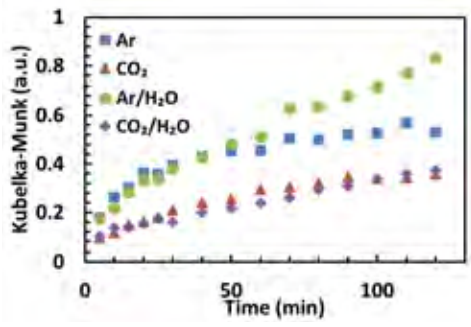

Fig 1. Time course of the LSPR absorption intensity at 450 nm under light irradiation.

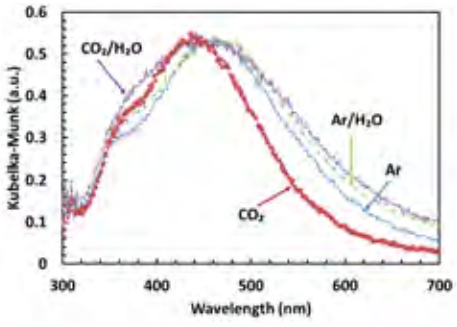

Fig 2. Normalized DR spectra measured at 120 min at four different atmospheres.

Detection of "color changes" with a single kind of opsin in the zebrafish pineal organ.

Seiji Wada[1], Baoguo Shen[1], Emi Kawano-Yamashita[1], Takashi Nagata[1], Masahiko Hibi[2], Satoshi Tamotsu[3], Mitsumasa Koyanagi[1,4], Akihisa Terakita[1,4]

[1]Department of Biology and Geosciences, Graduate school of Science, Osaka City University; [2]Division of Biological Science, Graduate School of Science, Nagoya University;[3]Department of Biological Sciences, Faculty of Science, Nara Women's University, Japan;[4]OCARINA, Osaka City University, Japan;

Pineal and its related organs in lower vertebrates discriminate UV and visible light. Our previous studies revealed that a pineal opsin, parapinopsin (PP) is responsible for UV-sensitivity in the wavelength discrimination of lamprey and teleost pineal organs [1-3]. PP has a unique property called bistable nature; upon UV light absorption, the dark state of PP converts to the visible light-sensitive photoproduct, which reverts to the original dark state by visible light-absorption. Accordingly, PP forms different "photoequilibrium-like states", depending on various spectral distributions between UV and visible light region [4]. In this study, we investigated how the PP-photoequilibrium is involved in the color opponency under natural light-like conditions with calcium imaging using transgenic zebrafish. We further investigated how the intensity and spectral distribution of natural sunlight varies depending on several factors. We found that the zebrafish pineal organ might respond to changes in the spectral distribution of natural light and discuss a physiological relevance of the pineal wavelength discrimination involving parapinopsin.

[1] Koyanagi M.; Kawano E,; Kinugawa Y.; Oishi T.; Shichida Y.; Tamotsu S.; Terakita A. *PNAS* **2004**, 101, 6687-6691

[2] Wada S.; Kawano-Yamashita E.; Koyanagi M.;Terakita A. *PLoS One* **2012**, e39003

[3] Koyanagi M.; Wada S.; Kawano-Yamashita E.; Hara Y.; Kuraku S.; Kosaka S.; Kawakami K.; Tamotsu S.; Tsukamoto H.; Shichida Y.; Terakita A. *BMC Biology* **2015**, 13, 73.

[4] Wada S.; Shen B.; Kawano-Yamashita E.; Nagata T.; Hibi M.; Tamotsu S.; Koyanagi M.;Terakita A. *PNAS* **2018**, 115:11310–11315

Behavioral investigation of non-visual photoreception with pineal-specific opsin-knockout zebrafish

Genki Nakata[1], Seiji Wada[1], Mitsumasa Koyanagi[1,2], Akihisa Terakita[1,2]

[1]Department of Biology and Geosciences, Graduate School of Science, Osaka City University, Osaka, Japan; [2]OCARINA, Osaka City University, Osaka, Japan

Pineal organs of most lower vertebrates capture light and the light information is utilized for regulating various physiological functions. Secretion of melatonin, which is known as a hormone that modulates locomotor activities in various animals, is one of major pineal functions. In teleosts, it was reported that melatonin secreted in the dark (night) is suppressed by light illumination. Previous reports including our recent works suggest that three kinds of light-sensitive proteins, opsins expressed in pineal organs might be involved in the melatonin suppression [1]. In this study, by using opsin-knockout zebrafish, we first investigated the contribution of a major opsin of the three to the light-induced melatonin suppression and then to light-modulated behaviors. We found that the opsin was largely responsible for the light-induced melatonin suppression. We also obtained evidence that suggested the opsin was involved in a light-modulated behavior(s). Functional relationship among the opsin, the light-induced melatonin suppression and the light-induced behavior is discussed.

[1] Koyanagi, M.; Wada, S.; Kawano-Yamashita, E.; Hara, Y.; Kuraku, S.; Kosaka, S.; Terakita, A. *BMC biology* **2015**, 13, 73.

Evaluation of the pineal wavelength discrimination based on a pineal-specific opsin parapinopsin in the zebrafish behaviours

Tomoka Saito[1], Seiji Wada[1], Baoguo Shen[1], Takashi Nagata[1, 2], Mitsumasa Koyanagi[1, 3] and Akihisa Terakita[1, 3]

[1]Department of Biology and Geosciences, Graduate School of Science, Osaka City University, Osaka, Japan; [2]PRESTO, JST; [3]OCARINA, Osaka City University, Osaka, Japan

Pineal and related organs in lower vertebrates discriminate UV and visible light. We previously found that a pineal opsin called parapinopsin (PP) is responsible for UV-sensitivity in the wavelength discrimination of the lamprey and teleost pineal organs as well as the lizard pineal related organ [1-3]. Recently, our calcium-imaging studies with PP-knockout zebrafish and a visual opsin introduced PP-knockout zebrafish revealed that a single kind of opsin PP generates color opponency in a single kind of pineal photoreceptor cell [4]. The PP-based color opponency depends on the unique molecular property called bistable nature; upon UV light absorption, the dark state of PP converts to the visible light-sensitive photoproduct, which reverts to the original dark state by visible light-absorption. Accordingly, PP forms different "photoequilibrium-like states" between the dark state (UV-sensitive) and photoproduct (visible light-senstive), depending on various spectral distributions between UV and visible light region. We found that PP-based color opponency requires "background light" with an intensity of approximately 1% or more of natural sunlight in the early afternoon. In this study, by using PP-knockout zebrafish we evaluated contribution of PP-based pineal color opponency to zebrafish behaviours under background light condtions containing different UV and visible light lintensities. Based on obtained results, we would attempt to discuss behavial relevance of the PP-based pineal wavelength discriminaiton.

[1] Koyanagi M.; Kawano E,; Kinugawa Y.; Oishi T.; Shichida Y.; Tamotsu S.; Terakita A. *PNAS* **2004**, 101, 6687-6691

[2] Wada S.; Kawano-Yamashita E.; Koyanagi M.;Terakita A. *PLoS One* **2012**, e39003

[3] Koyanagi M.; Wada S.; Kawano-Yamashita E.; Hara Y.; Kuraku S.; Kosaka S.; Kawakami K.; Tamotsu S.; Tsukamoto H.; Shichida Y.; Terakita A. *BMC Biology* **2015**, 13, 73.

[4] Wada S.; Shen B.; Kawano-Yamashita E.; Nagata T.; Hibi M.; Tamotsu S.; Koyanagi M.;Terakita A. *PNAS* **2018**, 115:11310–11315

A Nobel Type of Opsin with Optogenetic Potential: Animal Opsin-Based Photopigment as a Potential Dark-Active and Light-Inactivated G Protein-Coupled Receptor

Takashi Nagata[1,*], Mitsumasa Koyanagi[1,2], Robert Lucas[3], Akihisa Terakita[1,2]

[1]*Department of Biology and Geosciences, Graduate School of Science, Osaka City University, Osaka, Japan;* [2]*OCARINA, Osaka City University, Osaka, Japan;* [3]*Faculty of Biology, Medicine and Health, The University of Manchester, Manchester, UK;* **Current affiliation: PRESTO, JST*

Peropsin or retinal pigment epithelium-derived rhodopsin homolog, found in many animals, belongs to the opsin family. Most opsins bind to 11-*cis*-retinal as a chromophore and act as light-activated G protein-coupled receptors (GPCRs). In contrast, we previously reported that peropsins from an amphioxus and a spider bind all-*trans*-retinal and isomerize it into 11-*cis* form by light [1, 2]. Such a photo-isomerization activity is also found in a retinal photoisomerase retinochrome, which serves to produce 11-*cis*-retinal chromophore in squid retinas. However, our comparative analyses of catalytic enzyme activity of peropsin and retinochrome as a retinal photoisomerase revealed that the catalytic efficiency of spider peropsin is much lower than that of squid retinochrome, suggesting a possibility of a peropsin function other than a retinal photoisomerase [3]. On the other hand, peropsin has amino acid sequence motifs that are highly conserved among GPCRs. In this study, we therefore asked whether peropsin acts as a GPCR. We conducted cultured cell-based assays for G protein activation but did not detect any significant activation of major G proteins by peropsins. Interestingly, however, chimeric mutants of peropsins constructed by replacing the third intracellular loop region with that of Gs- or Gi-coupled opsin were active and drove Gs- or Gi-mediated signaling in the dark, respectively, and were inactivated upon illumination in cultured cells. These results suggest that peropsin could act as a dark-active, light-inactivated G protein-coupled receptor. In addition, the chimeric peropsin mutants would be useful as novel optogenetic tools that enable light-inactivated G protein signaling.

[1] Koyanagi, M.; Terakita, A.; Kubokawa, K.; Shichida, Y., Amphioxus homologs of Go-coupled rhodopsin and peropsin having 11-*cis*- and all-*trans*-retinals as their chromophores. *FEBS Lett* **2002,** *531* (3), 525-8

[2] Nagata, T.; Koyanagi, M.; Tsukamoto, H.; Terakita, A., Identification and characterization of a protostome homologue of peropsin from a jumping spider. *J Comp Physiol A* **2010,** *196* (1), 51-9.

[3] Nagata, T.; Koyanagi, M.; Lucas, R.; Terakita, A., An all-*trans*-retinal-binding opsin peropsin as a potential dark-active and light-inactivated G protein-coupled receptor. *Sci Rep* **2018,** *8* (1), 3535

Comparative analyses of light responses between the pineal photoreceptors expressing "bistable" and "bleaching" opsins using transgenic zebrafish.

Baoguo Shen[1], Seiji Wada[1], Emi Kawano-Yamashita[1], Mitsumasa Koyanagi[1,2], Akihisa Terakita[1,2]

[1]*Department of Biology and Geosciences, Graduate School of Science, Osaka City University, Osaka, Japan;* [2]*OCARINA, Osaka City University, Osaka, Japan*

Pineal and related organs in lower vertebrates discriminate UV and visible light, independently of ocular color vision. We previously found that in the pineal wavelength discrimination, a pineal-specific opsin, parapinopsin serves as a UV -sensitive pigment [1-4] and has a unique molecular property called "bistable nature" different from that of visual cone opsins: upon UV-light absorption, parapinopsin converts to a stable photoproduct, which reverts to the dark state upon subsequent visible light absorption whereas the visual opsin photoproducts are unstable, release chromophores and become colorless , showing the molecular property called "bleaching" nature [1]. Therefore, it is of interest to investigate how the different photoproduct stabilities relate to photoresponses or sensitivities of photoreceptor cells. In order to obtain a clue to this issue, we established a mutant zebrafish, which expresses UV-cone opsin instead of parapinopsin in the pineal photoreceptor cells. We performed calcium imaging of photoreceptor cells of the mutant and wild-type zebrafish with a multiphoton microscope. Based on the obtained results, we discussed how the different opsin properties are involved in a light adaptation process of the pineal photoreceptor cells.

[1] Koyanagi, M.; Kawano, E.; Kinugawa, Y.; Oishi, T.; Shichida, Y.; Tamotsu, S.; Terakita, A. *PNAS* **2004**, 101, 6687-6691.

[2] Wada, S.; Kawano-Yamashita, E.; Koyanagi, M.; Terakita, A. *PLoS One* **2012**, e39003.

[3] Koyanagi, M.; Wada, S.; Kawano-Yamashita, E.; Hara, Y.; Kuraku, S.; Kosaka, S.; Terakita, A. *BMC biology* **2015**, 13, 73.

[4] Wada, S.; Shen, B.; Kawano-Yamashita, E.; Nagata, T.; Hibi, M.; Tamotsu, S.; Koyanagi, M.; Terakita, A. *PNAS* **2018**, 115, 11310-11315.

Gliding ghost of *Mycoplasma gallisepticum*

Masaki MIZUTANI[1], Makoto MIYATA[1,2]
[1]*Graduate School of Science, Osaka City University, Osaka, Japan*
[2]*OCARINA, Osaka City University, Osaka, Japan*

Cytadherence and/or motility are essential factors to exert pathogenicity in many infectious bacteria. Mycoplasmas are commensal and occasionally pathogenic bacteria which lack a peptidoglycan layer and have small cell and genome sizes[1]. *Mycoplasma gallisepticum* is an avian pathogenic bacterium causing a chronic respiratory disease in chickens and an infectious sinusitis in turkeys. The infected cells transmit to their eggs from breeder birds. *Mycoplasma gallisepticum* is a related species of human pathogenic mycoplasma, *Mycoplasma pneumoniae*. They bind to sialylated oligosaccharides on host tissue surfaces and glide to spread by using unique gliding system, which is completely unrelated to other bacterial motility systems including *Mycoplasma mobile* gliding system or eukaryotic motility[2].

A previous study has shown that the gliding motility of *Mycoplasma mobile* is driven by ATP hydrolysis on the basis of gliding ghost experiments. In this experiment, *Mycoplasma mobile* cells were permeabilized with Triton X-100 and stopped for gliding, then gliding was reactivated by the addition of ATP[3]. However, the reactivation of permeabilized cells of *Mycoplasma pneumoniae*-type gliding has not been succeeded so far[1].

In the present study, we permeabilized *Mycoplasma gallisepticum* cells with Triton X-100, Triton X-100 containing ADP or Triton X-100 containing ATP, and observed the behaviours of permeabilized cells. The cells permeabilized with Triton X-100 or Triton X-100 containing ADP did not show gliding. The cells permeabilized with Triton X-100 containing ATP showed gliding at a speed of 0.014 ± 0.007 μm/s that is only 4% of intact cells, and 63% of permeabilized cells continuously glided through 17 min. Next, we permeabilized cells with Triton X-100 containing ATP and vanadate ion which gradually inhibits ATP hydrolysis. The cells permeabilized with Triton X-100 containing ATP and vanadate ion showed gliding at a speed of 0.011 ± 0.010 μm/s, and 33% of permeabilized cells continuously glided through 17 min. These results indicate that *Mycoplasma gallisepticum* gliding is also driven by ATP hydrolysis.

References

[1] Miyata, M.; Hamaguchi, T. *Current Opinion in Microbiology* **2016**, 29, 15–21.
[2] Nakane, D.; Miyata, M. *Journal of Bacteriology* **2009**, 191, 3256–3264.
[3] Uenoyama, A.; Miyata, M. *PNAS* **2005**, 102, 12754–12758.

Structural dynamics of epi-genome related heterochromatin protein HP1 studied by spin labeling ESR spectroscopy

Toshiaki Arata[1,3,4], Shigeaki Nakazawa[2], Yuichi Mishima[4], Kazunobu Sato[2], Takeji Takui[2], Toru Kawakami[4], Hironobu Hojo[4], Toshimichi Fujiwara[4], Makoto Miyata[1,3], and Isao Suetake[4,5]

[1]Dept. Biol. and [2]Dept. Chem., Grad. Sch. Sci., and [3]OCARINA, Osaka City Univ., Osaka; [4]Inst. Protein Res., Osaka Univ., Osaka; [5]Koshien Univ., Hyogo, Japan

Heterochromatin protein (HP1) is evolutionally conserved, and binds to epigenetic mark, lysine9 methylated histone H3 as a transcriptional repressor [1]. Here, we introduced site-specific spin labeling on HP1 and examined the dynamics of human HP1 with continuous wave (CW)-ESR and pulsed electron double resonance (DEER/PELDOR) spectroscopy [2,3]. HP1 has the chromodomain (CD) and the chromoshadow domain (CSD), which are linked by the flexible HR. It dimerizes *via* CSD to form NTE-CD-HR-CSD-CSD-HR-CD-NTE, where NTE is an N-terminal extension of CD. The ESR spectroscopy from the nitroxide spin label fixed at a cysteine of the CD or CSD of human HP1 indicated a highly flexible structure of HP1 molecule on nanosecond time scale. Different from yeast HP1, dimerization *via* CD-CD interaction is reported, CD was freely mobile by CW-ESR and the distance between two CD domains in the HP1 dimer was beyond the limit of DEER (>7 nm). HP1 is reported to bind lysine9 methylated histone H3 peptide (H3K9me) at CD domain and also bind DNA at HR domain while HP1γ does not bind DNA. The rotational dynamics of CD slowed down 1.5-fold by H3K9me either as CD alone or in full-length HP1, and also indirectly by DNA while that in HP1γ did not. Preliminary results showed that phosphomimic mutation of NTE slowed down CD dynamics 1.5-fold in full-length HP1 but made it apparently insensitive to DNA and H3K9me binding. The NTE region will play an important role for HP1 function by controlling the CD dynamics in phosphorylation-dependent manner. The HR which links between CD and CSD was highly dynamic on subnanosecond time scale as detected by CW-ESR. Dynamics of spin label located at several residues of HR in HP1α was restricted weakly with DNA only under high viscosity in glycerol. This weak motional restriction suggested loose translational diffusion of HP1α on DNA and *vice versa*. In contrast, the other domain (CSD) stably formed a dimer, while the interdomain distance was just expected based on crystal structure. In addition, the CSD dimer in full-length HP1 exhibited nearly free but isoform-specific motion; HP1α was 1.5-fold slower than HP1γ, but became identical when the N-terminal domain including HR was deleted. The distinct dynamics is due to the fact that HR is different between HP1α and HP1γ in length and sequence. It is likely that distinct dynamics contributes to the isoform-specific function of HP1.

[1]Mishima,Y.*et al.Nuc.Acid Res.***2015**,43,10200.[2]Abe,J.*et al.Appl.Mag.Reson.***2018**,42,473. [3]Arata,T. (In Japanese) *Seibutsu Butsuri* **2012**, 4, 172; *Bunko Kenkyu* **2006**, 54, 245.

Two different conformations of Gli123 protein, essential for *Mycoplasma mobile* gliding

Daiki Matsuike[1)], Yuhei O Tahara[1)], Tasuku Hamaguchi[3)], Hisashi Kudo[4)], Yuuki Hayashi[4)], Munehito Arai[4)], Makoto Miyata[1,2)]

1) Department of Biology, Graduate School of Science, Osaka City University,
2) OCARINA, Osaka City University
3)RIKEN, SPring-8 Center
4) Graduate School of Arts and Science, The University of Tokyo

Abstract: *Mycoplasma mobile*, a fish pathogenic bacterium glides on solid surfaces based on ATP energy by a unique energy-conversion mechanism. Four huge proteins clustering on the surface of gliding machinery are essential for this mechanism. Gli349 shaped like an eighth music note (♪), acts as a leg protein by binding to sialylated oligosaccharides on solid surfaces. Gli521 shaped an interrogation mark (?), transmits the force to Gli349 as a crank protein [1]. We focused on the structure of Gli123, a 123 kDa protein responsible for the assembly of surface gliding proteins [2].

Gli123 showed two different conformations under rotary-shadowing electron microscopy (EM), i.e. globular and rod structures in high and low ionic strength conditions, respectively. This conformational shift occurred reversibly as monitored by light scattering. We clarified the globular structure by single particle analysis of negative staining EM, as a "White-mushroom" with dimensions, 20.0, 14.5, and 16.0 nm. Reconstruction of higher resolution is undertaken by using cryo-EM. We clarified the rod structure by Small Angle X-ray Scattering (SAXS) analyses, as chained five masses about 34 nm long and 4 nm wide. We are currently also trying SAXS modeling of globular structure.

On the surface of gliding machinery, four proteins are organized to form a large complex. The conformational change of Gli123 may be involved in this organizing process.

Keywords

Mycoplasma mobile / Electron Microscopy / single particle analysis / SAXS

References:

[1] Miyata, M.; Hamaguchi, T. *Current Opinion in Microbiology* **2016**, 29, 15-21.

[2] Uenoyama, A.; Miyata M. *Journal of Bacteriology* **2005**, 187, 5578-5584.

Structure of motor evolved by combination of ATP synthase and phosphoglycerate kinase for *Mycoplasma mobile* gliding

Takuma Toyonaga[1], Takayuki Kato[2], Akihiro Kawamoto[3], Tasuku Hamaguchi[4]
Noriyuki Kodera[5], Toshio Ando[5], Keiichi Namba[2,4,6] and Makoto Miyata[1,7]
[1]Grad. Sch. Sci., Osaka City Univ., Japan, [2]Grad. Sch. Front. Biosci., Osaka Univ., Japan,
[3]IPR, Osaka Univ., Japan, [4]SPring-8, Riken, Japan,
[5]WPI NanoLSI, Kanazawa Univ., Japan, [6]BDR, Riken, Japan
[7]OCARINA, Osaka City Univ., Japan

Mycoplasma mobile, a fish pathogenic bacterium, glides on host cell surfaces with a unique mechanism. The gliding machinery is divided into two parts: internal and surface structures. Our previous study showed that the motor in the internal structure including an ATP synthase homolog and phosphoglycerate kinase (PGK) forms chains along the cell membrane [1, 2]. Both ATP synthase and PGK are essential enzymes for life in most living organisms and synthesize ATP in electron transport chain and glycolytic pathway, respectively. Recently, electron cryomicroscopy (cryoEM), which can visualize biomolecules in a frozen hydrated state has been developed drastically, resulting in resolving biomolecular structures at near atomic resolution. In the present study, we determined the structure of the internal motor by single-particle cryoEM at 7.4 Å resolution. The structure showed that two hexamers are paired by a rectangular frame with eight arm-like extensions. This structure allowed us to dock the crystal structure of ATP synthase catalytic subunits from *Bacillus sp.* into the two hexamers at secondary-structure level. PGK was assigned to each of four arms extending horizontally from the homolog of ATP synthase catalytic subuits. A coiled-coil structure deeply penetrates the center of hexamers, as seen in ATP synthases generally. The coiled coil should be composed of MMOB1630, which has no homology with any subunit of ATP synthase, based on analyses of isolated single hexamer including the coiled coil. Our data suggested that the motor of *Mycoplasma mobile* evolved by the combination of two essential enzymes for life with several novel proteins.

Figure. CryoEM structure of the internal motor fitted with atomic models of ATP synthase from *Bacillus sp.* (α-subunits, red; β-subunits, yellow; PDB ID code 2QE7 [3]) and PGK from *Thermus sp.* (blue; PDB ID code 2IE8 [4]).

[1] Miyata, M.; Hamaguchi, T. *Curr. Opin. Microbiol.* **2016**, 29, 15-21.
[2] Nakane, D.; Miyata, M. *Proc. Natl. Acad. Sci. USA* **2007**, 104, 19518-19523.
[3] Stocker, A.; Keis, S.; Vonck, J.; Cook, G.M.; Dimroth, P. *Structure* **2007**, 15, 904-914
[4] Lee, J.H.; Im, Y.J.; Bae, J.; Kim, D.; Kim, M.K.; Kang, G.B.; Lee, D.S.; Eom, S.H. *Biochem. Biophys. Res. Commun.* **2006**, 350, 1044-1049

Internal Ribbon Structure Driving Helicity-Switching Swimming in Spiroplasma

Yuya SASAJIMA[1)], Makoto MIYATA[1,2)]

[1)] *Graduate School of Science, Osaka City University, Japan*
[2)] *OCARINA, Osaka City University, Japan*

Spiroplasma eriocheiris, a helical-shaped swimming bacterium lacking peptidoglycan layer, a bacterial cell wall, swims in a high viscosity solution by reversing its helical orientation from front to back [1, 2, 3]. In the present study, we analyzed the ribbon of about 110 nm in width that exists inside the helical helix by electron microscopy, to elucidate the mechanism of helical reversal. The isolated ribbon had 840 nm pitch very similar with the cell. The protofilament obtained by separating the ribbon was a double helix composed of fibers in a ring-like repeating structure, the pitch of which was roughly consistent with the pitch of the ribbon and the cell. Based on these observations, we concluded that the swimming is caused by the structural change in Fibril protein forming protofilaments of about 11 nm in diameter. When the ribbon containing three kinds of MreB protein in addition to Fibril was treated with A22, MreB polymerization inhibitor, separation of each bundled protofilament was observed, suggesting that the MreBs orient fibril filaments to the ribbon. Therefore, any of these four proteins is expected to be responsible for the helical switch. We are clarifying the structure and its changes of isolated Fibril by using electron microscopy and single particle analysis.

Helicity-switching swimming in Spiroplasma

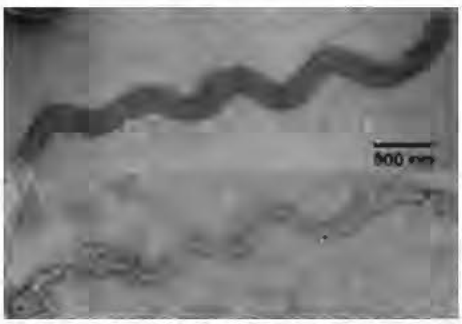

Internal helical ribbon structure

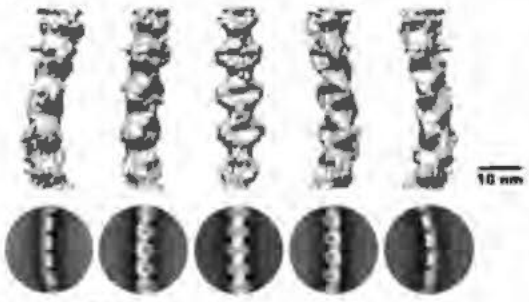

Fibril filament

[1] Miyata M and Hamaguchi T. Frontiers in Microbiology. 2016, 7, 960.

[2] Terahara N, Tulum I, and Miyata M. Biochemical and Biophysical Research Communication. 2017, 487, 488-93.

[3] Liu P, Zheng H, Meng Q, Terahara N, Gu W, Wang S, Zhao G, Nakane D, Wang W, and Miyata M. Frontiers in Microbiology. 2017, 8, 58.

Dynamics and Structure of MreB proteins from *Spiroplasma eriocheiris*

Daichi Takahashi[1], Makoto Miyata[1, 2]

1. Graduate School of Science, Osaka City University
2. OCARINA, Osaka City University

Abstract: MreB is a bacterial protein capable of polymerization using ATP (adenosine 5'-triphosphate) and Mg^{2+} [1]. The polymer of MreB play a critical role to form rod shapes of bacteria by binding to the inside of the cell membrane [2]. MreB is coded as a single copy of gene in many bacteria, and its role has been considered to be conserved. A novel type MreBs were discovered in genus *Spiroplasma* belonging to the same class with *Mycoplasma* [3]. Each *Spiroplasma* species has more than five classes of MreBs. These MreBs are thought to be involved in making *Spiroplasma* helical shapes and twisting their bodies for swimming motility [4]. To clarify the characters of these novel MreBs, two kinds of MreBs (MreB3 and MreB5) among five derived from *Spiroplasma eriocheiris* were purified and analyzed for the structures and the polymerization dynamics. When these MreBs were put into a polymerization condition, paired two filaments were observed under electron microscopy. The structure was similar to MreBs of other species. Both MreB3 and 5 required 1.5 to 2 hours for the equilibration of polymerization although conventional MreBs needed only 20 - 30 minutes as traced by light scattering technique. Polymerizations by using GTP (guanosine 5'-triphosphate) were faster than by using ATP. Addition of Mg^{2+} slowed the polymerization of these MreBs, although increase of Mg^{2+} made polymerization of conventional MreBs faster. Sedimentation experiments suggested that more than half of the MreBs remained as monomers although more than half polymerized in conventional MreBs [1]. These results suggest that MreBs from *Spiroplasma eriocheiris* have evolved a unique reaction mechanism and lower polymerization ability.

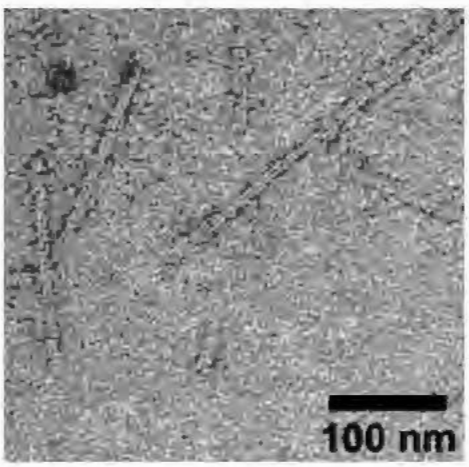

References

[1] Bean GJ *et al. Biochemistry* **2008**, 47, 826-35.
[2] Salje J *et al. Mol Cell* **2011**, 43, 478-87.
[3] Ku C *et al. Biochem Biophys Res Commun* **2014**, 446, 927-32.
[4] Liu P *et al. Front Microbiol* **2017**, 8, 58.

Reproduction of *Spiroplasma* swimming motility using synthetic bacteria and elucidation of its mechanism

Hana Kiyama[1], Shigeyuki Kakizawa[2], and Makoto Miyata[1,3]

1. Graduate School of Science, Osaka City University, Japan

2. The National Institute of Advanced Industrial Science and Technology (AIST)

3. OCARINA, Osaka City University, Japan

The class *Mollicutes*, a small group of bacteria, is thought to have caused extraordinary evolution. *Spiroplasma*, belonging to class *Mollicutes*, performs a unique swimming motility by switching the helical core of cell clockwise and counterclockwise. The cell helicity is composed of Fibril protein unique to *Spiroplasma* genus and five classes of MreB homologous to eukaryotic actin [1]. MreB is a universal protein in bacteria and acts as a scaffold for cell wall synthesis by forming short filaments [2], but interestingly it is involved in swimming motility in *Spiroplasma* which does not have a cell wall. In this study, for the purpose of reproducing swimming motility, a group of genes involved in *Spiroplasma eriocheiris* swimming was introduced and expressed in synthetic bacteria (*Mycoplasma mycoides* JCVI-syn3.0B) having no motility at all [3]. Synthetic bacteria made from mycoplasma have a genome designed only with essential genes.

When Fibril protein was expressed, about 30% cells elongated 4.4 times longer than the original. In addition, about 26% of the elongated cells formed a clear helicity with a pitch of 0.66 μm, similar to that *S. eriocheiris* shows in the starved state. The filaments isolated from these synthetic bacteria and observed by electron microscopy were very similar to the Fibril filaments from *S. eriocheiris*.

In addition, when MreB2, the most abundant MreB in *S. eriocheiris* was expressed, about 11% of the cells expanded to filamentous form with a length of 3.0 times. When MreB2 fused with mCherry was expressed, intense fluorescence was observed in the filamentous part.

As the cell shape can be changed by expressing genes in synthetic bacteria, the *Spiroplasma* swimming motility can be reproduced by further expressing the genes involved in swimming in the future studies.

[1] Liu, P. *et al*. *Front Microbiol*. **2017**, 8, 58.

[2] Shi, H. *et al*. *cell*. **2018**, 172, 1294-1305.

[3] Hutchison, CA 3rd. *et al*. *Science*. **2016**, 351, aad6253.

Structural and functional analysis of fatty acid kinase of *Thermus thermophilus* HB8

Maya Nakatani[1], Taihei Murakami[1,2], Hiroki Okanishi[3,4], Norie Araki[4], Makoto Miyata[1,5] and Ryoji Masui[1]

[1]*Grad. Sch. Sci., Osaka City Univ.,* [2]*Fac. Sci. Eng., Waseda Univ.,*[3]*Grad. Sch. Med., Osaka Univ.,* [4]*Grad. Sch. Med. Sci., Kumamoto Univ.,* [5]*OCARINA, Osaka City Univ.*

Fatty acid kinase (Fak), which has been identified recently [1], consists of two subunits, FakA and FakB. FakA phosphorylates the fatty acid bound to FakB. Fak is essential for synthesis of membrane lipids in bacteria such as *Mycoplasma* that do not have fatty acid synthase. Furthermore, Fak is reported to be involved in gene expressions of virulence factors. However, the structure and reaction mechanism of Fak remain largely unknown. In this study, we analyzed the subunit composition and domain organization of Fak from *Thermus thermophilus* HB8 (ttFak). Fatty acid kinase subunit of ttFak, TTHA0214 (ttFakA), was overexpressed in *E. coli* and purified to homogeneity. ttFakA was shown to be monomeric, which differs from the result of the previous study [1]. Pull-down assay using the cell extract of *T. thermophilus* coupled with mass spectrometry revealed that ttFakA interacts with TTHA0951 (ttFakB1), which is a fatty acid binding protein belonging to DegV family. Native PAGE also detected interaction of ttFakA with another DegV family protein TTHA0950 (ttFakB2). These results suggested that these three proteins, ttFakA, ttFakB1, and ttFakB2 constitute ttFak. Limited proteolysis of ttFakA with two proteases yielded two fragments of almost the same sizes each of which corresponded to the N- and C-terminal fragments. This agreed to the sequence-based prediction that ttFakA consists of two domains. The observation that the resulted fragments could not be separated by gel filtration suggested that the N- and C-terminal domains strongly interact with each other. Unexpectedly, when ttFakA was incubated with ATP in the presence of divalent cations, ttFakA was auto-phosphorylated. By mass spectrometry, the major phosphorylation site was identified as Ser249, which was reported to be phosphorylated in the previous proteomic analysis [2]. In the predicted structure, N-terminal domain might be the catalytic domain containing the ATP-binding site and Ser249 might be located in the loop region between the two domains. Based on these results, we discuss the structural organization and the role of auto-phosphorylation of ttFakA.

[1] Parsons, J. B., Broussard, T. C., Bose, J. L., Rosch, J. W., Jackson, P., Subramanian, C. and Rock, C. O. *Proc. Natl. Acad. Sci. U. S. A.* **2014**, 111, 10532-10537.

[2] Wu, W., Liao, J., Lin, G., Lin, M., Chang, Y., Liang, S., Yang, F., Khoo, K. and Wu, S. *Mol. Cell. Proteomics* **2013**, 12, 2701-2713.

Application to microbial surface structure observation of Quick-Freeze and Deep-Etch (QFDE) replica microscopy

Yuhei O Tahara[1,2], Makoto Miyata[1,2]
1)Graduate School of Science, Osaka City University, Japan
2)OCARINA, Osaka City University, Japan

Quick-Freeze and Deep-Etch (QFDE) replica microscopy is an electron microscopy method in which a sample is frozen and fixed in a moment by hitting a sample against a cooled metal and metal corted to exposed sample surface, and observed the metal membrane with resolution of nanometer order and time resolution of submillisecond.
In this technology, it is possible to observe the microstructure on the sample surface with high contrast, and it is particularly suitable for the surface of microorganisms.

This technology was developed and implemented in the new academic field, Ministry of Education, Culture, Sports, Science and Technology in 2012 - 2016. As technical support from 2018, 24 researchers and students from 16 research groups inside and outside the campus conducted a rapid freeze replica method and related electron microscope observations for 180 days in total.

1, *E. coli* infected with T phage (Fig. 1)
2, S-layer structure of *Caulobacter crescentus*
3, Intracellular structure of vesicle-releasing bacteria (Fig.2)
4, Detailed structure of artificial synthesis life Syn 3.0 (Fig. 3)
5, Surface structural change during germination of fission yeast spores (Fig 4)

Fig.1

Fig. 2

Fig.3

Fig.4

The effect of Ca^{2+} on molecular mass and viscosity of poly-γ-glutamic acid infermentative production

Presenter Nanako IWAMOTO [1], Yoshihiro YAMOGUCHI[1,2], Akira OGTA[1,3], Toshio TANAKA[1], Ken-ichi FUJITA[1]

Affiliation [1] *Grad. Sch. Sci. Osaka City Univ.*
[2] *OCARINA, Osaka City Univ.*
[3] *Res. Center. Urban Health & Sports, Osaka City Univ.*

Poly-γ-glutamic acid (PGA) is one of high viscus constituents of Japanese traditional fermentative food Natto. When PGA is left at room temperature, gradual decrease in its molecular mass is observed as incubation period increasing. Decrease in the molecular mass is accelerated by heat treatment at 100ºC. We previously reported that decrease in molecular mass occurred by heat treatment is restricted by divalent metal cation chelating agents such as EDTA and citric acid. In addition, the restrictive effect is enhanced by the Ca^{2+}-specific chelating agents such as BAPTA and EGTA. Based on the results, we assumed the involvement of Ca^{2+} in decrease in molecular mass of PGA occurred by heat treatment and increase in molecular mass during fermentative production of PGA. In this study, PGA was fermentatively produced using a synthetic culture medium with or without Ca^{2+} and we then estimated the molecular mass of PGA obtained.

We found that viscosity of the culture supernatant disappeared and the molecular mass of PGA was relatively low in the case using Ca^{2+} less synthetic medium. The low molecular mass is thought to depend on low L-glutamic acid concentration in the synthetic medium. Therefore, L-glutamic acid concentration was elevated to 10 fold in the medium. As a result, viscosity still disappeared in the culture supernatant. However, the molecular mass was equally high as compared with a control PGA sample. These results obtained above could not explain the involvement of Ca^{2+} in heat sensitive nature of PGA molecules. Therefore, further investigations are in progress to prove the involvement.

Exploration of novel factors related to gene expression of drug efflux pumps in *S. cerevisiae*

Masahiro Oyama[1], Yoshihiro Yamaguchi[1,2], Akira Ogita[1,3],
Toshio Tanaka[1], Ken-ichi Fujita[1]

[1]*Graduate School of Science, Osaka City University,*
[2] *OCU Advanced Research Institute for Natural Science and Technology,*
[3]*Research Center for Urban Health and Sports, Osaka City University*

Abstract: Recently, drug-resistant fungi have been frequently emerged by abuse of antifungal drugs. Especially resistant fungi against azole drugs are the problem in clinical sites [1]. Combining drugs that restrict drug resistance mechanisms with already approved drugs is one of the superior methods for overcoming infection caused by drug-resistant fungi. We have reported that trans-anethole (anethole), which is the principal component of anise oil, inhibits the drug efflux [2]. When *S. cerevisiae* cells were treated with dodecanol, viable cell number temporally reduced. Anethole restricted over-expression of multidrug efflux pump's gene *PDR5* induced by dodecanol to control levels thereby expressing durable antifungal effects. However, the detailed mechanism has been unsolved.

At first, we examined the susceptibility of dodecanol in gene-deficient strains related to regulation of intracellular Ca^{2+} levels. Among them, *pmr1Δ* was highly susceptible to doecanol. Next, we examined the change in cell viability of *pmr1Δ*. The recovery of the cell viability delayed in treatment with dodecanol. We indicated that the involvement of *PMR1* in over-expression of *PDR5* induced by dodecanol. Increase in intracellular Ca^{2+} levels was significantly observed in treatment with dodecanol and combination of dodecanol with anethole. Furthermore, *pmr1Δ* maintained elevated Ca^{2+} levels as compared with the parental strain. The expression of *PMR1* was restricted in the treatment with dodecanol and drug combination. Dodecanol did not induce the expression of *PDR5* in *pmr1Δ*. Above all, we suggested that elevated Ca^{2+} levels provably depend on the decreased expression level of *PMR1* caused by dodecanol. In addition, the elevated Ca^{2+} levels possibly restrict over-expression of *PDR5*.

References:

[1] Masiá Canuto M.; Gutiérrez Rodero F. *Lancet Infect. Dis.* **2002**, 2, 550.

[2] Fujita, K.; Ishikura, T.; Jono, Y.; Yamaguchi, Y.; Ogita, A.; Kubo, I.; Tanaka, T. *Biochim. Biophys. Acta Gen. Subj.* **2017**, 1861(2), 477.

Molecular dissection of the transport of the spore surface protein Isp3 in fission yeast.

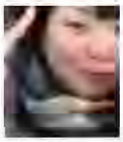

Karina YOSHIKAWA[1], and Taro NAKAMURA[1,2]

1) Graduate School of Science, Osaka City University, Japan

2) The OCU Advanced Research Institute for Natural Science and Technology (OCARINA), Osaka City University, Japan

Spores of fission yeast are dormant cells resistant to various stresses such as heat and alcohol. To date, we have found that the outermost layer of the fission yeast spore wall is composed of a protein called Isp3 (Isp3 layer) and that the Isp3 layer plays an important role in spore tolerance to environmental stresses [1]. Isp3 is a protein that is specifically found in fission yeast and has very characteristic regions (Fig. 1). Isp3 is expressed

MGLGNLCSYKQDDSLDILQKKVLIDAFNKVTIDC
PNVQHQQPTYWYPPPPPRHHKEHKKSHHHWE
SDDDSSDDEESCEKKKPKCCEKKKPKCCES
EQNNGCGRRNQLARRLAFLGSFGDGDCDGCN
AFTVTGPITYFRTCPDPLTGITPAVAAAAAATPA
AATPATPAAAATPAAPAA

Blue: the basic amino acid-rich region. Red: the acidic amino acid region. Pink: the repeat sequence. Green: the alanine-rich region.

specifically during sporulation, accumulates in the forming spores and subsequently exported to the outside of the spore, i.e. the cytoplasm of the ascus. Since signal sequence is not found in Isp3, it is possible that Isp3 may be transported by an unknown mechanism. The aim of this study is to address the novel mechanism of protein transport using Isp3 as a model.

The various deletion mutants of Isp3 were constructed and their localizations were observed. Surprisingly, the characteristic regions as described above were not involved in the export. Isp3 lacking the N terminal 45 amino acids accumulated in the spores. These data suggest that the N-terminal region is necessary for export of Isp3(Fig. 2).

ıre 2. The images show the rescence of Isp3-GFP and ΔN-terminal region-GFP in rulating cells.

[1] Fukunishi, K. et al., *Mol. Biol. Cell* **2014,** 25, 1549-1559

Identification and characterization of genes involved in constructing spike structure of fission yeast spore surface

Daiki Masuda[1], Yuhei Tahara[1,2], Makoto Miyata[1,2], and Taro Nakamura[1]

[2] *The OCU Advanced Reseach Institute for Natural Science and Technology (OCARINA), Osaka City University, Japan*

Introduction: Fission yeast spore surfase is coverd by the characteristics spike structure. How is this spike structure constructed? *mde10*$^+$ was idenified as a gene involved in the construction of the spike structure[1] (Figure). *mde10*$^+$ encodes an ADAM family protein which is conserved widely in higher organisms including human. ADAMs are responsible for important life phenomena on cell surface such as membrane fusion of sperm and egg or signaling, in association with various proteins. Therefore, we assumed that the additional genes cooperate with *mde10*$^+$ to construct spike structure. The aim of this study is to identify and characterize the additional genes involved in constructing the spike structure and elucidate its molecule mechanism.

Results: To identify target genes, we observed 191 deletion strains of genes whose expression are upregulated during sporulation (*mug* and *meu*) [2][3]. At first, we roughly selcected 40 mutants whose spore periphery was different from wild-type by phase contrast microscopy. Next, we observed the fine structure of these strains by electron microscopy and identified 10 mutants, two of which (*mug57*Δ and *meu30*Δ) exhibited abnormal surface morphology. *mug57*$^+$ and *meu30*$^+$ encode a fasciclin I domain protein which is involved in cell adhesion and an α-amylase homolog, respectivly. Interestingly, although spike structure remained in these mutants, they were smaller and a number of spike was increased. These data suggest that the presense of pathway to surpress the number of spike structure on the spore surface.

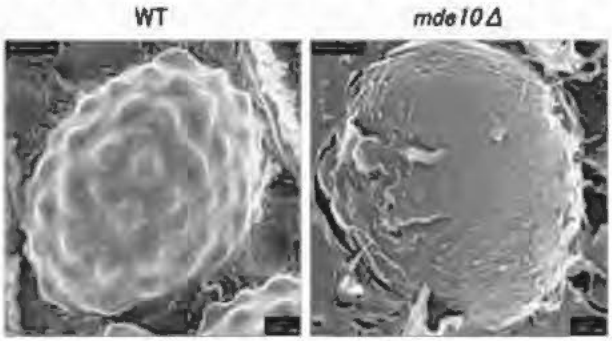

Figure. Fission yeast spore by electron microscopy

[1] Nakamura T *et al. Eukaryotic Cell* 2004, 3, 27-39.

[2] Martin C *et al. Curr Biol* 2005, 15, 2056-2062.

[3] Watanabe T *et al. Nucleic Acids Res* 2001, 29, 2327-2337.

Excess accumulation of carotenoids in a siphonous green alga, *Codium fragile* upon different light strengths

Soichiro Seki[1], Ryuichi Kano[2], Ritsuko Fujii[1,2,3]
[1]Department of Chemistry, Faculty of Science, [2]Graduate school of Science, and [3]The OCU Advanced Research Institute for Natural Science and Technology, Osaka City University, Japan

The major carotenoids accumulated in chloroplast of higher plants and algae are highly conserved: β-carotene, lutein, violaxanthin (Vx) and neoxanthin. Solo conformation of neoxanthin as 9'-*cis* has been reported for more than 140 species [1], but several "primitive" green algae were reported to contain all-*trans* neoxanthin (tNx) [2]. Our group has shown for the first time that the accumulation of tNx is associated to the strong illumination during cultivation for *Codium intricatum* [3]. *Codium* sp. belongs to the "siphonous alga" which is a branch of green algae accumulating siphonaxanthin (Sx) and/or siphonein (Sn), and α-carotene instead of lutein and β-carotene, respectively. These species show negligible "xanthophyll cycle" [4], which is a well-known photoprotective adaptation of green linage including accumulation of Vx upon strong light exposure. Therefore, we addressed a question that accumulated tNx may be involved in an unknown photoprotective adaptation representative to the xanthophyll cycle.

In this study, we focused on to clarify the precise relationship between accumulation of tNx and photosynthetic photon flux density (photon flux density of 400 to 700 nm photons, PPFD, in μmol photon m^{-2} sec^{-1}). We cultivated the gametophyte of *C. fragile* having 50 μm i.d. filamentous form (Kobe University Macro-Algal Culture Collection, KU-0654). Approximately 0.7 g (wet weight) aliquots of the cultivated cells were put into glass vials (32 mm inner diameter) and were incubated under four different irradiation strengths of 50, 100, 200, 300 PPFD from white LED for 7 days. Pigment compositions were determined by using HPLC system [3] and normalized with eight molecules of chlorophyll *b*.

As shown in the Fig. (a), the relative number of tNx increased with the incubation days at all irradiation strengths tested. It also increases with irradiation strengths as plotted in Fig. (b). Interestingly, the increment of tNx accumulation was large for 0-100 PPFD and about one sixth for 100-300 PPFD. This may indicate that the numbers of tNx may reach a sort of saturation in thylakoid membranes between 100-200 PPFD, and the photoprotective adaptation also reaches the maximum at the irradiation condition if tNx plays photoprotective function. Further experiments are necessary to clarify this.

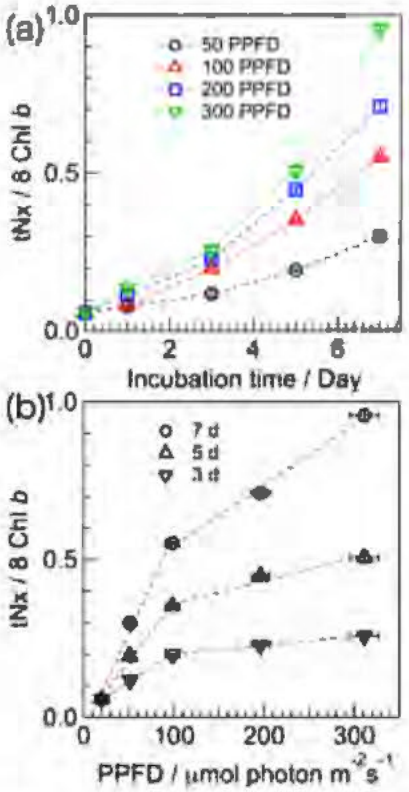

Figure. Relative numbers of all-*trans* neoxanthin (tNx) in cultivated *Codium fragile* against incubation time (a) and irradiance (b).

<References>

1. Takaichi, S.; Mimuro, M. *Plant Cell Physiol.* **1998,** *39(9)*, 968–977.

2. Yoshii, Y. *Phycolog. Res.* **2006**, *54*, 220–229.

3. Uragami. C. et al. *Photosynth. Res.* **2014,** *121*, 69-77.

4. Giovagnetti, V. et al. *Planta* **2018,** *247(6)*, 1293-1306.

Fabrication of Diamond/Cu Direct Bonding for Power Device Applications

Shinji Kanda[1], Satoshi Masuya[2], Makoto Kasu[2], Naoteru Shigekawa[1], and Jianbo Liang[1]

[1]*Graduate School of Engineering, Osaka City University, 3-3-138 Sugimoto, Sumiyoshi-ku, Osaka 558-8585, Japan*

[2]*Department of Electrical and Electronic Engineering, Saga University, 1 Honjo-machi, Saga 840-8502, Japan*

m18tb019@ab.osaka-cu.ac.jp

Abstract:

Diamond is the best potential candidate as the next generation semiconductor material for high power and high frequency devices[1],[2]. Diamond devices with high frequency, high thermal stability, high-current and low-loss capability have been reported[3]-[5]. The high operating electrical power in such devices would result in an increase in temperature near the active region, which would degrade devices performance and reliability.

Power devices were generally directly mounted onto the heat sink by solder bonding or hydrophilic bonding. However, the thermal conductivity of the solder materials is very low in comparison with those of metals such as Cu and Al. The thermal resistance of the solder layer limits the heat dissipation of the devices. We previously reported the direct bonding of diamond and Al using surface activated bonding (SAB) at room temperature and obtained diamond/Al bonding interface with high thermal stability[6].

In this work, we present the direct bonding of diamond and Cu using SAB at room temperature. The optical microscope image of the diamond/Cu bonded sample surface without annealing is shown in Fig. 1. Although a small unbonded region was observed on the upper left side of the bonded sample, an about 99 % area bonding of diamond and Cu was achieved.

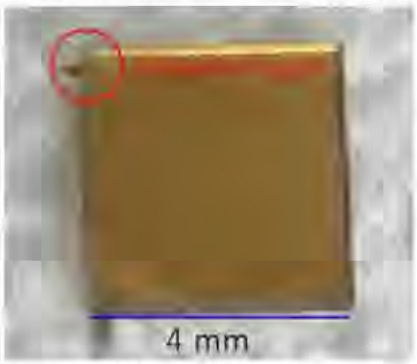

Figure 1. The optical microscope image of the diamond/Cu bonded sample surface without annealing.

References:

[1] J. Isberg, J. Hammersberg, E. Johanssion, T. Wikström, D. J. Twitchen, A. J. Whitehead, S. E. Core, and G. A. Scarsbrook, Science 297 (2002) 1670.

[2] A. T. Collins, In Properties and Growth of Diamond, IEE: Inspec, London, 1994.

[3] M. Kasu, K. Ueda, H. Ye, Y. Yamauchi, S. Sasaki, and T. Makimoto, Electron. Lett. 41 (2005) 1249.

[4] M. Kasu, H. Sato, and K. Hirama, Appl. Phys. Express 5 (2012) 025701.

[5] H. Umezawa, Y. Kato, and S. I. Shikata, Appl. Phys. Express 6 (2013) 011302.

[6] J. Liang, Shoji Yamajo, Martin Kuball, N. Shigekawa, Scripta Materialia 159 (2019) 58.

Bonding strength evaluation of Al foil/AlN junctions by surface activated bonding

S. Horikawa, S. Morita, J. Liang, Y. Kaneko, and N. Shigekawa
Graduate School of Engineering, Osaka City University,
3-3-138 Sugimoto, Sumiyoshi-ku, Osaka 558-8585, Japan
m18tb050@hg.osaka-cu.ac.jp

Abstract:

The thermal tolerance of widegap semiconductors, which largely outperforms of that of conventionally-used Si, has not yet fully exploited in the present power electronics modules since the highest temperature of normal operations of such modules is limited by several factors such as the thermal tolerance of die attaches and the thermal resistance of ceramic plates[1]. We previously fabricated Al-foil/AlN and SiC-die/Al-foil/AlN junctions by using the surface-activation bonding (SAB), i.e., without using die attaches, and confirmed that no fractures appeared at the Al/AlN interfaces even after annealing at 600 °C. We also showed that bonded SiC Schottky diodes normally operated in an ambient temperature up to 300 °C[2].

In this work, we fabricated an Al foil/AlN junction by An Al foil/AlN junction is fabricated by bonding a 30-μm Al foil and a 650-μm AlN plate at room temperature and 473 K. The peel strengths of the two junctions were evaluated by a 180 ° peel test in a schematic shown in Fig. 1. The relationship between the peel strength and the stroke of the respective junctions is shown in Fig. 2. The peel strength, which revealed ununiform features, was ~30 and ~60 N/m for the junctions fabricated by the room-temperature bonding and the 473-K bonding, respectively.

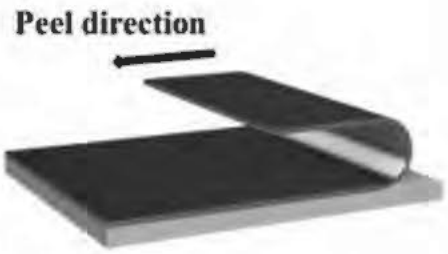

Fig. 1. Schematic of 180° peel test.

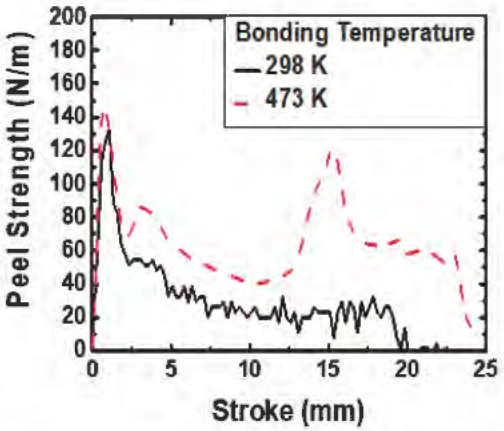

Fig. 2. Peel Strength of Al foil/AlN junctions.

References:

[1] R. Kisiel, et al. *Microelectronics Reliability*, vol. 49, pp. 627–629, 2009.

[2] S. Morita, et al. *ECS Trans.*, vol.86, pp. 137-142, 2018.

Analysis of SiC/Si Bonding Interface with Thermal Annealing Treatment by XPS

Zexin Wan, Jianbo Liang, Naoteru Shigekawa

Graduate School of Engineering, Osaka City University, 3-3-138 Sugimoto, Sumiyoshi, Osaka 558-8585, Japan

Abstract: It was reported that the reaction between Schottky contacts and SiC layers limits their thermal tolerance [1]. The usage of heavily doped Si substrates as substitute for Schottky contacts is a practicable method to solve the problem. We applied the surface-activated bonding (SAB) to fabricate the SiC/Si heterojunctions [2]. During the irradiation of fast atom beam (FAB) of Ar, damages were introduced to the substrate and the electrical properties of the SiC/Si junctions were largely affected. We previously found that the effects of damages were recovered by the thermal treatment. In this research, the variation in properties of SiC/Si bonding interfaces due to the thermal treatment is investigated by using X-ray photoelectron spectroscopy (XPS).The process of experiment is shown in Fig.1. We annealed the SiC/Si junctions at 400, 700, and 1000°C, and measured their current-voltage characteristic at room temperature. Then we removed the Si substrate and analyzed the exposed surface of SiC by using XPS. The C1s core level spectra of the respective SiC surfaces are shown in Fig.2. By fitting the XPS spectra, we find that the annealing of junctions brings about the shift in binding energy of C-Si bonding, which is in correlation with the reverse-bias current of SiC/Si heterojunction. The change in the binding energy is assumed to be attributed to the shift of Fermi level at the SiC surface due to the annealing.

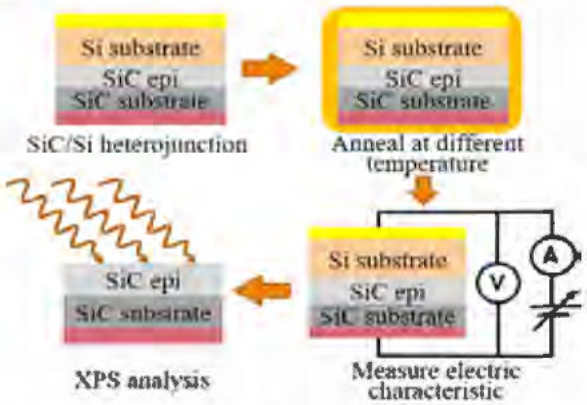

Fig.1 Schematic of the process applied to SiC/Si heterojunction.

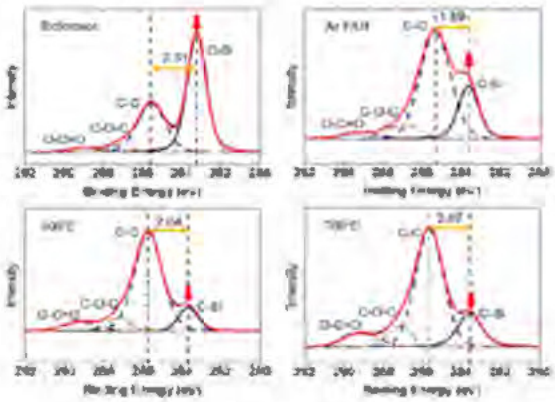

Fig.2. Spectra of C 1s core level of SiC surface

Acknowledge:

The XPS analysis was supported by Prof. Kouichi Tsuji, Graduate School of Engineering, Osaka City University.

References:

[1] Bhanumurthy K., Schmid-Fetzer R., "Solid-state reaction bonding of silicon carbide (HIP-SiC) below 1000℃" Materials Science and Engineering A 220(1):35-40.

[2] J. Liang, S. Nishida, M. Arai, and N. Shigekawa, "Improved electrical properties of n-n and p-n Si/SiC junctions with thermal annealing treatment," J. Appl. Phys. 120, 034504 (2016).

Photoinduced Shape Change of Crystals Composed of a Diarylethene with a Long Alkyl Chain

Takuya Higashiguchi, Daichi Kitagawa, Seiya Kobatake
Department of Applied Chemistry, Graduate School of Engineering, Osaka City University, Osaka 558-8585, Japan

Diarylethene crystals exhibit various photomechanical behaviors such as contraction, expansion, bending, fragmentation, and twisting, which are expected to be applied to photoactuators [1]. In particular, crystals consisting of a diarylethene with a long alkyl group exhibit unique photomechanical behavior accompanying a reversible thrmodynamic single-crystal-to-single-crystal phase transition [2]. In this study, we investigated on crystal shape changes of a diarylethene having undecyl group at both sides (DE-(C11)$_2$) upon photoirradiation.

DE-(C11)$_2$

Upon irradiation with UV light, the crystal bent toward the incident light, but the degree of bending depended on the illumination directions (i.e. left or right) as shown in Figure 1. Furthermore, when another plane of the rod-like crystal was irradiated with UV light, the crystal twisted toward the incident light. The degree of twisting also depended on illumination directions as shown in Figure 2. Moreover, in the course of study, it was found that crystals of DE-(C11)$_2$ were "twin crystal", as can be seen from single crystal X-ray diffraction analysis. The crystals always have striations at twin boundaries as observed by scanning electron microscopy. The two crystals in the twin crystal have different thickness. The mechanism of these photomechanical behaviors will be discussed based on the molecular packing of a diarylethene and each thickness in the twin crystal.

Figure 1. Photoinduced bending behavior depending on illumination sides. UV irradiation was performed for 10 s.

Figure 2. Photoinduced twisting behavior depending on illumination sides. UV irradiation was performed for 10 s.

[1] M. Irie, T. Fukaminato, K. Matsuda, S. Kobatake, *Chem. Rev.*, **2014**, 114, 12174-12277.
[2] D. Kitagawa, K. Kawasaki, R. Tanaka, S. Kobatake, *Chem. Mater.*, **2017**, 29, 7524-7532.

Photoluminescence Switching of Quantum Dot Coated with Diarylethenes by Photochromic Reaction

Yuya Seto, Daichi Kitagawa, DaeGwi Kim, Seiya Kobatake
Graduate School of Engineering, Osaka City University,
3-3-138 Sugimoto, Sumiyoshi-ku, Osaka 558-8585, Japan

Diarylethene (DE) is one of the photochromic compounds which has excellent properties such as fast response and high repeating durability[1]. Quantum dots (QD) have high emission quantum yield and narrow emission band[2]. Research on photoluminescence on/off switching of QD coated with DE has been conducted so far, but no report shows the high quenching ratio [3]. In this study, CdSe/ZnS core-shell type of QDs coated with DE (QD-DE) were synthesized (Fig. 1) and the photoluminescence on/off switching behavior accompanying with the photochromic reactions was investigated.

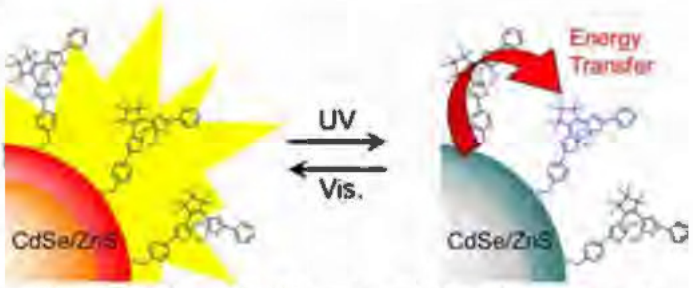

Figure 1. Schematic illustration of photochromism and photoluminescence ON/OFF switching of QD-DE.

The photoluminescence intensity drastically decreased with increasing absorption intensity of the DE closed-ring form, as shown in Fig. 2. The photocyclization conversion increased with the irradiation time, but the rate of the conversion became slow with increasing coated number of DE, as shown in Fig. 3a. On the other hand, the F/F_0 value relative to the photocyclization conversion largely decreased with increasing coated number of DE as shown in Fig. 3b. We succeeded in fabricating quantum dots coated with diarylethenes exhibiting fast quenching speed and high contrast of photoluminescence on/off switching.

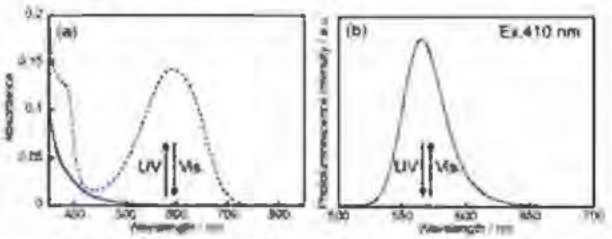

Figure 2. (a) Absorption and (b) photoluminescence spectral changes of QD-DE (DE/QD = 87.4) in toluene upon alternating irradiation with 313 nm light and visible light.

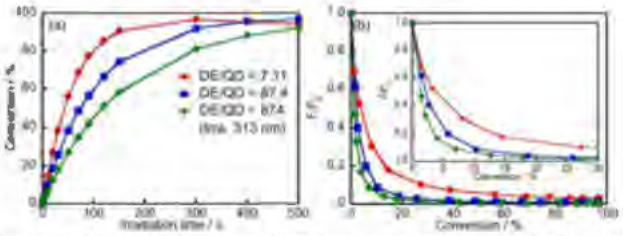

Figure 3. (a) Photocyclization conversion relative to irradiation time and (b) normalized photoluminescence intensity relative to photocyclization conversion of QD-DE.

References:

[1] M. Irie, T. Fukaminato, K. Matsuda, S. Kobatake, *Chem. Rev.* **2014**, 114, 12174-12277.
[2] W. W. Yu, L. Qu, W. Guo, X. Peng, *Chem. Mater.* **2003**, 15, 2854-2860.
[3] S. A. Díaz, L. Giordano, T. M. Jovin, E. A. Jares-Erijman, *Nano Lett.* **2012**, 12, 3537-3544.

Bright and Tunable Emission of BODIPY in Solid State

Katsuya Shimizu, Seiya Kobatake
Department of Applied Chemistry, Graduate School of Engineering, Osaka City University, Osaka 558-8585, Japan

Boron dipyrro methene (BODIPY) shown in **Figure 1** has attracted much attention because of high fluorescence quantum yield (Φ_f) and molar extinction coefficient (ε) in solution. However, Φ_f significantly decreases and the emission spectrum is red-shifted due to intermolecular interaction such as π-π stacking and reabsorption of fluorescence derived from high planarity and a small Stokes shift in concentrated solution and in the solid state [1]. If it is easily possible to change the emission color using a single fluorophore without molecular modification and to create solid emissive BODIPY, then that strategy would be very useful for application to optoelectronic materials for solid-state dye lasers and organic light-emitting diodes. Here, we report on the design and fabrication of random copolymers (poly(BO_x-*co*-St_y)) consisting of BODIPY monomer (BO) and styrene (St) to achieve multi-color and efficient emission in the solid state using St as a spacer (**Figure 2**). As shown in **Figure 3**, the emission color of the resulting copolymers changed from green to red by changing the content of BO from 0.042 to 100 mol%. Φ_f also increased with the content of St (Φ_f = 0.05-0.88) because the intermolecular distance between the BO fluorophores became longer. In particular, poly(BO_x-*co*-St_y) (y/x = 2400) exhibited a very high Φ_f (0.88) which is the highest value among BODIPY derivatives in the solid state reported to date [2].

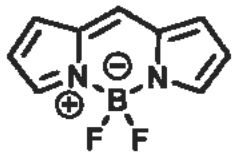

Figure 1. Typical structure of BODIPY.

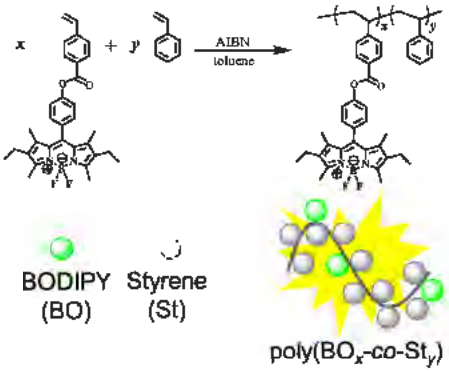

Figure 2. Synthetic scheme of poly(BO_x-*co*-St_y).

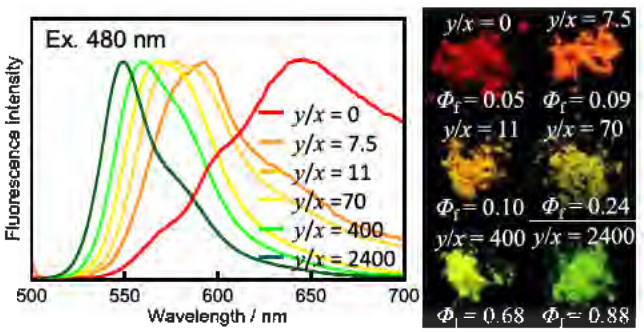

Figure 3. Fluorescence spectra of poly(BO_x-*co*-St_y) in the bulk powder excited with 480 nm light.

References:

[1] A. Loudet, K. Burgess, *Chem. Rev.*, **2007**, 107, 4891-4932.

[2] K. Shimizu, D. Kitagawa, S. Kobatake, *Dyes Pigm.*, **2019**, 161, 341-346.

Simultaneous observation of nanoparticles and hexane droplets in hexane/water emulsion by quick freeze replica electron microscopy

Kazuya Tamejima[1], Takuya Okamoto[1], Yuhei O Tahara[1,2], Makoto Miyata[1,2], Tomoyuki Yatsuhashi[1,2]

[1]*Graduate School of Science, Osaka City University, Japan*

[2]*The OCU Advanced Research Institute for Natural Science and Technology, Osaka City University, Japan*

Gold nanoparticles (AuNPs) are widely used as catalysts and biomedical materials. Femtosecond laser irradiation to gold (III) chloride trihydrate ($HAuCl_4$) aqueous solution has been reported as one of the single-nano-sized AuNPs synthesis methods [1]. However, a dispersant, which is indispensable to control particle size, might contaminate the resultant AuNPs. We recently succeed synthesizing single-nano-sized AuNPs in hexane/water mixture by femtosecond laser irradiation. The key to form single-nano-sized AuNPs without the use of dispersant is the emulsion formed by stirring $HAuCl_4$ aqueous solution and hexane. In this study, we try to observe both AuNPs and hexane droplets in water by quick freeze replica electron microscopy to clarify the AuNPs production mechanism.

Hexane / $HAuCl_4$ aqueous solution was exposed to femtosecond laser pulses (0.8 μm, 40 fs, 0.4 mJ, 1 kHz). The AuNPs collected from water layer was observed by a transmission electron microscope (TEM). The mean diameter of AuNPs was 6.1±2.0 nm (Fig. 1a, n = 300). It is emphasized that the probability of capturing droplets is extremely small since the quick freeze replica method samples only a small part of solution. Therefore, we optimized pre-freezing operation procedures, freezing tools, fracturing position, and sample sublimation time. As a result, the shape of hexane droplet and AuNPs was successfully transferred to the replica made of platinum (Fig.1b, thickness 1.3 nm). The mean diameter of AuNPs on the hexane droplet was 12 nm (n = 65). We are now planning to improve the experimental conditions for better statistics.

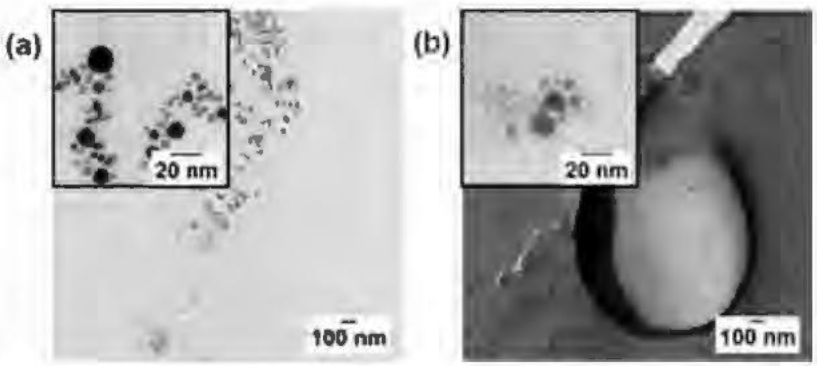

Fig. 1 TEM images of (a) solution and (b) replica.

[1] Nakamura, T.; Mochidzuki, Y.; Sato, S., *J. Mater. Res.*, **2008,** *23*(4), 968–974.

Study on Micro-Tomographically Functional Imaging of Blood Flow in Vascular Plexuses using Optical Coherence Doppler Velocigraphy

Daisuke FURUKAWA[1], Souichi SAEKI[1],
, Takafumi ITO[2], Yoshiaki NISHINO[2], Yusuke HARA[1,3]

[1] *Graduate School of Engineering, Mechanical & Physical Engineering, Osaka City University. 3-3-138, Sugimoto, Sumiyoshi-ku, Osaka, 558-8585*

[2] *TOKOTAKAOKA Co., Ltd, Hamamatsu, Japan*

[3] *SHISEIDO Research Center, Yokohama, Japan*

Abstract:

The skin aging process, e.g. wrinkles and saggings, caused by not only aging but also ultraviolet irradiation, could be related to the depression of metabolic function. The microcirculation system should be an important guideline of skin care for the anti/smart-aging. Rheological behavior of interstitial in epidermal and dermal tissue, including blood micro-circulation, can vary skin mechanics in micro scale, i.e. visco-elasticity. Therefore, an *in vivo* quantitative measurement of capillary blood flow velocity is crucial to clarify their properties. The purpose of this study is to visualize the tomographic flow velocity of red blood cell in capillaries below human epidermal skin using Optical Coherence Doppler Velocigraphy, i.e. OCDV [1]. This is constructed on a low coherence interferometer [2], which is based on Hilbert transform and adjacent auto-correlation. In order to validate OCDV system, this was *in vivo* applied to human forearm skin under the condition with or without vasodilation, respectively. As a result of skin tomography obtained by OCDV, A *en-face* cross-sectional MIP can display horizontal networks of capillary blood vessels. Additionally, it was confirmed that capillary vasculature and blood velocity can be visualized tomographically even in the upper subpapillary layer. In summary, OCDV system could be quite useful for a micro-tomographic imaging of blood flow velocity of capillary vessels inside skin.

References:

[1] Daisuke Furukawa, et al., "In vivo Micro-Tomographic Visualization of Capillary Angio-Dynamics Around Upper Dermis Under Mechanical Stimulus Using Low Coherence Interferometer "Optical Coherence Doppler Velocigraphy", American Journal of Physics and Application, Vol.6(4), (2018), pp.89-96.

[2] Joseph M. Schmitt, "Optical Coherence Tomography (OCT): A Review", IEEE Journal on Selected Topics in Quantum Electronics, Vol.5, No.4 (1999), pp.1134-1142.

Development of Micro-tomographic Visualizing System of Mechanical Properties inside Regenerated Tissue using UA-OCDV

Koji YAMANE [1], Daisuke FURUKAWA [2], Souichi SAEKI [2]

[1] *Department of Mechanical Engineering, Faculty of Engineering, Osaka City University. 3-3-138, Sugimoto, Sumiyoshi-ku, Osaka, 558-8585*

[2] *Graduate School of Engineering, Mechanical & Physical Engineering, Osaka City University. 3-3-138, Sugimoto, Sumiyoshi-ku, Osaka, 558-8585*

Abstract:

In recent years, the regenerative therapy of osteoarthritic cartilage has attracted attention due to clinical transplantation of autologous cultured cartilage. However, a non-contact and invasive diagnosing method of bio-mechanical functions, e.g. viscosity and elasticity, has never been established yet. The purpose of this research is to construct and validate the ultrasonic-assisted Doppler OCT system (UA-OCDV), which can provide viscoelastic characteristics inside tissue tomographically and non-contactly using a high intensity focused ultrasound transducer as a loading devise. UA-OCDV was applied to porcine cartilages with or without collagenase treatment. Figure 1 shows tissue discrimination via tomographic phase map, where left and right sides are normal and digested cartilage, respectively. Consequently, UA-OCDV can visualize water permeability inside tissue micro-tomographically. Furthermore, this is effective to a non-contact diagnosing tool of viscoelastic properties correlated with water permeability.

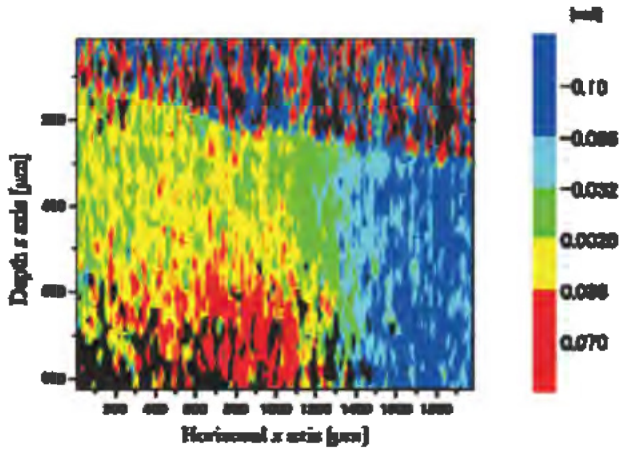

Fig.1 Cross-section color map of phase difference to acoustic radiation pressure

Construction on Medical Diagnosing System by Photo-thermal Doppler OCT (PT-OCDV) using photosensitizer

Miki YANAGISA[1], Daisuke FURUKAWA[2], Souichi SAEKI[2]

[1] *Department of Engineering, Mechanical Engineering, Osaka City University. 3-3-138, Sugimoto, Sumiyoshi-ku, Osaka, 558-8585*

[2] *Graduate School of Engineering, Mechanical & Physical Engineering, Osaka City University. 3-3-138, Sugimoto, Sumiyoshi-ku, Osaka, 558-8585*

Abstract:

Medical diagnosis using near-infrared fluorescence emitted from a photosensitizer [1], e.g. Indocyanine green (ICG), has attracted attention as a clinical and surgical visualizing tool of tumor and vasculature. The purpose of this study is to construct and validate an in vivo micro-tomographic visualizing system of pharmacokinetics of delivered drug, namely PT-OCDV. The proposed system, based on Doppler OCT, can provide tomographic detection of photo-thermal effect by a photosensitizer inside tissue. *in vivo* animal experiment was carried out using a mouse administered intraperitoneally with ICG. As a result, PT-OCDV displayed the tomographic distribution of not only capillary blood flow but also drug diffusion to tissue. It was proven that the present system had good potential as a diagnostic modality of various disease and Drug Delivery System.

References:

[1] Nakamichi, Y., et al , Journal of Biomechanical Science and Engineering, Vol.12, No.2, 2017, 16-00591.